UNIVERSITY OF CALIFORNIA SAN DIEGO

Design, Synthesis and Biological Evaluation of Chimeric Small Molecules

A dissertation submitted in partial satisfaction of the requirements for the degree Doctor of Philosophy

in

Chemistry

by

Troy Allen Bemis

Committee in charge:

Professor Michael D. Burkart, Chair
Professor Guy Bertrand
Professor Daniel J. Donoghue
Professor Kamil Godula
Professor Christian M. Metallo

2022

The dissertation of Troy Allen Bemis is approved, and it is acceptable in quality and form for publication on microfilm and electronically.

University of California San Diego

2022

DEDICATION

I would like to dedicate this work to my parents, Kenneth and Judith Bemis. Their love and support was paramount to my success in completing this work, and they have pushed me to be my best self for as long as I can remember.

I would also like to recognize my three sisters, Tiera, Carissa, and Tessa. Through all of the stress and uncertainty inherent in graduate school, they always made themselves available to me in times of need. They provided both the resolute support and the comic relief necessary to not simply survive but thrive in my environment.

Lastly, I would like to recognize my high school science teacher Ms. Rhonda Schultz. As a mischievous young student, she managed to spark my initial interest in chemistry which has flourished into a lifelong passion. Who knew throwing elemental sodium into water could be so fun! Thank you for the hard work and passion you bring to your classroom.

EPIGRAPH

One of the symptoms of an approaching nervous breakdown is the belief that one's work is terribly important.

Bertrand Russell

TABLE OF CONTENTS

LIST OF FIGURES

LIST OF SCHEMES

LIST OF TABLES

ACKNOWLEDGEMENTS

I would like to acknowledge Professor Michael D. Burkart for his support as the chair of my committee. The mentorship received from him over the years was paramount to my own success and I look forward to our future relationship as colleagues going forward.

I would also like to acknowledge Dr. James J. La Clair and Dr. Christopher J. Gartshore for the inumerable conversations throughout this work. Their guidance was invaluable to my development as a chemist.

Chapter 1, in full, is a reprint of the material as it appears in Chemical Communications. Bemis, Troy A.; La Clair, James J.; Burkart, Michael D., Royal Society of Chemistry, 2021. The dissertation author was the primary investigator and author of this paper.

Chapter 2, in full, is a reprint of the material as it appears in the Journal of Medicinal Chemistry. Bemis, Troy A.; La Clair, James J.; Burkart, Michael D., American Chemical Society, 2021.

Chapter 3, in part, is currently being prepared for submission for publicaiton of the material. O'Herin, Conor; Bemis, Troy A.; Kohlbrand, Alysia J.; La Clair, James J.; Burkart, Michael D.; Cohen, Seth M. The dissertation author is a primary coauthor of the manuscript in preparation with Conor O'Herin and the primary author of this chapter.

VITA

2013 Bachelor of Science, University of Wisconsin Madison

2017 Master of Science, University of California San Diego

2022 Doctor of Philosophy, University of California San Diego

PUBLICATIONS

Bemis, T. A.; La Clair, J. J.; Burkart, M. D. Unraveling the role of linker design in proteolysis targeting chimeras. *J. Med. Chem.* **2021**, *64*, 8042-8052.

Bemis, T. A.; La Clair, J. J.; Burkart, M. D. Traceless Staudinger ligation enabled parallel synthesis of proteolysis targeting chimera linker variants. *Chem. Commun.* **2021**, *57*, 1026-1029.

Gunawan, N. R.; Tessman, M.; Schreiman, A. C.; Simkovsky, R.; Samoylov, A. A.; Neelakantan, N. K.; Bemis, T. A.; Burkart, M. D.; Pomeroy, R. S.; Mayfield, S. P. Rapid biodegradation of renewable polyurethane foams with identification of associated microorganisms and decomposition products. *Bioresour. Technol. Reports* **2020**, *11*, 100513.

Decato, S.; Bemis, T.; Madsen, E.; Mecozzi, S. Synthesis and characterization of perfluoro-*tert*-butyl semifluorinated amphiphilic polymers and their potential application in hydrophobic drug delivery. *Polym. Chem.* **2014**, *5*, 6461-6471.

ABSTRACT OF THE DISSERTATION

Design, Synthesis and Biological Evaluation of Chimeric Small Molecules

by

Troy Allen Bemis

Doctor of Philosophy in Chemistry

University of California San Diego, 2022

Professor Michael D. Burkart, Chair

Chimeric small molecules offer a wide array of potential biological functionalties where metabolic pathways may be redirected towards non-cognate substrates for applications in biological research and pharmaceutical development. Here we explore the design of a class of chimeric small molecules known as proteolysis targeting chimeras through structure-activity relationships (SARs), provide synthetic methodology to access PROTAC linker variants, and biologically evaluate a suite of

human carbonic anhydrase II (hCAII) degrading chimeric small molecules through mammalian cell culture and western blotting techniques.

INTRODUCTION

The ability to rewire cellular metabolic pathways through the use of chimeric small molecules has been of great interest for use in pharmaceutical intervention and the general study of cell biology.[1] A chimeric small molecule consists of two functional moieties (ligands, fluorophores, bioactive functionalities, ect.) tethered together by a linker region (see Chapter 1 for details). These bifunctional molecules can be used to elucidate or induce both cognate and non-cognate interactions and have garnered attraction for their plug-and-play architecture and utility in a plurality of unique biological systems.

For cognate interactions, chimeric small molecules have been used to elucidate the transient protein-protein interactions of processive biosynthetic pathways. Our lab has published studies[2] on the protein-protein interactions formed in fatty acid biosynthesis (FAS) through the use of chimeric pantetheine analogs containing an electrophilic warhead used to covalently crosslink the various tailoring domains which can then be used for X-ray crystallography. The pantetheine analog can be chemoenzymatically loaded onto the acyl-carrier protein (AcpP) using a one-pot methodology developed previously. For further details please see the following.[2]

Chimeric small molecules have also been used to stimulate cellular signaling through chemically induced dimerization (CID) of transmembrane receptors, kinases, small GTPases, guanine nucleotide exchange factors (GEFs), phosphoinositide modifying enzymes, heterotrimeric G-protein subunits, and adaptor proteins. A detailed review of the advances in CID can be found here.[3]

There have been many examples of chimeric small molecules being used to rewire cellular pathways to induce non-cognate interactions to yield desired signaling effects. Below is a brief overview of the different modalities that have been recently demonstrated but will not be covered in further detail.

RNA-Degrading Ribonuclease Targeting Chimeras (RIBOTACs)[4] have been demonstrated that bind the three-dimensional folds of pre-miRNA (pre-miR21) and recruit a promiscuous RNase (RNase L) in order to degrade the RNA. The compounds showed significant *in vivo* activity in mouse models, and it is hypothesized that this platform will be generalizable to target other RNAs with sufficiently ligandable three-dimensional structure.

Protein Phosphatase Recruiting Chimeras (PhoRCs)[5] have been developed to recruit the phosphatase (PP1) to a phosphorylated protein

target in order induce de-phosphorylation. This strategy could have a broad application for the study of signaling pathways and offers an interesting opportunity for pharmaceutical intervention.

Conversely, phosphorylation-inducing chimeric small molecules (PHICs)[6] have demonstrated both PHICs-mediated native and neo-phosphorylation events. Both kinases, AMP-activated protein kinase (AMPK) and protein kinase C (PKC), could be recruited to facilitate a neo-phosphorylation event on bromodomain containing 4 (BRD4) or a signaling relevant native phosphorylation of Bruton's tyrosine kinase (BTK) in cells.

Extracellular protein target degradation has been demonstrated through the development of Lysosome Targeting Chimeras (LYTACs).[7] This approach utilizes an antibody with specificity for the extracellular protein of interest (POI) fused to agonist glycopeptide ligands targeting a lysosome-targeting cell surface receptor (CI-M6PR) which allows for internalization and subsequent degradation of the target protein.

There have been demonstrations of Autophagy-Targeting Chimeras (AUTACs)[8] that utilize guanine-based degradation tags that are capable of inducing autophagy of their targeted protein of interest (POI). The proof of concept study showed effective degradation of methionyl aminopeptidase

2 (MetAP2) and FK506-binding protein 12 (FKBP12) and a limited degradation of the nuclear protein target, bromodomain containing 4 (Brd4), which would be expected to only be available for degradation during mitosis.

Targeted protein acetylation has been achieved via chimeric small molecules using the acetylation tagging system (AceTAG).[9] Here a bifunctional small molecule recruiting the lysine acetyltransferase (p300/CBP) and mutant FK506-binding protein 12 ($FKBP12^{F36V}$) fusion proteins produced dose-dependent, selective, rapid, and reversible acetylation of fusion partner proteins; histone (H3.3), REL-associated protein involved in NF-kB heterodimer formation, nuclear translocation and activation (p65/RelA), and tumor suppressor protein (p53).

Currently, the most prevalent use of chimeric small molecules is to hijack the ubiquitin-proteasome system (UPS) through the recruitment of a ubiquitin E3 ligases in order to induce targeted proteolysis. Known as proteolysis targeting chimeras (PROTACs), these small molecules consist of an E3 ligase recruiting moiety tethered to a ligand for a target protein of interest (POI). In a compatible system, a ternary complex is formed, ubiquitin is transferred to a peripheral lysine on the POI, and this marks the target to be degraded by the proteasome. This modality signifies a

bifurcation from traditional occupancy-based pharmaceutical intervention to an event-based pharmaceutical intervention, which offers unique opportunities for the development of new medicines. My progress in this chemical space will be the focus of the subsequent chapters.

REFERENCES

1. Schneider, M.; Radoux, C. J.; Hercules, A.; Ochoa, D.; Dunham, I.; Zalmas, L. P.; Hessler, G.; Ruf, S.; Shanmugasundaram, V.; Hann, M. M.; Thomas, P. J.; Queisser, M. A.; Benowitz, A. B.; Brown, K.; Leach, A. R. The PROTACtable Genome. *Nat. Rev. Drug Discov.* **2021**, *20*, 789–797.

2. (*a*) Mindrebo, J. T.; Chen, A.; Kim, W. E.; Re, R. N.; Davis, T. D.; Noel, J. P.; Burkart, M. D. Structure and Mechanistic Analyses of the Gating Mechanism of Elongating Ketosynthases. *ACS Catal.* **2021**, *11* (12), 6787–6799. (*b*) Misson, L. E.; Mindrebo, J. T.; Davis, T. D.; Patel, A.; Andrew McCammon, J.; Noel, J. P.; Burkart, M. D. Interfacial Plasticity Facilitates High Reaction Rate of E. Coli FAS Malonyl-CoA:ACP Transacylase, FabD. *Proc. Natl. Acad. Sci. U. S. A.* **2020**, *117*, 24224–24233. (*c*) Mindrebo, J. T.; Patel, A.; Kim, W. E.; Davis, T. D.; Chen, A.; Bartholow, T. G.; La Clair, J. J.; McCammon, J. A.; Noel, J. P.; Burkart, M. D. Gating Mechanism of Elongating β-Ketoacyl-ACP Synthases. *Nat. Commun.* **2020**, *11*, 1–15. (*d*) Nguyen, C.; Haushalter, R. W.; Lee, D. J.; Markwick, P. R. L.; Bruegger, J.; Caldara-Festin, G.; Finzel, K.; Jackson, D. R.; Ishikawa, F.; O'Dowd, B.; McCammon, J. A.; Opella, S. J.; Tsai, S. C.; Burkart, M. D. Trapping the Dynamic Acyl Carrier Protein in Fatty Acid Biosynthesis. *Nat.* **2013**, *505*, 427–431.

3. Voß, S.; Klewer, L.; Wu, Y. W. Chemically Induced Dimerization: Reversible and Spatiotemporal Control of Protein Function in Cells. *Curr. Opin. Chem. Biol.* **2015**, *28*, 194–201.

4. Costales, M. G.; Aikawa, H.; Li, Y.; Childs-Disney, J. L.; Abegg, D.; Hoch, D. G.; Velagapudi, S. P.; Nakai, Y.; Khan, T.; Wang, K. W.; Yildirim, I.; Adibekian, A.; Wang, E. T.; Disney, M. D. Small-Molecule Targeted Recruitment of a Nuclease to Cleave an Oncogenic RNA in a Mouse Model of Metastatic Cancer. *Proc. Natl. Acad. Sci. U. S. A.* **2020**, *117*, 2406–2411.

5. Yamazoe, S.; Tom, J.; Fu, Y.; Wu, W.; Zeng, L.; Sun, C.; Liu, Q.; Lin, J.; Lin, K.; Fairbrother, W. J.; Staben, S. T. Heterobifunctional Molecules Induce Dephosphorylation of Kinases–A Proof of Concept Study. *J. Med. Chem.* **2020**, *63*, 2807-2813.

6. Siriwardena, S. U.; Munkanatta Godage, D. N. P.; Shoba, V. M.; Lai, S.; Shi, M.; Wu, P.; Chaudhary, S. K.; Schreiber, S. L.; Choudhary, A. Phosphorylation-Inducing Chimeric Small Molecules. *J. Am. Chem. Soc.* **2020**, *142*, 14052–14057.

7. Banik, S. M.; Pedram, K.; Wisnovsky, S.; Ahn, G.; Riley, N. M.; Bertozzi, C. R. Lysosome-Targeting Chimaeras for Degradation of Extracellular Proteins. *Nature* **2020**, *584*, 291–297.

8. Takahashi, D.; Moriyama, J.; Nakamura, T.; Miki, E.; Takahashi, E.; Sato, A.; Akaike, T.; Itto-Nakama, K.; Arimoto, H. AUTACs: Cargo-Specific Degraders Using Selective Autophagy. *Mol. Cell* **2019**, *76*, 797-810.

9. Wang, W. W.; Chen, L. Y.; Wozniak, J. M.; Jadhav, A. M.; Anderson, H.; Malone, T. E.; Parker, C. G. Targeted Protein Acetylation in Cells Using Heterobifunctional Molecules. *J. Am. Chem. Soc.* **2021**, *143*, 16700–16708.

CHAPTER 1: Unraveling the Role of Linker Design in Proteolysis Targeting Chimeras

ABSTRACT

A current bottleneck in the development of proteolysis targeting chimeras (PROTACs) is the empirical nature of linker length structure–activity relationships (SARs). A multidisciplinary approach to alleviate the bottleneck is detailed here. First, we examine four published synthetic approaches that have been developed to increase synthetic throughput. We then discuss advances in structural biology and computational chemistry that have led to successful rational PROTAC design efforts and give promise to *de novo* linker design *in silico*. Lastly, we present a model generated from a curated list of linker SARs studies normalized to reflect how linear linker length affects the observed degradation potency (DC_{50}).

INTRODUCTION

Since the first proof of concept in 2001,[1] small-molecule-induced targeted protein degradation has become an exciting modality for pharmacological intervention. The two main strategies used to induce the degradation are the use of molecular glues which are small molecules that alter the substrate recognition domain of an E3 ligase, thereby allowing the recruitment of neosubstrates for proteolysis, and the use of chimeric small molecules that consist of an E3 ligase binding moiety linked to a motif that binds desired target protein.[2] The latter will be the focus of this perspective. Coined proteolysis targeting chimeras (PROTACs, also known as SNIPERs, uSMITEs, or degraders), bifunctional small-molecule degraders have become known for their catalytic activity (potency), ability to induce isozyme selectivity through interprotein interaction, and deviation from the 'rule-of-five'.[3-6] The utility of six unique chimeric degrader molecules in humans is currently being investigated in clinical trials.[7] Of note are the indications of metastatic castration-resistant prostate cancer (ARV-110)[8] and metastatic breast cancer (ARV-471),[9] through the targeted degradation of the androgen receptors and estrogen receptors, respectively, and the nononcogenic target IRAK4 degrader (KT-474) which could demonstrate their use in chronic dosing.[7] Their advance into

the clinic along with their unique ability to degrade challenging protein targets highlights the importance of understanding the salient features that guide successful PROTAC discovery. In this miniperspective, we explore the strategies involved in enhancing throughput, examine successful rational design efforts, and provide a synopsis of the molecular trends within the current linker designs.

The unique metabolic activity of PROTACs comes from their ability to appropriate RING ubiquitin ligases from the ubiquitin-proteasome system (UPS), which regulates protein homeostasis by tagging proteins with polyubiquitin chains, thereby marking them for proteolysis.[10] The UPS signal cascade (Figure 1-1a) begins with the E1 activating enzyme, which adenylates the C-terminus of ubiquitin, followed by a transfer of the ubiquitin to an active site cysteine. The E1 activating enzyme then engages an E2 conjugating enzyme and transfers the ubiquitin to the E2 active site cysteine through a trans-thioesterification. The ubiquitin-loaded E2 conjugating enzyme then binds a multisubunit E3 ligase complex, which transfers the ubiquitin to a peripheral lysine residue on the substrate protein, labeling the substrate for degradation by the proteasome.[11] With each step of the cascade (Figure 1-1a), the UPS confers specificity for its

substrate protein. Efforts have been made at therapeutic intervention at each step in the UPS cascade.[12-14]

Figure 1-1: Metabolic activity of a PROTAC. (a) Representative comparison of UPS pathway for cullin-RING E3 ligases in both the presence and absence of PROTAC molecules. Step 1: Ubiquitin activation by E1. Step 2: Engagement of ubiquitin loaded E1 with E2 conjugating enzyme. Step 3: Transfer of ubiquitin to E2 via trans-thioesterification and subsequent formation of E3 ligase complex. Introduction of PROTAC molecules can redirect the E3 ligase from its cognate substrate (sub) to a noncognate POI. (b) Representative example of a noncognate ternary complex formed by the PROTAC dBET23, bromodomain BRD4, and E3 ligase substrate binding domain CRBN (PDB 6BN7). Note: E3 cartoon represents a multicomponent complex in which the PROTAC is able to bind the substrate adapter protein in order to redirect its metabolic activity.

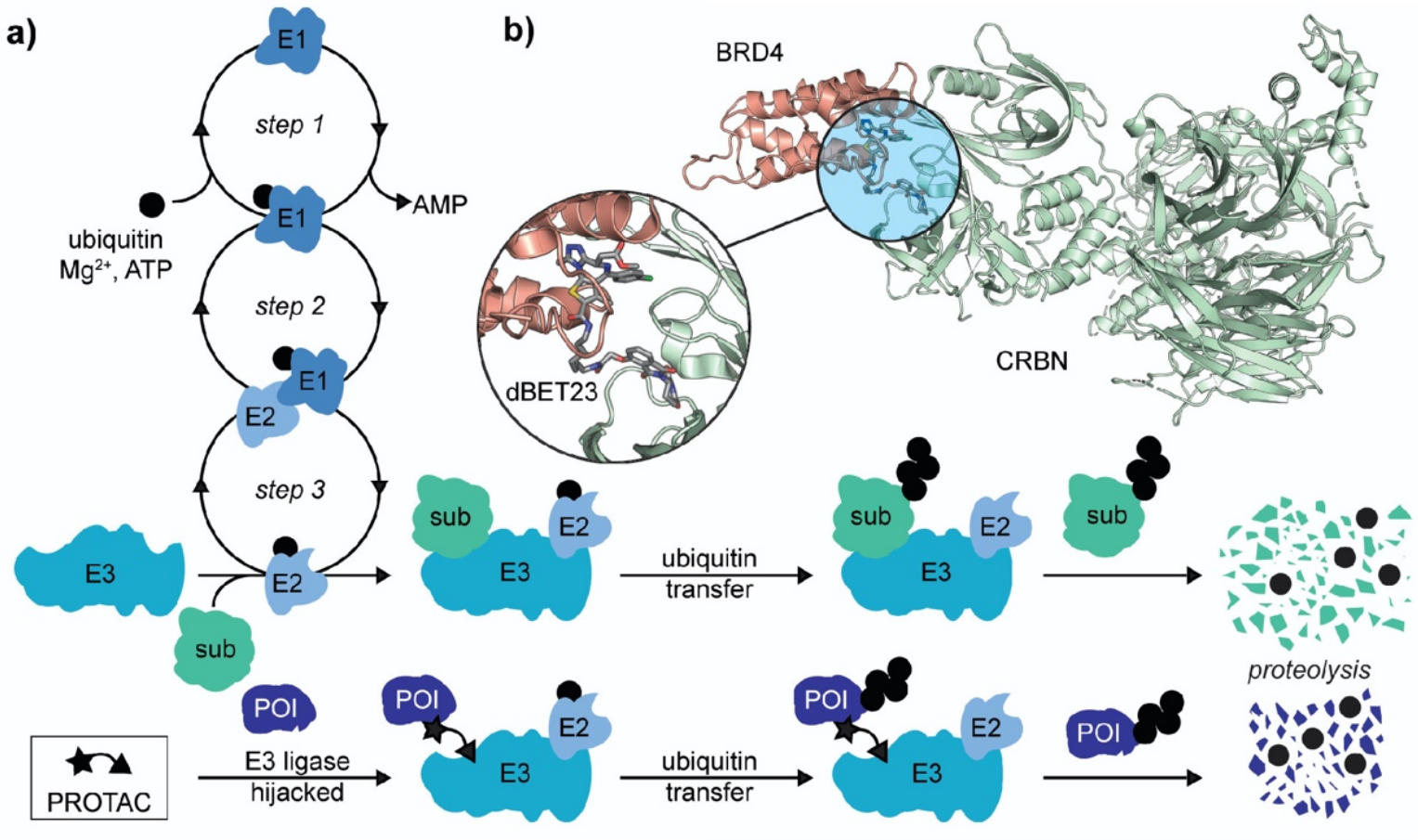
a)
E1
step 1
E1
AMP
ubiquitin
Mg2+, ATP
step 2
E1
E2
step 3
E2
E3
sub
sub
E2
E3
ubiquitin
transfer
sub
E2
E3
sub
proteolysis
POI
POI
E2
E3
ubiquitin
transfer
POI
E2
E3
POI
PROTAC
E3 ligase
hijacked
b)
BRD4
dBET23
CRBN

PROTACs are chimeric small molecules that are able to engage the substrate recognition domain of an E3 ligase and a protein of interest (POI) simultaneously, thereby inducing noncognate ubiquitination and subsequent degradation of the POI (Figure 1-1a).[15] A number of E3 ligases have been targeted for PROTAC development;[16] however, here we focus on PROTACs that hijack the substrate adapter domains cereblon ($CRL4^{CRBN}$)[17] and Von Hippel–Lindau ($CRL2^{VHL}$)[18] RING E3 ligases. Interestingly, PROTACs can exhibit an alluring 'plug-and-play' architecture,[19] where in some cases the same POI can be degraded by recruiting different E3 ligases. For example, the bromodomain (BRD4) degraders MZ1 and dBET-23 (Figure 1-1b) recruit Von Hippel–Lindau ($CRL2^{VHL}$) and cereblon ($CRL4^{CRBN}$) E3 ligases, respectively.[20,21] In other cases, swapping E3 ligase recruitment can show exquisite target selectivity through tertiary interaction, as demonstrated by the development of tyrosine kinase (ABL/BCR-ABL) degraders developed with promiscuous kinase inhibitor warheads.[19]

The potency and isozyme selectivity of PROTACs can be optimized through structure–activity relationships (SARs) within the linker (Figure 1-1b). Here, the length and chemical composition has been shown to influence, among others, a PROTAC's structural rigidity, hydrophobicity,

and solubility.[22] To date, linker length SAR studies are largely empirical and have proven to be time and labor intensive. While great strides have been made toward rational PROTAC design through structural biological and computational studies, linker design still presents a significant synthetic burden.

APPROACHES TO ENHANCE THROUGHPUT

The current approaches to streamline linker variant SAR studies involve increasing synthetic throughput via use of orthogonally protected bifunctional linkers[23] solid-phase synthesis,[24] copper-catalyzed click chemistry,[25] activated esters,[26] and Staudinger ligation chemistry[27] (Figure 1-2). PROTAC synthesis involves an asymmetric three-part diversification between the two binding motifs and a linker region (Figure 1-2b). By exploiting simplified purification procedures and parallel synthetic strategies, these approaches decrease material lead time without altering the empirical nature of the study.

Figure 1-2: Published synthetic methods for accessing PROTACs. (a) Synthesis of a BTK degrader using TPR. Secondary amine shown highlighted in color is used as a linker diversification handle. (b) Representative structure of a PROTAC bearing amide linker chemistry. (c) Synthesis of bromodomain degraders using copper-catalyzed click chemistry. (d) Synthesis of dBET1 utilizing Pfp activated esters. (e) Synthesis of dBET1 via Staudinger ligation chemistry. Reagents: (a) iodoacetic acid, *N*,*N*′-diisopropylcarbodiimide, DCM, rt; (b) despropenoyl ibrutinib, diisopropylethylamine (DIPEA), DMSO, rt then TFA/DCM (1:1), rt, 49% overall for (a and b); (c) $CuSO_4$ (20 mol %), sodium ascorbate (20 mol %), THF/H_2O, rt, 67–90%; (d) *N*-Boc-1,4-butanediamine, DIPEA, DMF, rt, 81%; (e) TFA/DCM (1:5), rt, 99%; (f) DIPEA, DMF, rt, 81%; (g) 4-azido-1-butanamine, O-(7-azabenzotriazol-1-yl)-*N*,*N*,*N*′,*N*′-tetramethyluronium hexafluorophosphate, 1,4-diazabicyclo[2.2.2]octane, DMF, rt, 50%; (h) DMF, 40°, 54%. Note: Steps (g and h) can be accomplished in a one-pot fashion.

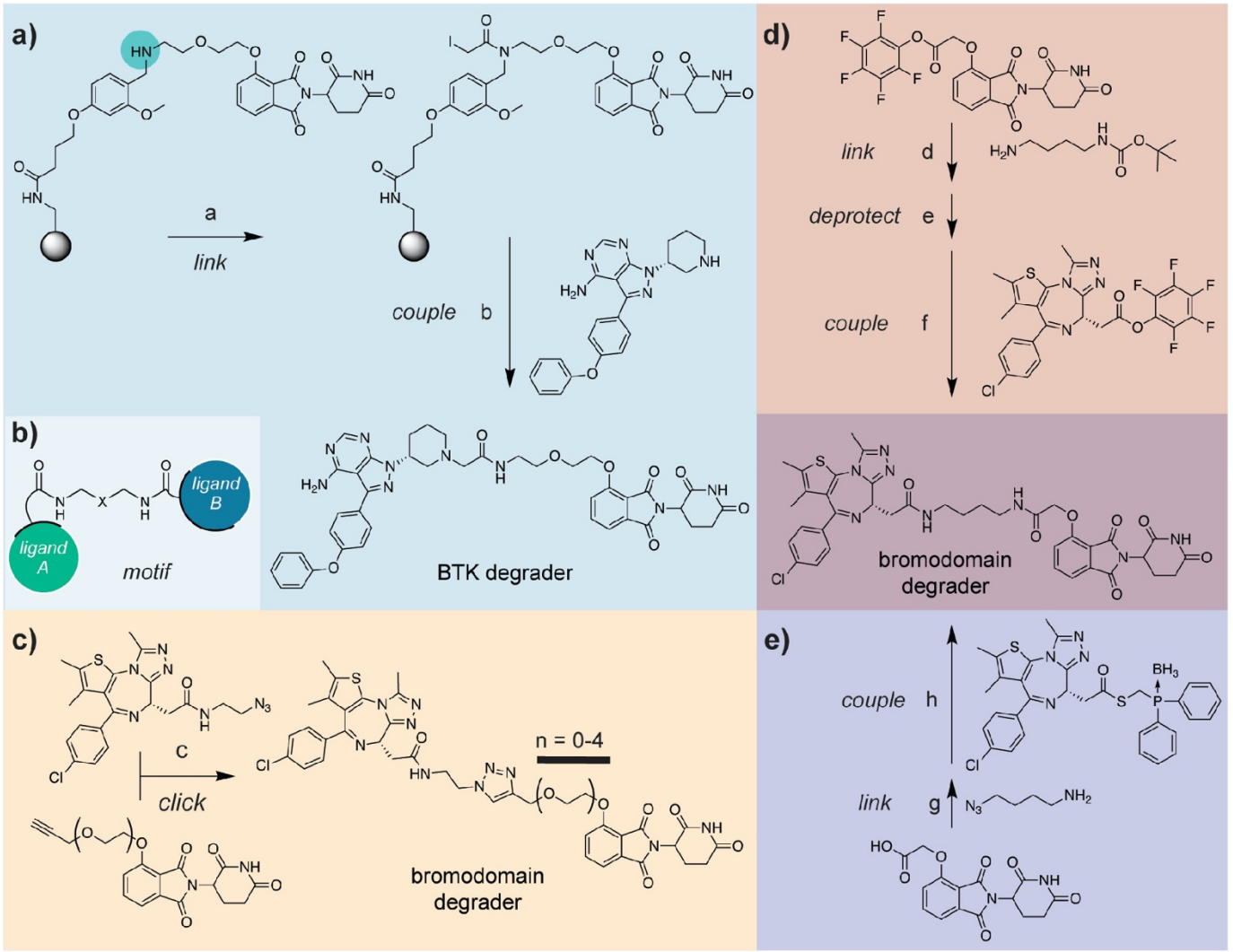
a)
a
link
couple b
b)
ligand A
ligand B
motif
BTK degrader
c)
c
click
n = 0-4
bromodomain degrader
d)
link d
deprotect e
couple f
bromodomain degrader
e)
couple h
link g

Krajcovicova et al.[24] were able to prepare a suite of PROTACs consisting of five different kinase inhibitors using a thalidomide preloaded resin (TPR) (Figure 1-2a). The aminomethyl polystyrene-divinylbenzene resin (PS-DVB) was acylated with 4-(4-formyl-3-methoxyphenoxy)-butanoic acid yielding a terminal aldehyde, which after amidation and subsequent reduction to a secondary amine provided a synthetic handle for linker diversification. The resulting resin was then treated with iodoacetic acid (with and without an additional polyethylene glycol (PEG) spacer), producing electrophilic TPR.

Subsequent reactions of this electrophilic TPR with a family of nucleophilic kinase inhibitors yielded a family of PROTACs. The fully elaborated PROTACs were then cleaved from the PS-DVB resin with trifluoroacetic acid (TFA) yielding the crude PROTACs in 24–85% yield and 78–98% purity and were then further purified by reverse-phase high-pressure liquid chromatography (HPLC) on a 200 mg scale. Though in this study, the authors prepared a PROTAC library using an electrophilic TPR and nucleophilic kinase inhibitors, they noted that this methodology is generalizable and other synthetic strategies to append POI-targeting inhibitors to the TPR can be accommodated, including use of electrophilic inhibitors with a nucleophilic TPR. If TPR resin is stable upon storage, this

strategy will undoubtedly buoy efforts to produce “user friendly” tool kits for the diversification of CRBN-recruiting PROTACs.

The copper-catalyzed click chemistry platform demonstrated by Wurz et al.[25] (Figure 1-2c) relied upon the preparation of a library of alkyne-terminal PEG-linked CRBN ligands and VHL ligands (not shown) as well as an azide-linked derivative of known bromodomain inhibitor JQ1. The two ligands were then united through triazole formation using copper-catalyzed click chemistry.[28] A panel of 10 bromodomain targeting PROTACs (five CRBN recruiting, five VHL recruiting) were prepared on 100 mg scale in 55–90% yields, and purity was demonstrated via liquid chromatography-mass spectrometry. Purification was accomplished using reverse-phase chromatography (ISCO Combiflash). This is the only published synthetic platform that directly synthesized both VHL recruiting PROTACs in addition to CRBN recruiting PROTACs.

An approach developed out by Papatzimas et al.[26] utilized pentafluorophenyl (Pfp)-esters as synthons to access previously published PROTAC dBET1[17] (Figure 1-2d) in 81% yield on 40 mg scale and could be readily purified on normal-phase silica gel. This strategy entailed isolating both the E3 ligase ligand and bromodomain inhibitor JQ1 as Pfp-esters. In a three-step sequence, a Boc-protected amine linker was then

reacted with the thalidomide-Pfp-ester to yield the first amide bond formation, the Boc-protecting group was removed with TFA, and finally the JQ1 Pfp-ester was added to yield dBET1[17] (Figure 1-2d).

We recently developed[27] a synthetic method that leverages the chemoselectivity of the Staudinger ligation in order to assemble PROTACs in an asymmetric, one-pot fashion (Figure 1-2e). We also targeted dBET1[17] (BRD4 degrader) and two analogs as a model system to demonstrate that the entire PROTAC assembly could be choreographed in a single reaction flask. However, the resulting reaction mixture was quite complex and would require HPLC purification. We then chose to isolate azido-terminal-linked thalidomide intermediates and showed that all of the linker variants could be synthesized in parallel in 39–85% yields from a stock solution of JQ1 borane-protected phosphine thioester. This only required silica microcolumn purification to obtain highly pure compound on 10 mg scale.

Taken together, there are a number of strategies that have been demonstrated to achieve modular synthesis of PROTAC linker variant suites for immunomodulatory imide drug-based (CRBN recruiting) systems, although none of them appear to have widespread application in the field as of yet. Although it is conceivable that most of the strategies

presented could be translatable to VHL or other E3 ligase recruiting systems, only the copper-catalyzed click platform[25] specifically demonstrated this, however introduction of the triazole moiety to the linker may not yield desirable physiochemical properties due to its high topological total polar surface area.[29] All of these strategies would greatly benefit from the availability of libraries of functionalized (alkyne, Boc-protected amine terminal, or azide terminal) linked E3 ligase ligands prepared and aliquoted for posterity. Indeed, many are commercially available. Key considerations for choosing a platform include stability upon long-term storage of the linked E3 ligase ligand libraries, purification capabilities of the laboratory, and desired linker chemistry (linear vs triazole containing). Collectively, these strategies increase the synthetic throughput of linker length SAR studies, and we see them as a first step (potentially coupled with computational techniques) in PROTAC development to determine POI·E3 ligase compatibility. Once an optimal linker length hit is detected, further linker SAR could be implemented to optimize rigidity, solubility, cell permeability, and pharmacological (pharmacokinetic/pharmacodynamic) profile to produce a lead degrader compound. This is commonly done by replacing PEG and linear aliphatic linkers with piperine and piperazine-based linkers which reduce the

degrees of freedom in the degrader and provide more favorable pharmacological properties, such as in the development of mutant BRAF kinase degrader SJF-0628[30] and recently released structures of ARV-110 and ARV-471, two of the degraders currently in the clinic. However, we view the linker rigidifying SAR as a next step in lead degrader development after the optimal linker length has been determined either by biological evaluation or computational prediction.

RATIONAL PROTAC DESIGN

Alternatively, efforts have been made toward rational PROTAC design utilizing both X-ray crystallographic data and computational modeling.[31] The first X-ray structure of a degrader (MZ1) in ternary complex was solved by Gadd et al.,[32] and using these data, they were able to rationally design a more selective bromodomain degrader (AT1). Farnaby and co-workers[33] were able to identify crucial stabilizing interactions between the PEG linker of PROTAC 1 (Figure 1-3a) and VHL from cocrystal structures of SMARCA2:PROTAC 1:VHL (PDB 6HAY). Based on these data, they introduced an additional T-shaped stacking interaction and increased rigidity via insertion of a phenyl moiety in the linker region without sacrificing the key PEG interactions yielding ACBI1 (Figure 1-3a); an improved SMARCA2/4 degrader.

Figure 1-3: Exemplary rational PROTAC development campaigns. (a) Development of improved SMARCA2/4 degrader ACBI1 through identification of key interactions with the PEG linker. (b) Design of isozyme selective bromodomain degrader ZXH-3-26 through limitation of the degrees of freedom via computationally aided linker length reduction. (c) Development of isozyme selective bromodomain degrader macroPROTAC-1 through limitation of the degrees of freedom via introduction of a macrocyclic linker.

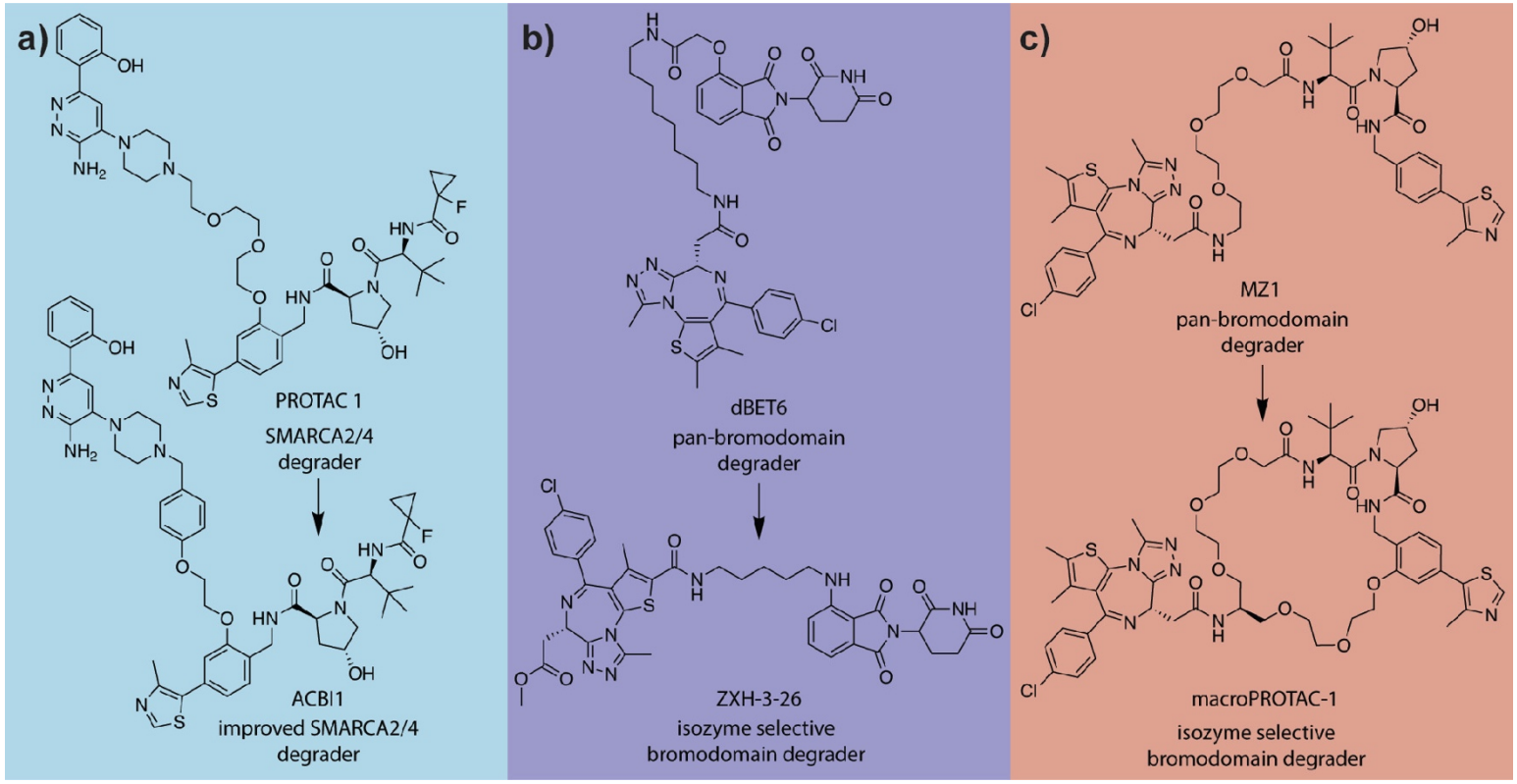
a)
PROTAC 1
SMARCA2/4
degrader
ACBI1
improved SMARCA2/4
degrader
b)
dBET6
pan-bromodomain
degrader
ZXH-3-26
isozyme selective
bromodomain degrader
c)
MZ1
pan-bromodomain
degrader
macroPROTAC-1
isozyme selective
bromodomain degrader

Notably, Nowak et al.[21] were able to develop a novel BRD4 selective degrader ZXH-3-26 based upon a known pan-bromodomain degrader, dBET6, (Figure 1-3b) by performing RosettaDock simulations that utilized the X-ray structures of a set of related, PROTAC-bound ternary complexes.[34] Stochastic sampling of low-energy conformations using Rosetta[34] was able to recapitulate experimental structures. Structural predictions also suggested that minimization of PROTAC linker length would enhance degrader selectivity by reducing the number of favorable binding modes for the POI–PROTAC–ligase ternary complex.

Testa and co-workers[35] have also demonstrated the utility of computer-aided PROTAC design. They identified a potent and isoform selective ($BRD4^{BD2}$ selective) bromodomain degrader using molecular dynamics simulations of the complex of $BRD4^{BD2}$ and VHL bound with known bromodomain degrader MZ1 (PDB 5T35) (Figure 1-3c). Analysis of the simulations suggested that a macrocyclic linker could improve MZ1 effectiveness by reducing the degrees of freedom of the PROTAC, preorganizing its POI and ligase moiety for ternary complex formation. Synthesis of a macrocyclic analog of MZ1 was realized using a “bespoke” PEG-based linker. The resulting macrocyclic PROTAC demonstrated a lower binding affinity for both BRD4 and VHL in binary complex compared

to MZ1, while maintaining a comparable degradation potency. Taken together, this suggests an increase in ternary complex formation efficiency.

More rigorous computational methods have been developed in efforts toward rationally designed *de novo* PROTAC development using both Molecular Operating Environment (MOE) and the open source Rosetta software suites. These methods have not only successfully reproduced, *in silico*, PROTAC binding modes identified from X-ray crystallography but are also consistent with trends in potency and selectivity based upon prior biological evaluation. Herein, we describe select examples to illustrate the value of such efforts. Further reading on computer-aided PROTAC development may be found here.[36-41]

Using the MOE software suite, Drummond et al.[42,43] developed a series of protocols for generating and analyzing PROTAC ternary complexes (Figure 1-4). Of these protocols, the most effective sampled the conformational space of the degrader in the absence of both POI and ligase in order to identify degrader conformations that in a subsequent step would be subjected to docking simulations. These methods used cocrystal structures of the binding moieties of the PROTAC (no linker) bound to their respective targets. This team has also shown that

computationally docked structures may also be used as input. Next global protein–protein docking simulations were performed using MOE's docking protocol in order to generate an ensemble of states and determine how the proteins might interact proximal to their ligated pockets.

Figure 1-4: Recent advances in computational approaches to PROTAC development. MOE: General approach and highlights of the protocol used by Drummond et al.[42] on the MOE platform. PRosettaC: General approach and highlights of the protocol used by Zaidman et al.[48] on the Rosetta platform. Rosetta: General approach and highlights of the protocol used by Bai et al.[52] on the Rosetta platform.

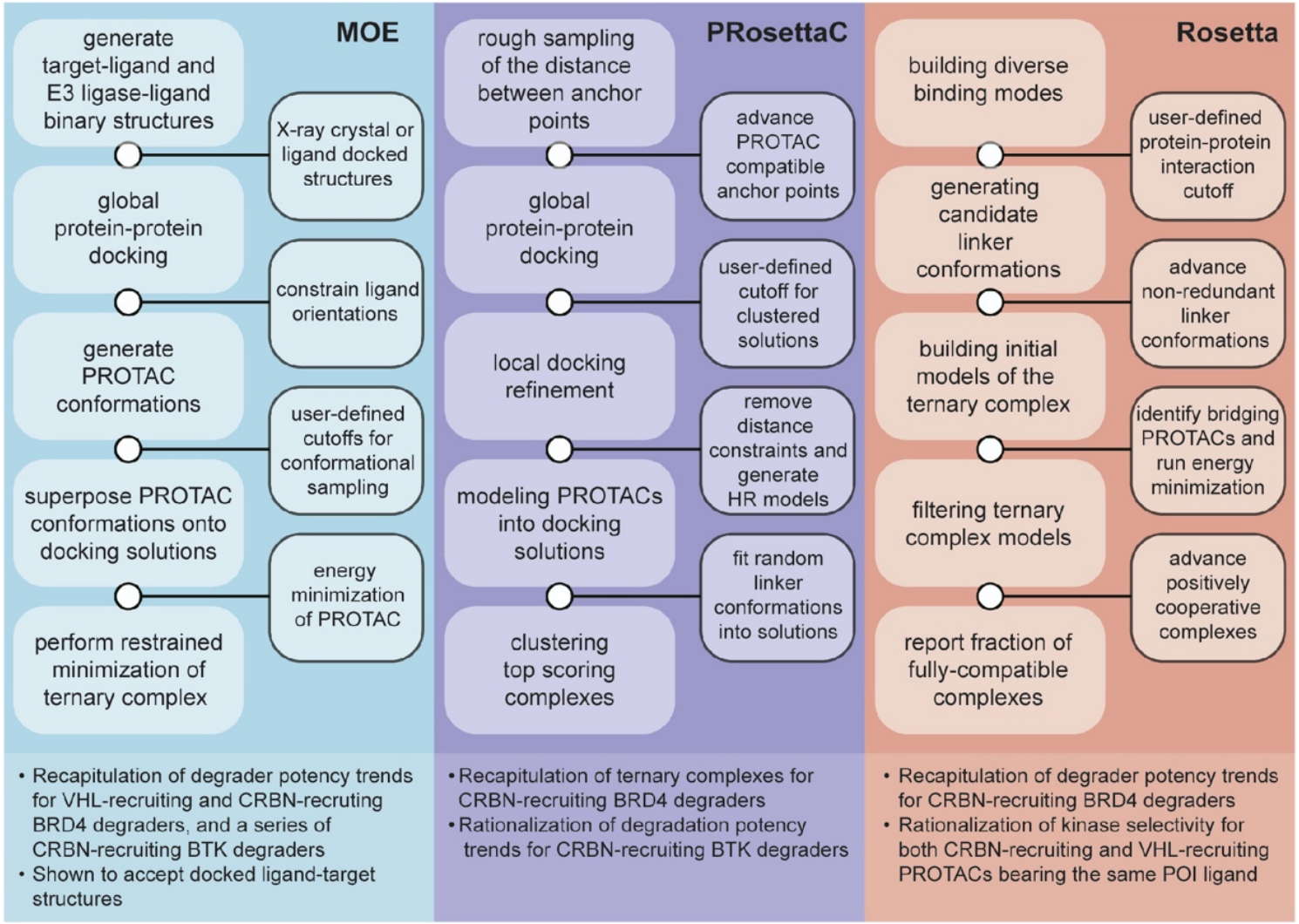
MOE
generate target-ligand and E3 ligase-ligand binary structures
X-ray crystal or ligand docked structures
global protein-protein docking
constrain ligand orientations
generate PROTAC conformations
user-defined cutoffs for conformational sampling
superpose PROTAC conformations onto docking solutions
energy minimization of PROTAC
perform restrained minimization of ternary complex
• Recapitulation of degrader potency trends for VHL-recruiting and CRBN-recruting BRD4 degraders, and a series of CRBN-recruiting BTK degraders
• Shown to accept docked ligand-target structures
PRosettaC
rough sampling of the distance between anchor points
advance PROTAC compatible anchor points
global protein-protein docking
user-defined cutoff for clustered solutions
local docking refinement
remove distance constraints and generate HR models
modeling PROTACs into docking solutions
fit random linker conformations into solutions
clustering top scoring complexes
• Recapitulation of ternary complexes for CRBN-recruiting BRD4 degraders
• Rationalization of degradation potency trends for CRBN-recruiting BTK degraders
Rosetta
building diverse binding modes
user-defined protein-protein interaction cutoff
generating candidate linker conformations
advance non-redundant linker conformations
building initial models of the ternary complex
identify bridging PROTACs and run energy minimization
filtering ternary complex models
advance positively cooperative complexes
report fraction of fully-compatible complexes
• Recapitulation of degrader potency trends for CRBN-recruiting BRD4 degraders
• Rationalization of kinase selectivity for both CRBN-recruiting and VHL-recruiting PROTACs bearing the same POI ligand

The ligands were then constrained to their bound conformation used in the global protein–protein docking operation, and a series of PROTAC conformers were generated using LowModeMD.[44] The resulting PROTAC conformers were then superimposed onto the docked POI–ligase structures, multiple energy minimizations were performed on the PROTAC, and the coordinates of the bound relaxed PROTACs were compared to the unlinked ligand-protein structures. Finally, a restrained minimization protocol was performed on the ternary complex as a whole to remove steric clashes between the proteins and the PROTAC. The method described was able to recapitulate degrader binding modes and potency trends for both VHL-recruiting and CRBN-recruiting degraders,[21,32,33] rationalize the degradation potency trends of macrocyclic PROTAC-1 (Figure 1-3c),[35] a series of CRBN-recruiting Bruton's tyrosine kinase (BTK) degraders,[45] PROTACs bearing a more rigid linker design,[46] and predict with reasonable accuracy the degradation selectivity among kinases of a degrader bearing a pan-kinase inhibitor.[47]

Alternatively, Zaidman et al.[48] used the open source Rosetta software suite in order to develop PRosettaC (Figure 1-4). PRosettaC is similar to that of Drummond and co-workers[42,43] insofar as that the structures of the binary complexes of both ligands with their respective

targets are requisite inputs. The PRosettaC protocol requires the definition of two anchor points corresponding to the binding epitopes on the degrader. The anchor points are then used to perform a rough sampling of the distances and ligand positions between the two anchor points that could accommodate a full length PROTAC, yielding an ensemble of degrader conformations that are binned based on the distance between the anchor atoms. These simulations provide information about the distance constraints for global protein–protein docking simulations using PatchDock.[49] This approach facilitates the rapid sampling of protein–protein interaction space. Restraint-free local protein–protein docking using RosettaDock[50] is subsequently performed to refine the structures of modeled POI–E3 ligase complexes.

Lastly, each of the solutions had their ligand positions fixed and were superposed with 100 full PROTAC conformations generated using RDkit, and the optimal conformation was chosen using Rosetta Packer.[51] The resulting ternary complexes were then filtered via Rosetta energy score and clustered with the assumption that the near native solutions would be sampled many times. This method was able to recapitulate experimentally determined ternary complexes of CRBN-

recruiting and VHL-recruiting degraders[21,32,33,35] as well as rationalize the degradation potencies of a series of CRBN-recruiting BTK degraders.[45]

Bai et al.[52] described an alternative Rosetta-based protocol (Figure 1-4). The protocol was still reliant on ligand-bound binary X-ray crystal structures as initial inputs, however it used a global docking protocol initially developed for antibody-antigen docking[53] to generate the initial ensemble of diverse poses of the POI and ligase about a fixed ligand position. Poses were evaluated based upon the stabilizing effect of protein–protein interactions formed between the POI and the ligase with the most highly scored decile of poses chosen for further refinement. Independently, the OMEGA software was used to generate a series of low energy linker conformations that were assembled from various linkers examined attached to small chemical moieties representing the functional group used at the binding moiety attachment site.[54] Up to 1000 conformers were generated for each linker and aligned with the ligand bound global docking solutions to determine if the linker adequately bridged the gap between proteins. The selected linkers were then merged with the bound ligands to create the full PROTAC, and an energy minimization was performed to eliminate steric clash and bond angle distortions. The resulting ternary complexes were then filtered based on

the median interaction energy of the initial protein–protein interaction and normalized by the number of initially docked models and linker conformations. The protocol was able to recapitulate degrader potency data for CRBN-recruiting BRD4 degraders[21,46] as well as rationalize kinase selectivity between both CRBN-recruiting and VHL-recruiting bearing the same kinase inhibitor.[37]

Both MOE and Rosetta were able to successfully recapitulate ternary complex binding modes elucidated from prior X-ray crystallographic studies, although these binding modes could represent thermodynamic artifacts from the process of crystallization.[52] For this reason, we find the ability of the protocols to rationalize biological trends in potency and target selectivity is, perhaps, a more apt benchmark of success as it pertains to *de novo* PROTAC development.

Due to the noncognate nature of the induced protein–protein interactions, a common theme between global docking strategies was the biasing toward hydrophobic interactions, which is consistent with the plastic protein–protein interface model[21] where multiple binding modes may be populated with direction-dependent polar interactions playing a secondary role in binding. A hurdle for the field to overcome will be the reliance on input of X-ray crystallographic data of ligand-bound POI

targets; however, Drummond et al.[42,43] have demonstrated moderate success with computationally docked structures, attributing the protocols shortcomings to the deviation of the position of the ligand anchor point atom in the docked structures from that of the X-ray crystal structure. Improvement in ligand docking protocols and strategies with reduced reliance on anchor points in global docking could overcome this issue.

Overall, these studies demonstrate that PROTAC development has benefitted from computer-aided optimization (Figure 1-3). Recent advances in computational protocols for small-molecule design presage an era of rational *de novo* PROTAC design (Figure 1-4), as recently demonstrated in the design of the enhancer lysine acetyltransferase (CBP/p300) degrader dCBP-1 where both the ligand and linkage point were successfully determined prior to synthesis using Rosetta.[55] With available tools, we envision a workflow that entails the computational protocols first being implemented as a method to determine POI–E3 ligase compatibility through examination of the energy landscapes of the protein–protein interfaces. Potent degrader hits could then be accessed through a mixture of *in silico* linker length prediction combined with the synthetic strategies outlined previously (Figure 1-2). Translating degrader leads that are selective between highly conserved protein targets would be carried

out more rigorously, such that degrader potency is maintained, while degrees of freedom of the ternary complex are minimized, as previously shown (Figure 1-3). Ultimately, the goal of *in silico* PROTAC development aims to increase throughput by minimizing the number of synthesized and biologically evaluated molecules in order to satisfactorily degrade a target protein. To this end, these protocols have already achieved their goal, and future advancements bode well for this hybrid approach.

TABULATING THE EMPIRICAL SAR OF LINKER LENGTH

One of the most critical features observed early in PROTAC discovery was the role of linker length.[22] Early studies[21,45] showed that there is complex interplay between having a too short or too long of a linker. In an effort to further reduce the synthetic burden of linker length SAR studies, we explored the PROTAC literature and systematically tabulated potency data as a function of linker length in order to search for trends. Our goal was to explore a possible model with predictive properties that would be agnostic to the PROTAC system under study and could suggest optimal linker length from minimal empirical inputs. This strategy would not eliminate the empirical nature of an SAR study but could potentially reduce the number of molecules needed to determine the linker length that produces the most potent degrader.

PROTACs are primarily characterized through binary and ternary complex formation dissociation constants (K_d), half maximal inhibitory concentrations (IC_{50} values), maximal degradation percentage (D_{max}), and half maximal degradation concentration (DC_{50} values).[56] For this study we chose to examine the reported DC_{50} values, defined as the concentration at which half-maximal degradation is observed, of the PROTACs in comparison to their relative linker lengths based on the fact that they

encapsulate in a single measured value the abundance of metabolic processes at play. Using DC_{50} values, one can assume that the effects of target protein degradation and resynthesis kinetics, cellular permeability and efflux, native protein expression levels, rate of ubiquitination and subsequent degradation, and other metabolic considerations between different protein targets and cell lines would be included within the data set.

Similar efforts have been made to correlate heterogeneous IC_{50} values with chemical structure, and it has been shown[57] that this strategy does not work due to variability in the assays and conditions used to measure the values as well as errors in data tabulation on large databases. To avoid errors in data tabulation, we chose to normalize the degradation potency data by hand, with careful consideration to compare PROTACs across different studies. Maple et al.[29] developed a degrader scoring measurement and compared 422 degraders from 73 different articles and were able to show correlations between degrader efficacy and increasing clogP, decreasing total polar surface area, and decreasing hydrogen bond donor count. Here we take a narrow view and attempt to add to these findings as it pertains to linker length specifically.

In terms of PROTAC structure, comparison of degradation values were only made when they utilized the same E3 ligase ligand, POI ligand, linkage point on each ligand, linkage functionality (such as amide bond or analine linkages) and linker chemical composition (exemplified by aliphatics or PEGs). Also, only linear linkers were considered for the study due to a lack of extensive published SAR series for more rigid (piperazine-type) linkers,[58] as it pertains directly to linear length versus DC_{50} values. We also excluded studies of covalent degraders and homodegraders due to their implicit differences in mechanism. In terms of biological evaluation, comparison was only made when they shared the same target, were evaluated in the same cell line, and DC_{50} values were collected at the same time points via the same methodology. These normalization restrictions effectively allow only for direct comparison of linker variants across an SAR series within the same study; however, it also allows comparison of all the various compound series for which there is a sufficiently large (>2 compounds) data set.

Due to the conservative normalization strategy pursued, the number of eligible SAR campaigns was greatly narrowed. An exhaustive review of the literature (as of July 12, 2020) revealed 26 series of compounds across 12 SAR studies[25,45,59-68] that were normalized and

compared for this analysis. There are likely more unpublished PROTAC DC_{50} values that were omitted from publication due to lackluster performance, and we urge the future publication of such negative data. Even though some compounds may not make useful preclinical candidates, there is great value in sharing all data sets for the *gestalt* of PROTAC development. To this end, we have provided the raw data from this analysis for others to access and elaborate upon the model (see Appendix).

To begin our analysis, we normalized our entire data set to the single most potent degrader across all 26 compound series and compared how linker length affected the degradation potency (ΔDC_{50} value). As might be expected, no coherent correlation was found when directly comparing the eligible literature degradation data as a whole (Figure 1-5a). In order to overcome the issues ingrained with direct comparison, we applied the normalization strategy described above. The most optimal degrader from each SAR compound series, as chosen by the authors, had both coordinates set to zero (ΔDC_{50} value) and zero linker length in order to observe how a change in the number of linear atoms affects potency. Other PROTACs from within the same series would then be normalized in reference to the most potent compound for linker length (number of linear

atoms) (Figure 1-5b). A final consideration had to be made pertaining to compounds reported as having a $DC_{50} > 3000$ nM.[25,60] We have reported these values as the maximum (3000 nM) for graphical representation only, however, the overall trend is apparent without their inclusion. We also expect evaluation of the less potent degraders to be complicated by the hook-effect,[69] as increasing concentrations of PROTAC are required.

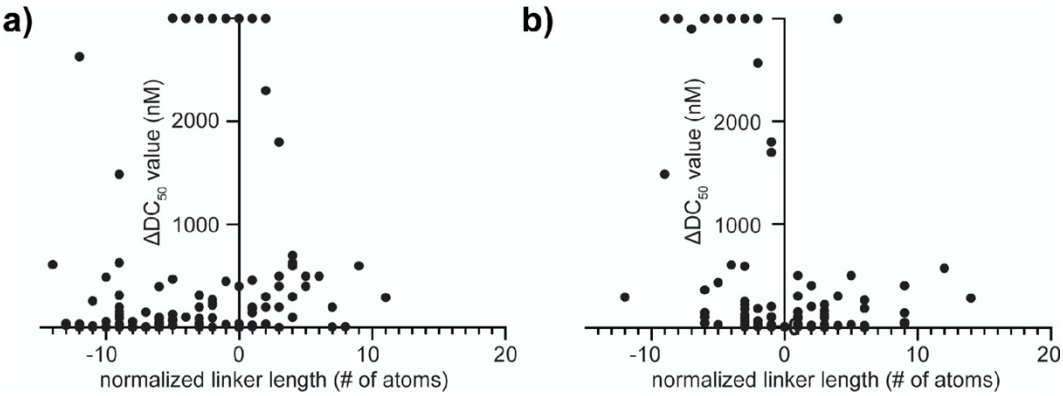

Figure 1-5: Comparison of aggregate and filtered linker length SAR studies after normalization. (a) The selected SAR studies normalized to the most potent reported compound as an aggregate. (b) The selected SAR studies normalized to other compounds that meet the more rigorous filtering criteria described.

The results of normalization (Figure 1-6) show an apparent "boot-shaped" pattern across all of the compound series examined, and although the data are not coherent enough to provide useful quantitative (nonlinear regression based) interpretation, useful qualitative inferences can be made. We qualitatively break this data into three sections relative

to linker length. The section left of Δlinker length = 0 yields a steep drop-off in PROTAC potency, which we attribute to increased contributions of steric clash due to shorter linker lengths, which likely diminishes ternary complex formation efficiency (Figure 1-6). The section centered around 0 yields the most potent PROTACs (due to normalization procedures), but when compared to the section on the left suggests this zone is likely where protein–protein interactions are most favorable for the given system, regardless of whether they are cooperative,[32,33,70] noncooperative,[45] or negatively cooperative.[21,45] The zone to the right of +6 yields effective PROTACs with diminishing potency, which we attribute to entropic effects intrinsic to longer linker lengths and more degrees of freedom in the ternary complex. Ongoing debate has focused on the importance of protein–protein interaction between the E3 ligase and POI as it pertains to PROTAC development, and although leveraging this interaction is likely paramount to considerations of selectivity, this analysis suggests the proximity model could also coexist with regard to degradation potency.

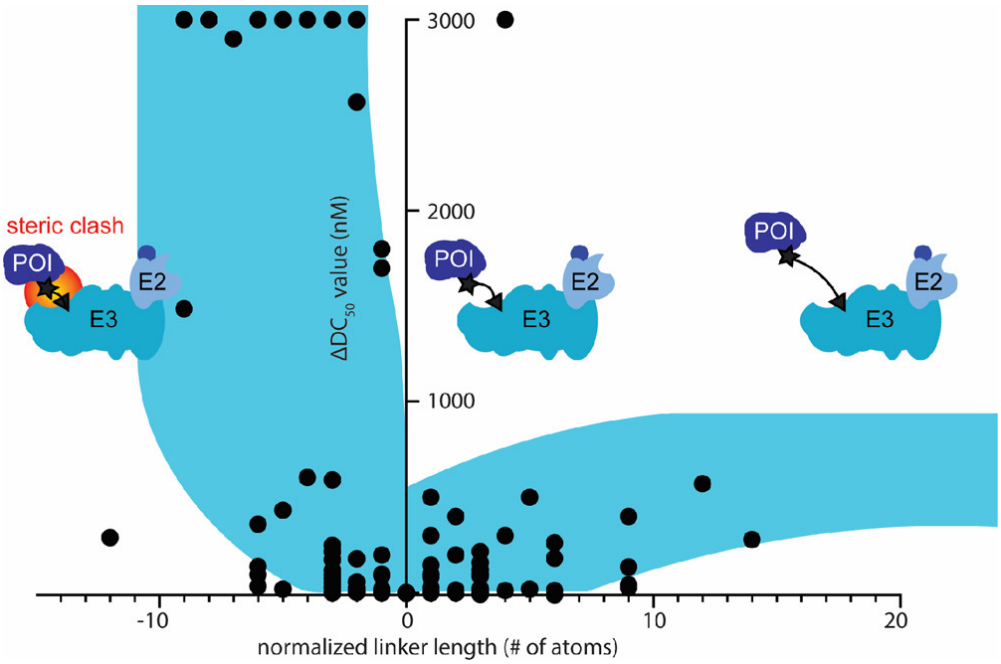

Figure 1-6: Representation of the qualitative inferences made. Qualitatively we describe this trend in three zones. Left of center represents a region where steric clash can hinder successful ternary complex formation, leading to a sharp drop off in degradation potency. Center represents the most potent degraders. Right of center represents the diminishing degradation potency due to increased entropy associated with longer linkers.

This analysis suggests that an empirical linker length SAR study might be best initiated with longer linker lengths as a means to test for compatibility between the E3 ligase and POI. However, the data do not necessarily suggest that any linker length larger than the optimum will produce a successful degrader; only that, in general, the chances of finding a degrader are increased with longer linkers due to the absence of

steric clash. If a compatible E3 ligase–POI system is identified, systematically shortening the length of the linker will identify the sharp cutoff point in potency and locate the linker length that induces potency abolishing steric clash. In general, this analysis suggests that the most potent PROTACs were found within a few atoms of that linker length. In addition, this region may provide the best chances of selectivity by minimizing degrees of freedom in the ternary complex while maintaining potency.

The model presented was comprised of limited published data and can only be used to make qualitative inferences about how linker length can affect degrader potency. We would expect that no such model could be generated for degrader selectivity, as each system will have its own unique interprotein contacts, and normalization for direct comparison would be difficult between systems. However, we can imagine that, were enough data reported and added to the normalization, a quantitative description of the trend may become relevant through nonlinear regression. This would likely take the form of a weakly fitted curve due to the intrinsic biological and pharmacological complexities inherent in DC_{50} measurements, yet it could wield suggestive power by fitting a novel limited linker SAR data set to the determined curve to examine which

zones (Figure 1-6) have been identified for a compound series in a novel system. For this reason, we intend to update and evaluate the publicly available data set in the future. This could offer another tool to reduce the synthetic bottleneck caused by linker length SAR studies.

SUMMARY

In conclusion, the empirical nature of PROTAC development campaigns is being eroded by the harmonious development in synthetic methodologies of chimeric small molecules, structural characterization of ternary complexes, advances in computational protocols, and systematic analysis of prior studies. PROTAC development presents a dramatic detour for drug design in that the focus has shifted to small molecules capable of stabilizing noncognate protein interactions long enough for polyubiquitination. This event-driven pharmacology allows for repurposing of previously abandoned ligands that had been shelved due to lack of potency or lack of selectivity. It also offers a method to effectively target noncatalytic protein targets, a significant expansion of possible leads. Through continued cooperation between the fields of expertise outlined here, we expect the coupled reduction of lead-time for development of PROTACs through the development of a solution to the empirical nature of the linker domain. We await further validation of this exciting pharmacological modality in the clinic.

Chapter 1, in full, is a reprint of the material as it appears in Chemical Communications. Bemis, Troy A.; La Clair, James J.; Burkart,

Michael D., Royal Society of Chemistry, 2021. The dissertation author was the primary investigator and author of this paper.

APPENDIX

Appendix Table 1-1: Compiled linker SAR data from reference 59. Data was normalized to the most potent compound in the series.

DOI	E3 Ligase C = CRBN V = VHL	Compound number in original manuscript	Linker type A = aliphatic, P = PEG or other oxygen containing	Number of atoms in the linker	DC50 (nM)	Cell Line	Normalized linker length	Normalized DC50 (nM)	Method	Targets	NOTES
											###3000 nM was used as maximum upper limit in this presentation of data
https://doi.org/10.1021/acsmedchemlett.0c00046	V	3j	A	25	7.1	MM1S	0	0	in-cell ELISA	HDAC6	
	V	3K	A	26	11		1	3.9	in-cell ELISA		

Appendix Table 1-2: Compiled linker SAR data from reference 60. Data was normalized to the most potent compound in the series.

DOI	E3 Ligase C = CRBN V = VHL	Compound number in original manuscript	Linker type A = aliphatic, P = PEG or other oxygen containing	Number of atoms in the linker	DC50 (nM)	Cell Line	Normalized linker length	Normalized DC50 (nM)	Method	Targets	NOTES
											###3000 nM was used as maximum upper limit in this presentation of data
https://doi.org/10.1021/acs.jmedchem.0c00339	C	11a	P	13		SRD15	-9	3000	Semi-quant immunoblotting	HMGCR	>3000 nm
	C	11b	P	14			-8	3000	Semi-quant immunoblotting		>3000 nm
	C	11c	P	15	3000		-7	2900	Semi-quant immunoblotting		
	C	11d	P	16			-6	3000	Semi-quant immunoblotting		>3000 nm
	C	11e	P	17			-5	3000	Semi-quant immunoblotting		>3000 nm
	C	11f	P	18			-4	3000	Semi-quant immunoblotting		>3000 nm
	C	11g	P	19			-3	3000	Semi-quant immunoblotting		>3000 nm
	C	11h	P	20			-2	3000	Semi-quant immunoblotting		>3000 nm
	C	11i	P	21	1800		-1	1700	Semi-quant immunoblotting		
	C	11j	P	22	100		0	0	Semi-quant immunoblotting		
	C	11k	P	22					Semi-quant immunoblotting		NEG. Control. Methylated glutarimide
	C	11l	P	23	400		1	300	Semi-quant immunoblotting		
	C	11m	P	24	500		2	400	Semi-quant immunoblotting		
	C	11n	P	25	200		3	100	Semi-quant immunoblotting		
	C	11o	P	26			4	3000	Semi-quant immunoblotting		>3000 nm
	C	11p	P	27	600		5	500	Semi-quant immunoblotting		
	C	12a	A	17					Semi-quant immunoblotting		DC50 N.D.
	C	12b	A	18	400		-1	200	Semi-quant immunoblotting		
	C	12c	A	19	200		0	0	Semi-quant immunoblotting		
	C	12d	A	20	300		1	100	Semi-quant immunoblotting		
	C	12e	A	21	400		2	200	Semi-quant immunoblotting		
	C	12f	A	22	300		3	100	Semi-quant immunoblotting		
	C	12g	A	23	500		4	300	Semi-quant immunoblotting		
	C	13a	P	31					Semi-quant immunoblotting		>3000 nm
	C	13b	P	30					Semi-quant immunoblotting		>3000 nm
	C	13c	P	33					Semi-quant immunoblotting		>3000 nm
	C	13d	P	34	300				Semi-quant immunoblotting		
	C	13e	P	35					Semi-quant immunoblotting		>3000 nm
	C	13f	P	37					Semi-quant immunoblotting		>3000 nm
	C	14a	A	17			-4	3000	Semi-quant immunoblotting		>3000 nm
	C	14b	A	18			-3	3000	Semi-quant immunoblotting		>3000 nm
	C	14c	A	19			-2	3000	Semi-quant immunoblotting		>3000 nm
	C	14d	A	20	300		-1	100	Semi-quant immunoblotting		
	C	14e	A	21	200		0	0	Semi-quant immunoblotting		
	C	14f	A	22	700		1	500	Semi-quant immunoblotting		
	C	15a	A	17			-4	3000	Semi-quant immunoblotting		>3000 nm
	C	15b	A	18			-3	3000	Semi-quant immunoblotting		>3000 nm
	C	15c	A	19			-2	3000	Semi-quant immunoblotting		>3000 nm
	C	15d	A	20	2300		-1	1800	Semi-quant immunoblotting		
	C	15e	A	21	500		0	0	Semi-quant immunoblotting		
	C	15f	A	22	600		1	100	Semi-quant immunoblotting		

Appendix Table 1-3: Compiled linker SAR data from reference 61. Data was normalized to the most potent compound in the series.

DOI	E3 Ligase C = CRBN V = VHL	Compound number in original manuscript	Linker type A = aliphatic, P = PEG or other oxygen containing	Number of atoms in the linker	DC50 (nM)	Cell Line	Normalized linker length	Normalized DC50 (nM)	Method	Targets	NOTES
											###3000 nM was used as maximum upper limit in this presentation of data
https://doi.org/10.1021/acs.jmedchem.9b01530	C	12	A	6	2630	Molm-16	-2	2570	Semi-quant immunoblotting	STAT3	
	C	13	A	7	260		-1	200	Semi-quant immunoblotting		
	C	14	A	8	60		0	0	Semi-quant immunoblotting		
	C	15	A	9	90		1	30	Semi-quant immunoblotting		
	C	16	A	11	150		3	90	Semi-quant immunoblotting		

Appendix Table 1-4: Compiled linker SAR data from reference 62. Data was normalized to the most potent compound in the series.

DOI	E3 Ligase C = CRBN V = VHL	Compound number in original manuscript	Linker type A = aliphatic, P = PEG or other oxygen containing	Number of atoms in the linker	DC50 (nM)	Cell Line	Normalized linker length	Normalized DC50 (nM)	Method	Targets	NOTES
											###3000 nM was used as maximum upper limit in this presentation of data
https://doi.org/10.1021/acs.jmedchem.9b01264	V	17	A	10	10.1	K562	2	1.6	Semi-quant immunoblotting	BCR-ABL	
	V	18	A	9	37.9		1	29.4	Semi-quant immunoblotting		
	V	19	A	8	8.5		0	0	Semi-quant immunoblotting		
	V	20	A	7	17.9		-1	9.4	Semi-quant immunoblotting		
	V	21	A	6	34.7		-2	26.2	Semi-quant immunoblotting		
	V	22	A	5	40.2		-3	31.7	Semi-quant immunoblotting		
	V	23	A	4	611.4		-4	602.9	Semi-quant immunoblotting		

Appendix Table 1-5: Compiled linker SAR data from reference 63. Data was normalized to the most potent compound in the series.

DOI	E3 Ligase C = CRBN V = VHL	Compound number in original manuscript	Linker type A = aliphatic, P = PEG or other oxygen containing	Number of atoms in the linker	DC50 (nM)	Cell Line	Normalized linker length	Normalized DC50 (nM)	Method	Targets	NOTES
											###3000 nM was used as maximum upper limit in this presentation of data
https://doi.org/10.1021/acs.jmedchem.9b00871	C	CP-10	P	10	2.1	U251	1	1	Semi-quant immunoblotting	CDK6	
	C	CP-5	P	9	1.1		0	0	Semi-quant immunoblotting		
	C	CP-6	P	12	24.2		3	23.1	Semi-quant immunoblotting		
	C	CP-7	P	15	14.3		6	13.2	Semi-quant immunoblotting		
	C	CP-8	P	18	31		9	29.9	Semi-quant immunoblotting		
	C	CP-15	P	9	1.6		0	0.5	Semi-quant immunoblotting		
	C	CP-13	A	10	5.3		0	3.6	Semi-quant immunoblotting		
	C	CP-14	A	11	10.6		1	8.9	Semi-quant immunoblotting		
	C	CP-16	A	10	1.7		0	0	Semi-quant immunoblotting		
	C	CP-A1	P	10	8.6		0	0	Semi-quant immunoblotting		
	C	CP-A2	P	13	129.7		3	121.1	Semi-quant immunoblotting		
	C	CP-A3	P	16	271.9		6	263.3	Semi-quant immunoblotting		
	C	CP-A4	P	19	145.5		9	136.9	Semi-quant immunoblotting		

Appendix Table 1-6: Compiled linker SAR data from reference 64. Data was normalized to the most potent compound in the series.

DOI	E3 Ligase C = CRBN V = VHL	Compound number in original manuscript	Linker type A = aliphatic, P = PEG or other oxygen containing	Number of atoms in the linker	DC50 (nM)	Cell Line	Normalized linker length	Normalized DC50 (nM)	Method	Targets	NOTES
											###3000 nM was used as maximum upper limit in this presentation of data
https://doi.org/10.1021/acs.jmedchem.9b00516	C	12a	A	8	3.41	MM1S	-3	1.77	In-cell ELISA	HDAC6	
	C	12d	A	11	1.64		0	0	In-cell ELISA		
	C	12i	A	10	2.54		-1	0.9	In-cell ELISA		

Appendix Table 1-7: Compiled linker SAR data from reference 65. Data was normalized to the most potent compound in the series.

DOI	E3 Ligase C = CRBN V = VHL	Compound number in original manuscript	Linker type A = aliphatic, P = PEG or other oxygen containing	Number of atoms in the linker	DC50 (nM)	Cell Line	Normalized linker length	Normalized DC50 (nM)	Method	Targets	NOTES
											###3000 nM was used as maximum upper limit in this presentation of data
https://doi.org/10.1021/jacs.8b08008	V	1	P	5	23.2	PC3	-1	20.2	Semi-quant immunoblotting	FAK	
	V	2	P	6	7.6		0	4.6	Semi-quant immunoblotting		
	V	3	P	6	3		0	0	Semi-quant immunoblotting		
	V	4	P	7	4		1	1	Semi-quant immunoblotting		
	V	5	P	9	20.8		3	17.8	Semi-quant immunoblotting		
	V	6	P	15	48.1		9	45.1	Semi-quant immunoblotting		
	V	8	P	7	8.2		1	5.2	Semi-quant immunoblotting		
	V	9	P	9	26.7		3	23.7	Semi-quant immunoblotting		

Appendix Table 1-8: Compiled linker SAR data from reference 45. Data was normalized to the most potent compound in the series.

DOI	E3 Ligase C = CRBN V = VHL	Compound number in original manuscript	Linker type A = aliphatic, P = PEG or other oxygen containing	Number of atoms in the linker	DC50 (nM)	Cell Line	Normalized linker length	Normalized DC50 (nM)	Method	Targets	NOTES
											###3000 nM was used as maximum upper limit in this presentation of data
https://doi.org/10.1073/pnas.1803662115	C	5	P	9	1487	RAMOS	-9	1485.9	Semi-quant immunoblotting	BTK	
	C	6	P	12	36.9		-6	35.8	Semi-quant immunoblotting		
	C	7	P	13	21.8		-5	20.7	Semi-quant immunoblotting		
	C	8	P	15	4.5		-3	3.4	Semi-quant immunoblotting		
	C	9	P	16	5.9		-2	4.8	Semi-quant immunoblotting		
	C	10	P	18	1.1		0	0	Semi-quant immunoblotting		
	C	11	P	19	9.7		1	8.6	Semi-quant immunoblotting		
	C	6	P	12	398.5	THP-1	-6	361.1	Semi-quant immunoblotting		
	C	7	P	13	469.9		-5	432.5	Semi-quant immunoblotting		
	C	8	P	15	90.5		-3	53.1	Semi-quant immunoblotting		
	C	9	P	16	217.7		-2	180.3	Semi-quant immunoblotting		
	C	10	P	18	37.4		0	0	Semi-quant immunoblotting		
	C	11	P	19	184.1		1	146.7	Semi-quant immunoblotting		

Appendix Table 1-9: Compiled linker SAR data from reference 66. Data was normalized to the most potent compound in the series.

DOI	E3 Ligase C = CRBN V = VHL	Compound number in original manuscript	Linker type A = aliphatic, P = PEG or other oxygen containing	Number of atoms in the linker	DC50 (nM)	Cell Line	Normalized linker length	Normalized DC50 (nM)	Method	Targets	NOTES
											###3000 nM was used as maximum upper limit in this presentation of data
https://doi.org/10.1021/acs.jmedchem.7b00635	V	3f	P	12	88	Panc.02.13	-3	76	Semi-quant immunoblotting	TANK-binding Kinase 1	
	V	3g	P	13	71		-2	59	Semi-quant immunoblotting		
	V	3h	P	14	103		-1	91	Semi-quant immunoblotting		
	V	3i	P	15	12		0	0	Semi-quant immunoblotting		Compound chosen in series to match selections made in original SAR study
	V	3j	P	16	95		1	83	Semi-quant immunoblotting		
	V	3k	P	17	29		2	17	Semi-quant immunoblotting		
	V	3l	P	18	6		3	-6	Semi-quant immunoblotting		
	V	3m	P	19	25		4	13	Semi-quant immunoblotting		
	V	3n	P	20	34		5	22	Semi-quant immunoblotting		
	V	3o	P	21	3		6	-9	Semi-quant immunoblotting		
	V	3p	P	29	292		14	280	Semi-quant immunoblotting		

Appendix Table 1-10: Compiled linker SAR data from reference 67. Data was normalized to the most potent compound in the series.

DOI	E3 Ligase C = CRBN V = VHL	Compound number in original manuscript	Linker type A = aliphatic, P = PEG or other oxygen containing	Number of atoms in the linker	DC50 (nM)	Cell Line	Normalized linker length	Normalized DC50 (nM)	Method	Targets	NOTES
											###3000 nM was used as maximum upper limit in this presentation of data
https://doi.org/10.1021/acs.jmedchem.6b01912	V	5	P	9	100	HeLa	-6	96	Semi-quant immunoblotting	BRD4 short	
	V	6	P	12	8		-3	4	Semi-quant immunoblotting		
	V	7	P	15	4		0	0	Semi-quant immunoblotting		
	V	8	P	9	126		-3	118	Semi-quant immunoblotting		
	V	9	P	12	8		0	0	Semi-quant immunoblotting		Ties in potency were given to those with largest Dmax
	V	10	P	15	8		3	0	Semi-quant immunoblotting		
	V	5	P	9	100		-3	97	Semi-quant immunoblotting	BRD4 Long	
	V	6	P	12	3		0	0	Semi-quant immunoblotting		
	V	7	P	15	10		3	7	Semi-quant immunoblotting		
	V	8	P	9	200		-3	175	Semi-quant immunoblotting		
	V	9	P	12	25		0	0	Semi-quant immunoblotting		
	V	10	P	15	32		3	7	Semi-quant immunoblotting		
	V	5	P	9	316		-3	216	Semi-quant immunoblotting	BRD3	
	V	6	P	12	100		0	0	Semi-quant immunoblotting		
	V	7	P	15	316		3	216	Semi-quant immunoblotting		
	V	8	P	9	158		-6	138	Semi-quant immunoblotting		
	V	9	P	12	50		-3	30	Semi-quant immunoblotting		
	V	10	P	15	20		0	0	Semi-quant immunoblotting		
	V	5	P	9	631		-3	591	Semi-quant immunoblotting	BRD2	
	V	6	P	12	40		0	0	Semi-quant immunoblotting		
	V	7	P	15	200		3	160	Semi-quant immunoblotting		

Appendix Table 1-11: Compiled linker SAR data from reference 25. Data was normalized to the most potent compound in the series.

DOI	E3 Ligase C = CRBN V = VHL	Compound number in original manuscript	Linker type A = aliphatic, P = PEG or other oxygen containing	Number of atoms in the linker	DC50 (nM)	Cell Line	Normalized linker length	Normalized DC50 (nM)	Method	Targets	NOTES
											###3000 nM was used as maximum upper limit in this presentation of data
https://doi.org/10.1021/acs.jmedchem.6b01781	C	11a	P	8	490	NCI-H661	-12	290	Semi-quant immunoblotting	BRD4	
	C	11b	P	11			-9	3000	Semi-quant immunoblotting		>5000
	C	11c	P	14			-6	3000	Semi-quant immunoblotting		>5000
	C	11d	P	17	450		-3	250	Semi-quant immunoblotting		
	C	11e	P	20	200		0	0	Semi-quant immunoblotting		
	V	12a	P	10	59		0	0	Semi-quant immunoblotting		
	V	12b	P	13	83		3	24	Semi-quant immunoblotting		
	V	12c	P	16	240		6	181	Semi-quant immunoblotting		
	V	12d	P	19	460		9	401	Semi-quant immunoblotting		
	V	12e	P	22	630		12	571	Semi-quant immunoblotting		

Appendix Table 1-12: Compiled linker SAR data from reference 68. Data was normalized to the most potent compound in the series.

DOI	E3 Ligase C = CRBN V = VHL	Compound number in original manuscript	Linker type A = aliphatic, P = PEG or other oxygen containing	Number of atoms in the linker	DC50 (nM)	Cell Line	Normalized linker length	Normalized DC50 (nM)	Method	Targets	NOTES
											###3000 nM was used as maximum upper limit in this presentation of data
https://doi.org/10.1016/j.ejmech.2020.112190	V	8	A	8		SR			Semi-quant immunoblotting	ALK	>50
	V	9	A	9	15				Semi-quant immunoblotting		
	V	10	A	10					Semi-quant immunoblotting		>50
									Semi-quant immunoblotting		
	V	15	A	8	9.1		-3	2.1	Semi-quant immunoblotting		
	V	16	A	9	20.9		-2	13.9	Semi-quant immunoblotting		
	V	17	A	10	7.2		-1	0.2	Semi-quant immunoblotting		
	V	18	A	11	7		0	0	Semi-quant immunoblotting		
									Semi-quant immunoblotting		
	V	23	A	8	11.4		-2	3.9	Semi-quant immunoblotting		
	V	24	A	9	25.1		-1	17.6	Semi-quant immunoblotting		
	V	25	A	10	7.5		0	0	Semi-quant immunoblotting		

REFERENCES

1. Sakamoto, K. M.; Kim, K. B.; Kumagai, A.; Mercurio, F.; Crews, C. M.; Deshaies, R. J. Protacs: Chimeric Molecules That Target Proteins to the Skp1-Cullin-F Box Complex for Ubiquitination and Degradation. *Proc. Natl. Acad. Sci. U. S. A.* **2001**, *98*, 8554–8559.

2. Faust, T. B.; Donovan, K. A.; Yue, H.; Chamberlain, P. P.; Fischer, E. S. Small-Molecule Approaches to Targeted Protein Degradation. *Annual Review of Cancer Biology* **2021**, *5*, 181–201.

3. António, J. P. M.; Goncalves, L. M.; Guedes, R. C.; Moreira, R.; Gois, P. M. P. Diazaborines as New Inhibitors of Human Neutrophil Elastase. *ACS Omega* **2018**, *3*, 7418–7423.

4. Dang, C. V.; Reddy, E. P.; Shokat, K. M.; Soucek, L. Drugging the "undruggable" Cancer Targets. *Nat. Rev. Cancer* **2017**, *17*, 502– 508.

5. Crews, C. M. Targeting the Undruggable Proteome: The Small Molecules of My Dreams. *Chem. Biol.* **2010**, *17*, 551–555.

6. Lipinski, C. A.; Lombardo, F.; Dominy, B. W.; Feeney, P. J. Experimental and Computational Approaches to Estimate Solubility and Permeability in Drug Discovery and Development Settings. *Adv. Drug Delivery Rev.* **2001**, *46*, 3–26.

7. Mullard, A. Targeted Protein Degraders Crowd into the Clinic. *Nat. Rev. Drug Discovery* **2021**, *20*, 247–250.

8. Trial of ARV-110 in Patients With Metastatic Castration Resistant Prostate Cancer (mCRPC). NCT03888612. https://clinicaltrials.gov/ct2/show/NCT03888612 (accessed May 10, 2021).

9. A Phase 1/2 Trial of ARV-471 Alone and in Combination With Palbociclib (IBRANCE) in Patients With ER+/HER2– Locally Advanced or Metastatic Breast Cancer (mBC). NCT04072952. https://clinicaltrials.gov/ct2/show/NCT04072952 (accessed May 10, 2021).

10. Pohl, C.; Dikic, I. Cellular Quality Control by the Ubiquitin Proteasome System and Autophagy. *Science* **2019**, *366*, 818–822.

11. Kleiger, G.; Mayor, T. Perilous Journey: A Tour of the Ubiquitin-Proteasome System. *Trends Cell Biol.* **2014**, *24*, 352–359.

12. Wertz, I. E.; Wang, X. From Discovery to Bedside: Targeting the Ubiquitin System. *Cell Chem. Biol.* **2019**, *26*, 156–177.

13. Huang, X.; Dixit, V. M. Drugging the Undruggables: Exploring the Ubiquitin System for Drug Development. *Cell Res.* **2016**, *26*, 484– 498.

14. Nalepa, G.; Rolfe, M.; Harper, J. W. Drug Discovery in the Ubiquitin-Proteasome System. *Nat. Rev. Drug Discovery* **2006**, *5*, 596– 613.

15. Sun, X.; Gao, H.; Yang, Y.; He, M.; Wu, Y.; Song, Y.; Tong, Y.; Rao, Y. Protacs: Great Opportunities for Academia and Industry. *Signal Transduct. Target. Ther.* **2019**, *4*, 64.

16. Konstantinidou, M.; Li, J.; Zhang, B.; Wang, Z.; Shaabani, S.; Ter Brake, F.; Essa, K.; Dömling, A. PROTACs a Game-Changing Technology. *Expert Opin. Drug Discovery* **2019**, *14*, 1255–1268.

17. Winter, G. E.; Buckley, D. L.; Paulk, J.; Roberts, J. M.; Souza, A.; Dhe-Paganon, S.; Bradner, J. E. Phthalimide Conjugation as a Strategy for in Vivo Target Protein Degradation. *Science* **2015**, *348*, 1376–1381.

18. Buckley, D. L.; Van Molle, I.; Gareiss, P. C.; Tae, H. S.; Michel, J.; Noblin, D. J.; Jorgensen, W. L.; Ciulli, A.; Crews, C. M. Targeting the von Hippel-Lindau E3 Ubiquitin Ligase Using Small Molecules to Disrupt the VHL/HIF-1α Interaction. *J. Am. Chem. Soc.* **2012**, *134*, 4465–4468.

19. Lai, A. C.; Toure, M.; Hellerschmied, D.; Salami, J.; JaimeFigueroa, S.; Ko, E.; Hines, J.; Crews, C. M. Modular PROTAC Design for the Degradation of Oncogenic BCR-ABL. *Angew. Chem., Int. Ed.* **2016**, *55*, 807–810.

20. Zengerle, M.; Chan, K. H.; Ciulli, A. Selective Small Molecule Induced Degradation of the BET Bromodomain Protein BRD4. *ACS Chem. Biol.* **2015**, *10*, 1770–1777.

21. Nowak, R. P.; Deangelo, S. L.; Buckley, D.; He, Z.; Donovan, K. A.; An, J.; Safaee, N.; Jedrychowski, M. P.; Ponthier, C. M.; Ishoey, M.; Zhang, T.; Mancias, J. D.; Gray, N. S.; Bradner, J. E.; Fischer, E. S. Plasticity in Binding Confers Selectivity in Ligand-Induced Protein Degradation. *Nat. Chem. Biol.* **2018**, *14*, 706–714.

22. Cyrus, K.; Wehenkel, M.; Choi, E. Y.; Han, H. J.; Lee, H.; Swanson, H.; Kim, K. B. Impact of Linker Length on the Activity of PROTACs. *Mol. BioSyst.* **2011**, *7*, 359–364.

23. Steinebach, C.; Kehm, H.; Lindner, S.; Vu, L. P.; Köpff, S.; López Mármol, A.; Weiler, C.; Wagner, K. G.; Reichenzeller, M.; Krönke, J.; Gütschow, M. PROTAC-Mediated Crosstalk between E3 Ligases. *Chem. Commun.* **2019**, *55*, 1821–1824.

24. Krajcovicova, S.; Jorda, R.; Hendrychova, D.; Krystof, V.; Soural, M. Solid-Phase Synthesis for Thalidomide-Based ProteolysisTargeting Chimeras (PROTAC). *Chem. Commun.* **2019**, *55*, 929– 932.

25. Wurz, R. P.; Dellamaggiore, K.; Dou, H.; Javier, N.; Lo, M. C.; McCarter, J. D.; Mohl, D.; Sastri, C.; Lipford, J. R.; Cee, V. J. A "Click Chemistry Platform" for the Rapid Synthesis of Bispecific Molecules for Inducing Protein Degradation. *J. Med. Chem.* **2018**, *61*, 453–461.

26. Papatzimas, J. W.; Gorobets, E.; Brownsey, D. K.; Maity, R.; Bahlis, N. J.; Derksen, D. J. A General Strategy for the Preparation of Thalidomide-Conjugate Linkers. *Synlett* **2017**, *28*, 2881–2885.

27. Bemis, T. A.; La Clair, J. J.; Burkart, M. D. Traceless Staudinger Ligation Enabled Parallel Synthesis of Proteolysis Targeting Chimera Linker Variants. *Chem. Commun.* **2021**, *57*, 1026–1029.

28. Himo, F.; Lovell, T.; Hilgraf, R.; Rostovtsev, V. V.; Noodleman, L.; Sharpless, K. B.; Fokin, V. V. Copper(I)-Catalyzed Synthesis of Azoles. DFT

Study Predicts Unprecedented Reactivity and Intermediates. *J. Am. Chem. Soc.* **2005**, *127*, 210–216.

29. Maple, H. J.; Clayden, N.; Baron, A.; Stacey, C.; Felix, R. Developing Degraders: Principles and Perspectives on Design and Chemical Space. *MedChemComm* **2019**, *10*, 1755–1764.

30. Alabi, S.; Jaime-Figueroa, S.; Yao, Z.; Gao, Y.; Hines, J.; Samarasinghe, K. T. G.; Vogt, L.; Rosen, N.; Crews, C. M. Mutant-Selective Degradation by BRAF-Targeting PROTACs. *Nat. Commun.* **2021**, *12*, 920.

31. Leissing, T. M.; Luh, L. M.; Cromm, P. M. Structure Driven Compound Optimization in Targeted Protein Degradation. *Drug Discovery Today: Technol.* **2020**, 005.

32. Gadd, M. S.; Testa, A.; Lucas, X.; Chan, K. H.; Chen, W.; Lamont, D. J.; Zengerle, M.; Ciulli, A. Structural Basis of PROTAC Cooperative Recognition for Selective Protein Degradation. *Nat. Chem. Biol.* **2017**, *13*, 514–521.

33. Farnaby, W.; Koegl, M.; Roy, M. J.; Whitworth, C.; Diers, E.; Trainor, N.; Zollman, D.; Steurer, S.; Karolyi-Oezguer, J.; Riedmueller, C.; Gmaschitz, T.; Wachter, J.; Dank, C.; Galant, M.; Sharps, B.; Rumpel, K.; Traxler, E.; Gerstberger, T.; Schnitzer, R.; Petermann, O.; Greb, P.; Weinstabl, H.; Bader, G.; Zoephel, A.; Weiss-Puxbaum, A.; Ehrenhöfer-Wölfer, K.; Wöhrle, S.; Boehmelt, G.; Rinnenthal, J.; Arnhof, H.; Wiechens, N.; Wu, M. Y.; Owen-Hughes, T.; Ettmayer, P.; Pearson, M.; McConnell, D. B.; Ciulli, A. BAF Complex Vulnerabilities in Cancer Demonstrated via Structure-Based PROTAC Design. *Nat. Chem. Biol.* **2019**, *15*, 672–680.

34. Sircar, A.; Chaudhury, S.; Kilambi, K. P.; Berrondo, M.; Gray, J. J. A Generalized Approach to Sampling Backbone Conformations with RosettaDock for CAPRI Rounds 13–19. Proteins: *Struct., Funct., Genet.* **2010**, *78*, 3115–3123.

35. Testa, A.; Hughes, S. J.; Lucas, X.; Wright, J. E.; Ciulli, A. Structure-Based Design of a Macrocyclic PROTAC. *Angew. Chem., Int. Ed.* **2020**, *59*, 1727–1734.

36. Smith, B. E.; Wang, S. L.; Jaime-Figueroa, S.; Harbin, A.; Wang, J.; Hamman, B. D.; Crews, C. M. Differential PROTAC Substrate Specificity Dictated by Orientation of Recruited E3 Ligase. *Nat. Commun.* **2019**, *10*, 131.

37. Bondeson, D. P.; Smith, B. E.; Burslem, G. M.; Buhimschi, A. D.; Hines, J.; Jaime-Figueroa, S.; Wang, J.; Hamman, B. D.; Ishchenko, A.; Crews, C. M. Lessons in PROTAC Design from Selective Degradation with a Promiscuous Warhead. *Cell Chem. Biol.* **2018**, *25*, 78–87.

38. Lebraud, H.; Wright, D. J.; Johnson, C. N.; Heightman, T. D. Protein Degradation by In-Cell Self-Assembly of Proteolysis Targeting Chimeras. *ACS Cent. Sci.* **2016**, *2*, 927–934.

39. Schiedel, M.; Herp, D.; Hammelmann, S.; Swyter, S.; Lehotzky, A.; Robaa, D.; Oláh, J.; Ovádi, J.; Sippl, W.; Jung, M. Chemically Induced Degradation of Sirtuin 2 (Sirt2) by a Proteolysis Targeting Chimera (PROTAC) Based on Sirtuin Rearranging Ligands (SirReals). *J. Med. Chem.* **2018**, *61*, 482–491.

40. Imrie, F.; Bradley, A. R.; van der Schaar, M.; Deane, C. M. Deep Generative Models for 3D Linker Design. *J. Chem. Inf. Model.* **2020**, *60*, 1983–1995.

41. Pérez-Benito, L.; Henry, A.; Matsoukas, M. T.; Lopez, L.; Pulido, D.; Royo, M.; Cordomí, A.; Tresadern, G.; Pardo, L. The Size Matters? A Computational Tool to Design Bivalent Ligands. *Bioinformatics* **2018**, *34*, 3857–3863.

42. Drummond, M. L.; Williams, C. I. In Silico Modeling of PROTAC-Mediated Ternary Complexes: Validation and Application. *J. Chem. Inf. Model.* **2019**, *59*, 1634–1644.

43. Drummond, M. L.; Henry, A.; Li, H.; Williams, C. I. Improved Accuracy for Modeling ProTAC-Mediated Ternary Complex Formation and Targeted Protein Degradation via New in Silico Methodologies. *J. Chem. Inf. Model.* **2020**, *60*, 5234–5254.

44. Labute, P. LowModeMD-Implicit Low-Mode Velocity Filtering Applied to Conformational Search of Macrocycles and Protein Loops. *J. Chem. Inf. Model.* **2010**, *50*, 792–800.

45. Zorba, A.; Nguyen, C.; Xu, Y.; Starr, J.; Borzilleri, K.; Smith, J.; Zhu, H.; Farley, K. A.; Ding, W. D.; Schiemer, J.; Feng, X.; Chang, J. S.; Uccello, D. P.; Young, J. A.; Garcia-Irrizary, C. N.; Czabaniuk, L.; Schuff, B.; Oliver, R.; Montgomery, J.; Hayward, M. M.; Coe, J.; Chen, J.; Niosi, M.; Luthra, S.; Shah, J. C.; El-Kattan, A.; Qiu, X.; West, G. M.; Noe, M. C.; Shanmugasundaram, V.; Gilbert, A. M.; Brown, M. F.; Calabrese, M. F. Delineating the Role of Cooperativity in the Design of Potent PROTACs for BTK. *Proc. Natl. Acad. Sci. U. S. A.* **2018**, *115*, E7285–E7292.

46. Qin, C.; Hu, Y.; Zhou, B.; Fernandez-Salas, E.; Yang, C. Y.; Liu, L.; McEachern, D.; Przybranowski, S.; Wang, M.; Stuckey, J.; Meagher, J.; Bai, L.; Chen, Z.; Lin, M.; Yang, J.; Ziazadeh, D. N.; Xu, F.; Hu, J.; Xiang, W.; Huang, L.; Li, S.; Wen, B.; Sun, D.; Wang, S. Discovery of QCA570 as an Exceptionally Potent and Efficacious Proteolysis Targeting Chimera (PROTAC) Degrader of the Bromodomain and Extra-Terminal (BET) Proteins Capable of Inducing Complete and Durable Tumor Regression. *J. Med. Chem.* **2018**, *61*, 6685–6704.

47. Huang, H. T.; Dobrovolsky, D.; Paulk, J.; Yang, G.; Weisberg, E. L.; Doctor, Z. M.; Buckley, D. L.; Cho, J. H.; Ko, E.; Jang, J.; Shi, K.; Choi, H. G.; Griffin, J. D.; Li, Y.; Treon, S. P.; Fischer, E. S.; Bradner, J. E.; Tan, L.; Gray, N. S. A Chemoproteomic Approach to Query the Degradable Kinome Using a Multi-Kinase Degrader. *Cell Chem. Biol.* **2018**, *25*, 88–99.

48. Zaidman, D.; Prilusky, J.; London, N. PRosettaC: Rosetta Based Modeling of PROTAC Mediated Ternary Complexes. *J. Chem. Inf. Model.* **2020**, *60*, 4894–4903.

49. Duhovny, D.; Nussinov, R.; Wolfson, H. J. Efficient Unbound Docking of Rigid Molecules. In Algorithms in Bioinformatics; Guigó, R., Gusfield, D., Eds.; *Springer Verlag: Berlin*, **2002**; Vol. *2452*, pp 185–200.

50. Lyskov, S.; Gray, J. J. The RosettaDock Server for Local Protein-protein Docking. *Nucleic Acids Res.* **2008**, *36*, W233–W238.

51. Kuhlman, B.; Baker, D. Native Protein Sequences Are Close to Optimal for Their Structures. *Proc. Natl. Acad. Sci. U. S. A.* **2000**, *97*, 10383–10388.

52. Bai, N.; Miller, S. A.; Andrianov, G. V.; Yates, M.; Kirubakaran, P.; Karanicolas, J. Rationalizing PROTAC-Mediated Ternary Complex Formation Using Rosetta. *J. Chem. Inf. Model.* **2021**, *61*, 1368–1382.

53. Weitzner, B. D.; Jeliazkov, J. R.; Lyskov, S.; Marze, N.; Kuroda, D.; Frick, R.; Adolf-Bryfogle, J.; Biswas, N.; Dunbrack, R. L.; Gray, J. J. Modeling and Docking of Antibody Structures with Rosetta. *Nat. Protoc.* **2017**, *12*, 401–416.

54. Hawkins, P. C. D.; Nicholls, A. Conformer Generation with OMEGA: Learning from the Data Set and the Analysis of Failures. *J. Chem. Inf. Model.* **2012**, *52*, 2919–2936.

55. Vannam, R.; Sayilgan, J.; Ojeda, S.; Karakyriakou, B.; Hu, E.; Kreuzer, J.; Morris, R.; Herrera Lopez, X. I.; Rai, S.; Haas, W.; Lawrence, M.; Ott, C. J. Targeted Degradation of the Enhancer Lysine Acetyltransferases CBP and P300. *Cell Chem. Biol.* **2021**, *28*, 503–514.

56. Hughes, S. J.; Ciulli, A. Molecular Recognition of Ternary Complexes: A New Dimension in the Structure-Guided Design of Chemical Degraders. *Essays Biochem.* **2017**, *61*, 505–516.

57. Kalliokoski, T.; Kramer, C.; Vulpetti, A.; Gedeck, P. Comparability of Mixed IC50 Data-A Statistical Analysis. *PLoS One* **2013**, *8*, e61007.

58. Krönke, J.; Steinebach, C.; Ng, Y. L. D.; Sosic, I.; Lee, C. S.; Chen, S.; Lindner, S.; Vu, L. P.; Bricelj, A.; Haschemi, R.; Monschke, M.; Steinwarz, E.; Wagner, K. G.; Bendas, G.; Luo, J.; Gütschow, M. Systematic Exploration of Different E3 Ubiquitin Ligases: An Approach towards Potent and Selective CDK6 Degraders. *Chem. Sci.* **2020**, *11*, 3474–3486.

59. Yang, K.; Wu, H.; Zhang, Z.; Leisten, E. D.; Nie, X.; Liu, B.; Wen, Z.; Zhang, J.; Cunningham, M. D.; Tang, W. Development of Selective Histone Deacetylase 6 (HDAC6) Degraders Recruiting von Hippel-Lindau (VHL) E3 Ubiquitin Ligase. *ACS Med. Chem. Lett.* **2020**, *11*, 575–581.

60. Li, M. X.; Yang, Y.; Zhao, Q.; Wu, Y.; Song, L.; Yang, H.; He, M.; Gao, H.; Song, B. L.; Luo, J.; Rao, Y. Degradation versus Inhibition: Development of Proteolysis-Targeting Chimeras for Overcoming Statin-Induced Compensatory Upregulation of 3- Hydroxy-3-Methylglutaryl Coenzyme a Reductase. *J. Med. Chem.* **2020**, *63*, 4908–4928.

61. Zhou, H.; Bai, L.; Xu, R.; Zhao, Y.; Chen, J.; McEachern, D.; Chinnaswamy, K.; Wen, B.; Dai, L.; Kumar, P.; Yang, C. Y.; Liu, Z.; Wang, M.; Liu, L.; Meagher, J. L.; Yi, H.; Sun, D.; Stuckey, J. A.; Wang, S. Structure-Based Discovery of SD-36 as a Potent, Selective, and Efficacious PROTAC Degrader of STAT3 Protein. *J. Med. Chem.* **2019**, *62*, 11280–11300.

62. Zhao, Q.; Ren, C.; Liu, L.; Chen, J.; Shao, Y.; Sun, N.; Sun, R.; Kong, Y.; Ding, X.; Zhang, X.; Xu, Y.; Yang, B.; Yin, Q.; Yang, X.; Jiang, B. Discovery of SIAIS178 as an Effective BCR-ABL Degrader by Recruiting von Hippel-Lindau (VHL) E3 Ubiquitin Ligase. *J. Med. Chem.* **2019**, *62*, 9281–9298.

63. Su, S.; Yang, Z.; Gao, H.; Yang, H.; Zhu, S.; An, Z.; Wang, J.; Li, Q.; Chandarlapaty, S.; Deng, H.; Wu, W.; Rao, Y. Potent and Preferential Degradation of CDK6 via Proteolysis Targeting Chimera Degraders. *J. Med. Chem.* **2019**, *62*, 7575–7582.

64. Wu, H.; Yang, K.; Zhang, Z.; Leisten, E. D.; Li, Z.; Xie, H.; Liu, J.; Smith, K. A.; Novakova, Z.; Barinka, C.; Tang, W. Development of Multifunctional Histone Deacetylase 6 Degraders with Potent Antimyeloma Activity. *J. Med. Chem.* **2019**, *62*, 7042–7057.

65. Cromm, P. M.; Samarasinghe, K. T. G.; Hines, J.; Crews, C. M. Addressing Kinase-Independent Functions of Fak via PROTAC-Mediated Degradation. *J. Am. Chem. Soc.* **2018**, *140*, 17019–17026.

66. Crew, A. P.; Raina, K.; Dong, H.; Qian, Y.; Wang, J.; Vigil, D.; Serebrenik, Y. V.; Hamman, B. D.; Morgan, A.; Ferraro, C.; Siu, K.; Neklesa, T. K.; Winkler, J. D.; Coleman, K. G.; Crews, C. M. Identification and Characterization of von Hippel-Lindau-Recruiting Proteolysis Targeting Chimeras (PROTACs) of TANK-Binding Kinase 1. *J. Med. Chem.* **2018**, *61*, 583–598.

67. Chan, K. H.; Zengerle, M.; Testa, A.; Ciulli, A. Impact of Target Warhead and Linkage Vector on Inducing Protein Degradation: Comparison of Bromodomain and Extra-Terminal (BET) Degraders Derived from Triazolodiazepine (JQ1) and Tetrahydroquinoline (I-BET726) BET Inhibitor Scaffolds. *J. Med. Chem.* **2018**, *61*, 504–513.

68. Sun, N.; Ren, C.; Kong, Y.; Zhong, H.; Chen, J.; Li, Y.; Zhang, J.; Zhou, Y.; Qiu, X.; Lin, H.; Song, X.; Yang, X.; Jiang, B. Development of a Brigatinib Degrader (SIAIS117) as a Potential Treatment for ALK Positive Cancer Resistance. *Eur. J. Med. Chem.* **2020**, *193*, 112190.

69. Pettersson, M.; Crews, C. M. Proteolysis TArgeting Chimeras (PROTACs)-Past, Present and Future. *Drug Discovery Today: Technol.* **2019**, *31*, 15–27.

70. Roy, M. J.; Winkler, S.; Hughes, S. J.; Whitworth, C.; Galant, M.; Farnaby, W.; Rumpel, K.; Ciulli, A. SPR-Measured Dissociation Kinetics of PROTAC Ternary Complexes Influence Target Degradation Rate. *ACS Chem. Biol.* **2019**, *14*, 361–368.

CHAPTER 2: Traceless Staudinger Ligation Enabled Parallel Synthesis of Proteolysis Targeting Chimera Linker Variants

ABSTRACT

A parallel, one-pot assembly approach to proteolysis targeting chimeras (PROTACs) is demonstrated utilizing activated esters generated *in situ*, and traceless Staudinger ligation chemistry. The method described allows for rapid structure–activity relationship studies of PROTAC linker variants. Two previously studied systems, cereblon and BRD4 degraders, are examined as test cases for the synthetic method. The two related strategies to assemble PROTAC linker variants discussed can accommodate the chromatographic separations capabilities of labs of many sizes and incorporates commercially available degrader building blocks, thereby easing synthetic entry into PROTAC chemical space.

SYNTHETIC METHODOLOGY

The development of highly efficient chemical processes lies at the foundation of serialized screening systems.[1] Effectively described as Click chemistry,[2] these reactions have provided a remarkable access to small molecule diversity and has profoundly impacted our ability to prepare biological probes. Over the last decade, proteolysis targeting chimeras (PROTACs), heterobifunctional small molecules,[3] have gained recognition as a powerful tool for targeting proteins for proteasomal degradation (Figure 2-1).[4] Recently, PROTACs have garnered interest due to their potency, catalytic activity, and ability to target 'undruggable' proteins.[5] This utility has not gone unrecognized, and was recently marked by entry into the first clinical trials of ARV-110 for metastatic castration-resistant prostate cancer and ARV-471 for metastatic breast cancer.[6]

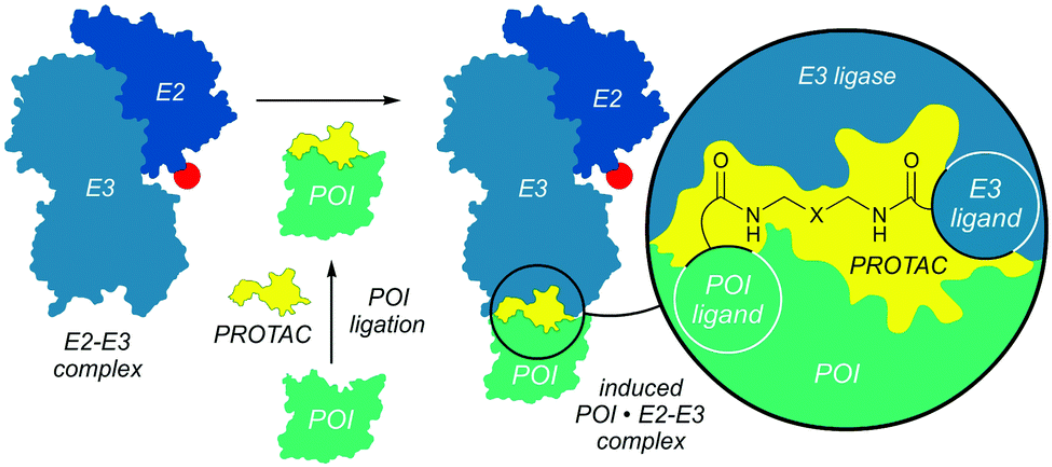

Figure 2-1: Schematic representation where a heterobifunctional molecule or PROTAC (yellow) is used to target the degradation of a protein of interest (POI, green). In this process, the PROTAC contains motifs that bind to both POI and E3 ligase (blue), yielding a ternary complex. Ubiquitin (red) can then be transferred to the POI in a proximity dependent manner, leading to proteolysis of the POI.

First described in 2001, the PROTAC concept (Appendix Figure 2-1) involves the preparation of chimeric molecules that contained two protein binding motifs that induce unnatural protein–protein interactions (PPIs).[7] While not limited to protein interactivity,[8] this concept offers a robust utility to link two pathways and molecularly rewire a cells function upon the presentation of a chimeric molecule. Developing tools to enable the preparation and screening of libraries of chimeric molecules will play a key role in our future development of concepts like PROTACs. While advances have been made to ease the synthetic entry into chimeric small molecule space,[9] preparations of linker variants remains a necessary and tedious task. One needs to consider a three-part diversification and optimization where structural variance can be introduced at the two-protein binding and linker motifs. The issue then exists as to how one can 'choreograph' these processes into a single operation, thereby streamlining the evaluation of PROTAC linker variants.

Over the last decade, our laboratory has explored the development of 4′-phosphopantetheinamide probes whose function serves as a chimeric molecule, wherein the one motif within serves to attach to a carrier protein (CP) and the second to a functional partner protein (PP).[10] In this system, a short but effective pantetheinamide linkage

enables a rapid multidentate processing between the CP and multiple PP domains. During the course of these studies, we realized the importance of developing a modular synthetic approach.[11] Ultimately, we were able to convert a task that began as multistep syntheses[12] into a single 'one-pot' reaction.[13]

With modularity in mind, we envisioned a similar 'one-pot' approach that could produce PROTACs in a parallel fashion, and ideally be devoid of intermediary purifications. Developing on advances from the Raines laboratory,[14] we targeted the use of a traceless Staudinger ligation[15] as a means to introduce asymmetry through a chemoselective amide bond formation.

The general process began with the *in situ* formation of an activated ester from one of the two proteins of interest (POI) ligands, as shown by activation of **4** by CDI (Scheme 2-1). This was then followed by a subsequent amide coupling with azidoamino-linkers **3a–3c**. The resulting azides **5a–5c** could then be coupled with thioester **6** to yield the second amide bond formation in a chemoselective manner through traceless Staudinger chemistry.[14,15] After engagement of the phosphine with the azide, the resulting aza-ylide intermediate[14a] is designed to undergo an intramolecular attack on the thioester, yielding **1a–1c** and **2a–**

2c after hydrolysis. We tested this approach by preparing two model PROTACs.

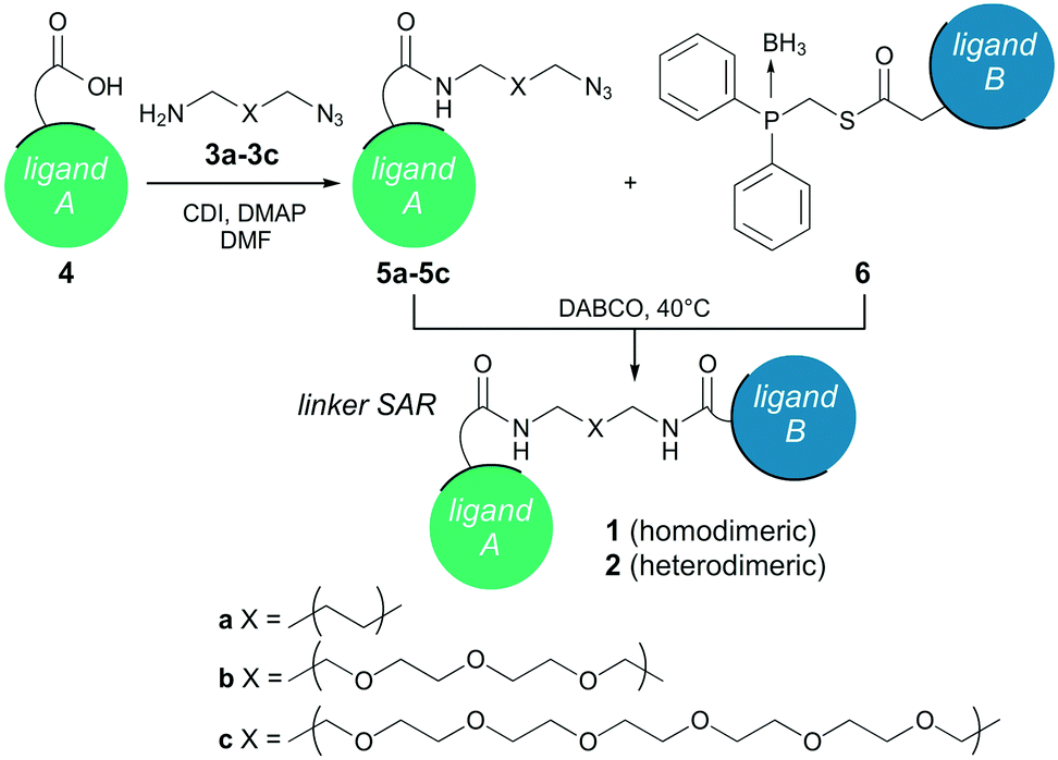

Scheme 2-1: The 'one-pot' PROTAC assembly approach begins with conversion of a carboxylic acid functional group **4** to its an acyl-imidazolate *in situ* followed by coupling to amines **3a–3c**. The resulting azides **5a–5c** are then coupled with thioester **6**, yielding bifunctional molecules **1a–1c** and **2a–2c**. We chose to use *N,N*-carbonyldiimidizole (CDI) for our initial study due to the ease of by-product removal, however other coupling reagents may be used.

In our first example, we examined the $CRL4^{CRBN}$ ubiquitin E3 ligase with IMiD-based ligands due to their documented risk of hydrolysis.[16] In comparison to other E3 ligase ligands,[17] the IMiD-based PROTACs pose greatest risk of hydrolysis under the Staudinger ligation conditions. This increases the likelihood of this method translating to other currently used E3 ligase ligands.[17] This was then partnered with the targeting of cereblon (CRBN) based on the recent demonstration of CRBN homodimeric PROTACs (**1a–1c**) (Scheme 2-1).[18]

We began by preparing thalidomide acid **7** in 6 steps with a 21% overall yield (Appendix Scheme 2-1),[19] which was accomplished on gram scale. Acid **7** was in turn coupled with thiol **9** to deliver borane-protected phosphine thioester **10** (Scheme 2-2). To our delight, **10** was obtained in high yield, and stored up to a month under dry conditions.

Scheme 2-2: Application to homobifunctional PROTACs. Three PROTACs **1a–1c** were assembled in a one-pot fashion beginning with thalidomide acid **7**. Compound **10** was synthesized and isolated from thiol **9** prior to the one-pot procedure. Intermediates **8a–8c** were formed *in situ* and were not isolated.

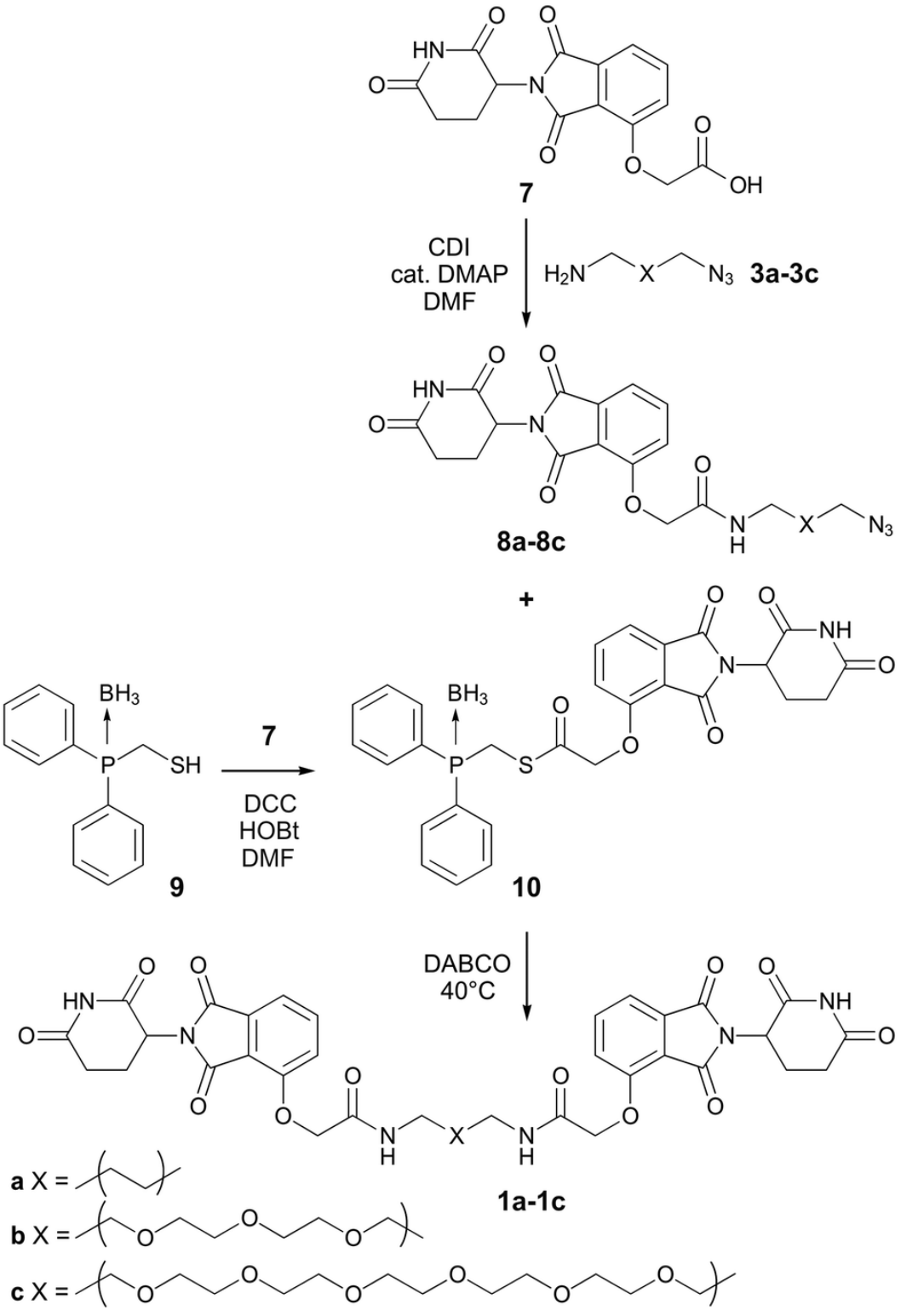
7
CDI
cat. DMAP
DMF
3a-3c
8a-8c
+
9
7
DCC
HOBt
DMF
10
DABCO
40°C
1a-1c
a X =
b X =
c X =

We then turned to explore the use of intermediate **10** as a tool to expedite the synthesis of homodimeric PROTACs. Targeting **1a–1c** (Scheme 2-2), a 55 mM stock solution the acyl imidazole was prepared by reacting **7** with 1.5 eq. of CDI in DMF. This solution was added to the respective reaction vessels containing 100 mM **3a**, **3b**, or **3c** in DMF along with 10 mol% of DMAP. After 3 h, TLC and LC/MS analyses indicated that the first bond formation reaction was complete, providing azides **8a–8c** in DMF. A 43 mM solution of thalidomide thioester **10** (1.5 eq.) was then added at room temperature followed by DABCO (4.5 eq.) as a 460 mM solution in DMF. Here, the DABCO played a key role in liberating the phosphine by forming lower energy complex with the borane.[20] This *in situ* phosphine liberation provided an excellent strategy to selectively engage reactivity as well as prevent unwanted phosphine oxidation.[21] The process was completed by the triggering of an intramolecular Staudinger ligation[14,15,21] through the addition of DABCO and heating the reaction to 40 °C, affording homo-PROTACs **1a–1c**, as confirmed by LC-MS analysis (Appendix Figures 2-3 – 2-5).

While an effective strategy, this approach provided only moderate yields due in part accumulation of azides **8a–8c** arising from the incomplete consumption of amines **3a–3c** during the first amide bond

formation, which ultimately reacted further with **10** to further yield additional **8a–8c**. While not a problem for homobifunctional **1** (ligand A = B, Scheme 2-1), this unwanted reactivity would scramble heterobifunctional **2** (ligand A ≠ B, Scheme 2-1) resulting in undesired mixtures of **1** and **2**. In our hands, the mixture of compounds **1a–b** and **8a–b**, respectively, proved to be inseparable on silica, and only modestly separable on reverse-phase UPLC (Appendix Figures 2-3 – 2-5). Compound **1c** was isolated with a 10% yield.

To this end, our attention shifted to the heterobifunctional bromodomain degrader dBET1[22] **2a** and its analogues **2b–2c** (Scheme 2-3). This system was chosen due to prior extensive chemical biological evaluation as exemplified by the structural studies showing ternary complex formation (Appendix Figure 2-2),[23] as well as its use as a model system for other PROTAC synthetic methodological studies.[9]

Scheme 2-3: Application to heterobifunctional PROTACs. Three heterodimeric PROTACs **2a–2c** were assembled in a one-pot fashion beginning with **7** (route A) or **8** (route B). The choice of coupling reagent should be optimized for each system in order to consume the linker amine **3** and avoid aberrant reactivity and consumption of thioester **6** (Scheme 2-1). This process can be conducted on analytical scales and evaluated prior to use. One-pot procedure beginning with **7** may require HPLC purification, however starting with a collection of degrader building blocks **8** (commercially available) enables purification *via* standard flash column chromatography. Both methods are conducive to parallel synthesis, thereby producing all linker variants in a concerted effort from a stock solution of thioester **6** (Scheme 2-1).

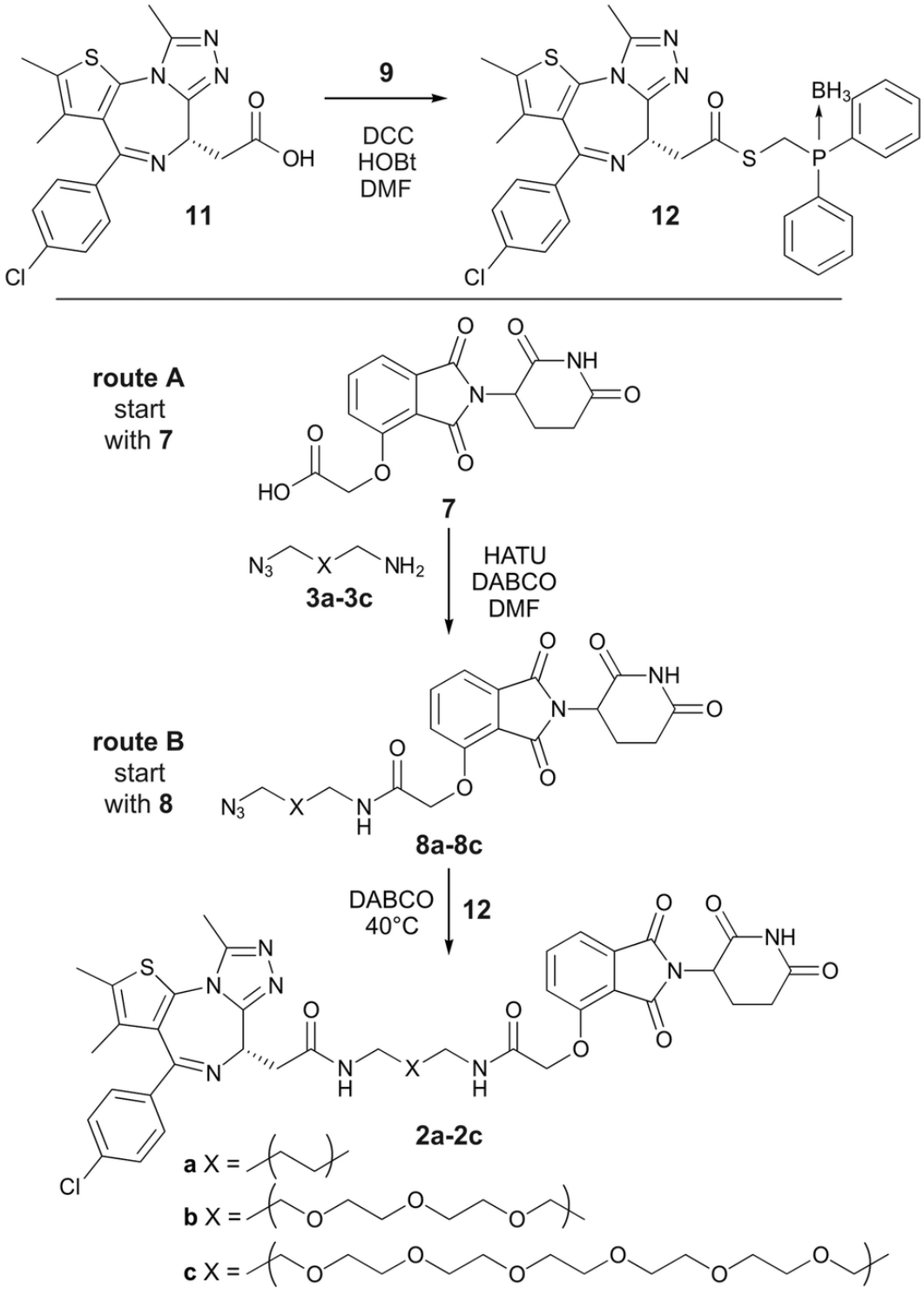
9
DCC
HOBt
DMF
11
12
route A
start
with 7
7
HATU
DABCO
DMF
route B
start
with 8
8a-8c
DABCO
40°C
12
2a-2c
a X =
b X =
c X =

Access to heterobifunctional PROTACs arose by reorganizing the approach to focus on proper choice in the thioester component. As shown in Scheme 2-1, (+)-JQ1 acid **11** was converted to thioester **12** (Scheme 2-3), which like its thalidomide counterpart **10** (Scheme 2-2), could be purified and stored under dry conditions.

Next, we optimized the coupling of **7** to **3b** and found improved yields with using HATU (route A, Scheme 2-3) over CDI (used in Scheme 2-2). Improving the yield of this step played a critical role in the success of the operation as it avoided aberrant reactivity and consumption of thioester **6** (Scheme 2-1). Starting with thalidomide acid **7** (1.3 eq.) and HATU (1.3 eq.), 110 mM linker amine **3b** (1 eq.), and 900 mM DABCO were added as solutions in DMF. This yielded azide **8b***in situ*. Upon addition of 73 mM (+)-JQ1 thioester **12** in DMF (1 eq.), followed by warming to 40 °C, the Staudinger ligation was initiated yielding compound **2b** in a 'one pot' fashion. LC-MS analyses indicated that **2b** was obtained in 48% yield (Appendix Figure 2-6). However, it also indicated that purification of **2b** from this mixture (Appendix Figures 2-7 – 2-10) likely required development of precise prep-HPLC techniques, a common issue associated with PROTAC synthesis.[24]

For our purposes, we sought a method that would deliver PROTACs in a parallel fashion that would be amenable to purification *via* conventional flash chromatography. To achieve this, we returned to our reaction design and identified an improved approach (route B, Scheme 2-3). Here, we chose to purify azides **8a** and **8c**, and perform the Staudinger ligation[14,15,21] in parallel with a stock solution of (+)-JQ1 thioester **12**. This simplification arose from the fact that many E3-ligase ligands with linker-azides and linker-primary amines (thioester **6** can be used directly as an activated ester) can be prepared, aliquoted, and stored on gram scales (several are now commercially-available). To our delight, this method yielded compounds **2a** and **2c** in 54% and 85%, respectively, after flash column chromatography (see Appendix). Here, we were able to repetitively add 66 mM (+)-JQ1 thioester **12** stock solution (1.2 eq.) in DMF to respective reaction vessels containing azides **8a** or **8c** (1 eq.). The Staudinger ligation[14,15,21] was then initiated by addition of 760 mM stock solution of DABCO (3.6 eq.), and heating to 40 °C. This yielded compounds **2a** and **2c** in a concerted effort. Most importantly, the impurity profile did not contain aberrant homobifunctional products (Appendix Figures 2-11 and 2-12), which even in small quantities could complicate

biological evaluation. Compound **2b** was later prepared and purified using this strategy with a 39% yield.

PROTAC linker design remains rather empirical, although considerable effort has been dedicated to exploring the role of linker chemistry on degrader potency and selectivity.[25] The one-pot strategy developed herein, provides an expedient approach that unites the availability of degrader building blocks, with the throughput of parallel synthesis as a means to expedite material delivery. Here, we define a practical strategy to efficiently assemble heterobifunctional small molecules. Effective desymmetrization was enabled through the chemoselectivity afforded by traceless Staudinger ligation chemistry, allowing PROTAC assembly in a single pot.

Overall, we have provided variants of the method to meet the various chromatographic capabilities of different laboratory settings. This type of strategy will enable rapid biological evaluation of PROTACs and will help 'demystify' the nuances of PROTAC linker chemistry by providing a platform for rapid liker diversification. Efforts are currently underway to explore other strategies, such as applications of one-pot SNAr reactions between amino terminal linkers and 4-fluoro-thalidomide,[26] and traceless

Staudinger ligation chemistry[14,15,21] with water-soluble phosphines,[27] therein further reducing the chromatographic complexity.

We thank Yongxuan Su (UCSD) for mass spectral analyses and Anthony Mrse (UCSD) for assistance with acquiring NMR spectral data. T. A. B. was supported in part by UC San Diego and NIH grant GM095970.

Chapter 2, in full, is a reprint of the material as it appears in the Journal of Medicinal Chemistry. Bemis, Troy A.; La Clair, James J.; Burkart, Michael D., American Chemical Society, 2021.

APPENDIX

Appendix Figure 2-1: Ubiquitin conjugation and associated-protein degradation. a) Schematic representation of the activation of an E3 (blue) ligase by ubiquitinylation of E1 (dark blue) followed by E2 engagement and trans-thioesterification. b) Schematic representation of how a normal E3 ligase targets its substrate (S, light blue) for proteolysis. c) Complementary process where a heterobifunctional molecule or PROTAC (p, yellow) is used to target the degradation of a protein of interest (POI, green). In this process, the PROTAC contains motifs that bind to both POI and E3 ligase.

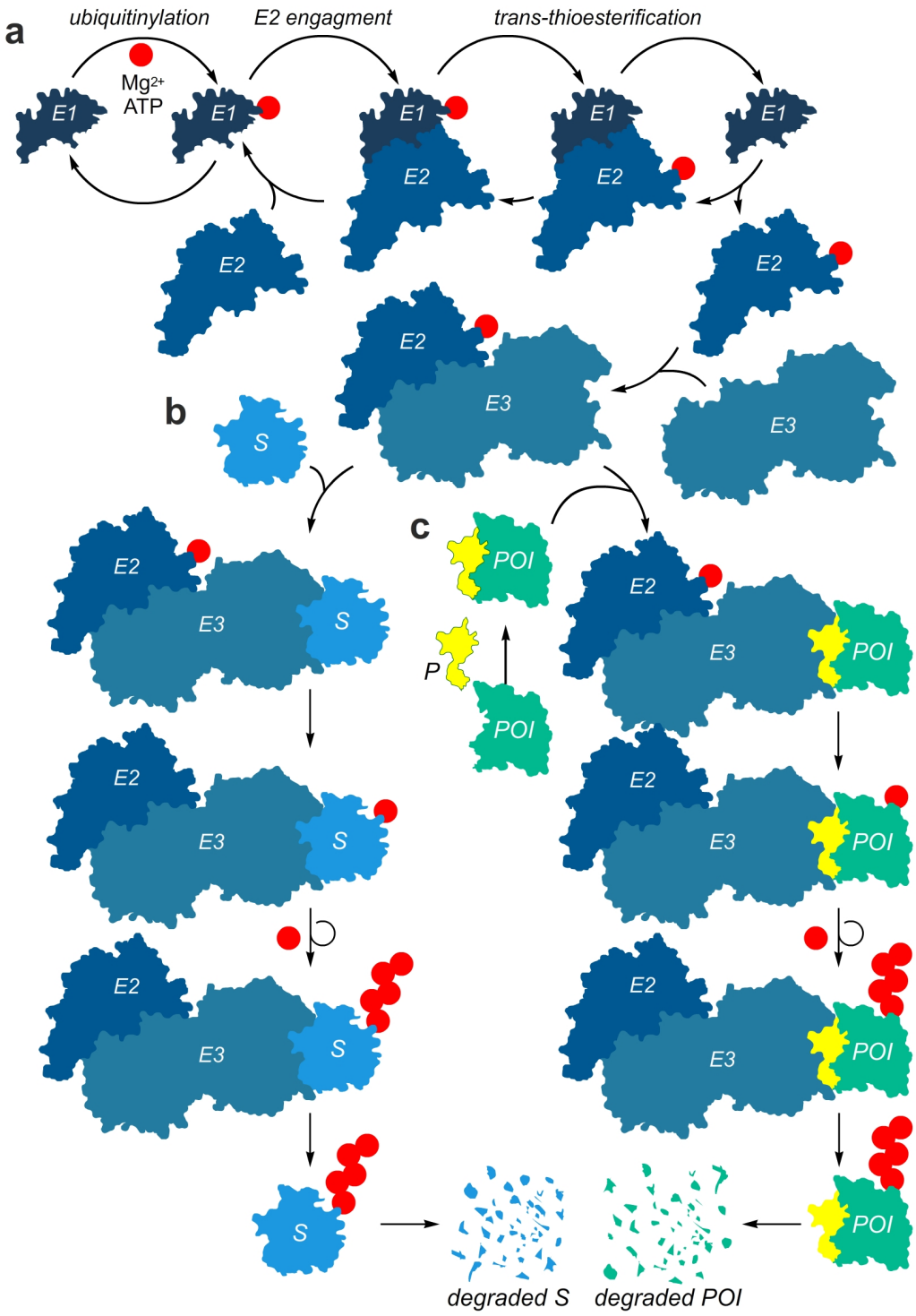
a
ubiquitinylation
E2 engagment
trans-thioesterification
Mg2+
ATP
E1
E2
b
E3
S
c
POI
P
degraded S
degraded POI

Appendix Figure 2-2: Structural-basis for PROTAC diversification. a) Structure of the dBET23 ligand. b) Structure of the dBET6 ligand. c) X-ray crystal structure (PDB = 6BN7)[23] depicting the binding of the dBET23 ligand (yellow) between the E3 ligase CRBN-CTD (blue) and protein of interest, $BRD4^{B01}$. d) X-ray crystal structure (PDB = 6BOY)[23] depicting the binding of the dBET6 ligand (yellow) between the E3 ligase CRBN-CTD (blue) and protein of interest, $BRD4^{B01}$.

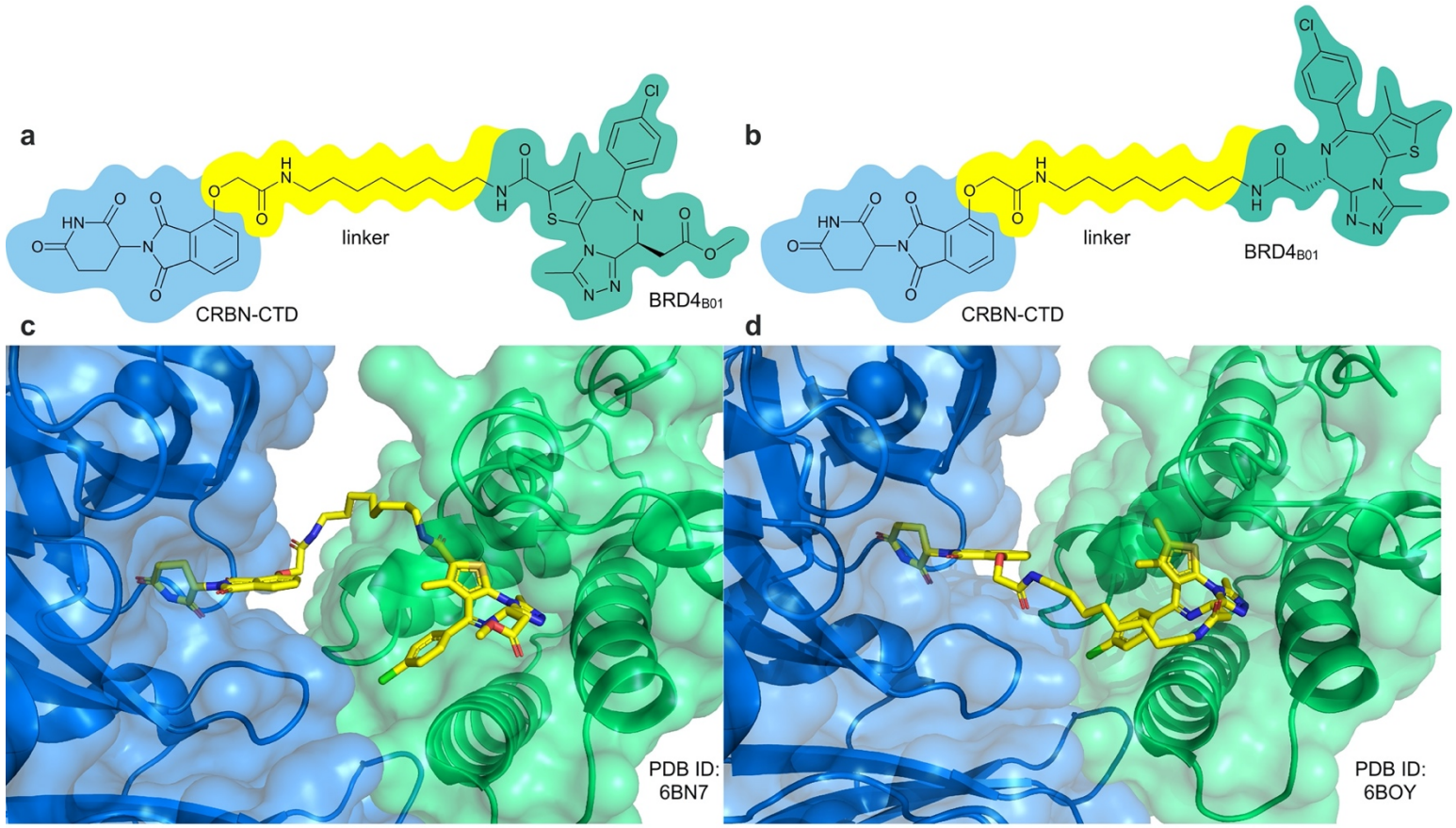
a
linker
CRBN-CTD
BRD4B01
b
linker
CRBN-CTD
BRD4B01
c
PDB ID:
6BN7
d
PDB ID:
6BOY

B. General Materials and Methods.

Chemical reagents were purchased from Acros, Fluka, Sigma-Aldrich, or TCI and any further purifications will be denoted in the following section. Deuterated NMR solvents were purchased from Cambridge Isotope Laboratories. All reactions were conducted with rigorously dried anhydrous solvents that were obtained by passing through a solvent column composed of activated A1 alumina and dispensed under an atmosphere of argon. An exception was N,N-dimethylformamide (DMF), which was purchased anhydrous (EMD Millipore) and used without further purification via provided septa. Acetonitrile and amines were dried via storage over molecular sieves and used as provided. DABCO was purified fresh before use through sublimation under reduced pressure at 45 °C. All reactions were performed under a positive pressure of argon via balloons unless otherwise noted and glassware was oven-dried and sealed with septa. Stirring was accomplished using Teflon coated stir-bars using an IKA RCT-basic mechanical stirrer. Solutions were heated using silicon oil baths. Analytical Thin Layer Chromatography (TLC) was performed on Silica Gel 60 F254 precoated glass plates (EMD Millipore). Preparative TLC (pTLC) was conducted on Silica Gel 60 F254 plates (EMD Millipore) that were pre-run with chloroform in order to minimize binder grease.

Visualization was achieved with UV light (254 nm, 365 nm) and/or $KMnO_4$. Flash column chromatography was carried out with Geduran Silica Gel 60 (230-400 mesh) from Fischer Scientific. ^1H NMR spectra were recorded on Varian Mercury Plus 400 or Varian VX500 spectrometers. ^{13}C NMR spectra were recorded at 125 MHz on a Varian VX500 spectrometer equipped with an Xsens Cold probe or at 100 MHz on a Varian Mercury 400 Plus spectrometers. Chemical shifts for ^1H NMR and ^{13}C NMR were referenced to the reported values of Gottlieb[28] using the signal from the residual solvent ^1H or ^{13}C signals from the deuterated solvent. Chemical shift δ values for ^1H and ^{13}C spectra are reported in parts per million (ppm) relative to these referenced values. Multiplicities are abbreviated as; s = singlet, d = doublet, t = triplet, q = quartet, m = multiplet, bs = broad signal. All ^{13}C spectra were recorded with complete proton decoupling. FID files were processed using MestreNova 14.0.1 (MestreLab Research). LC-MS was performed on a Waters SQ detector (quadrupole) in either positive or negative electrospray ionization (ESI) modes with a serial Waters Acquity TUV detector, Waters Acquity column manager and Waters Acquity binary solvent manager. Spectral data and procedures are provided for all compounds and spectral data for key compounds are explicitly provided.

Compounds not cited in the paper from here on will be numbered starting with **S1**.

C. Synthesis of thalidomide acid 7. Samples of acid 7 were synthesized from furan-2(5H)-one (**S1**) and Boc-glutamine (**S5**) in 8 steps as shown in Scheme S1.

Appendix Scheme 2-1: Synthetic route used to synthesize thalidomide acid **7**, adapted from the conditions outlined by Lohbeck and Millller.[29]

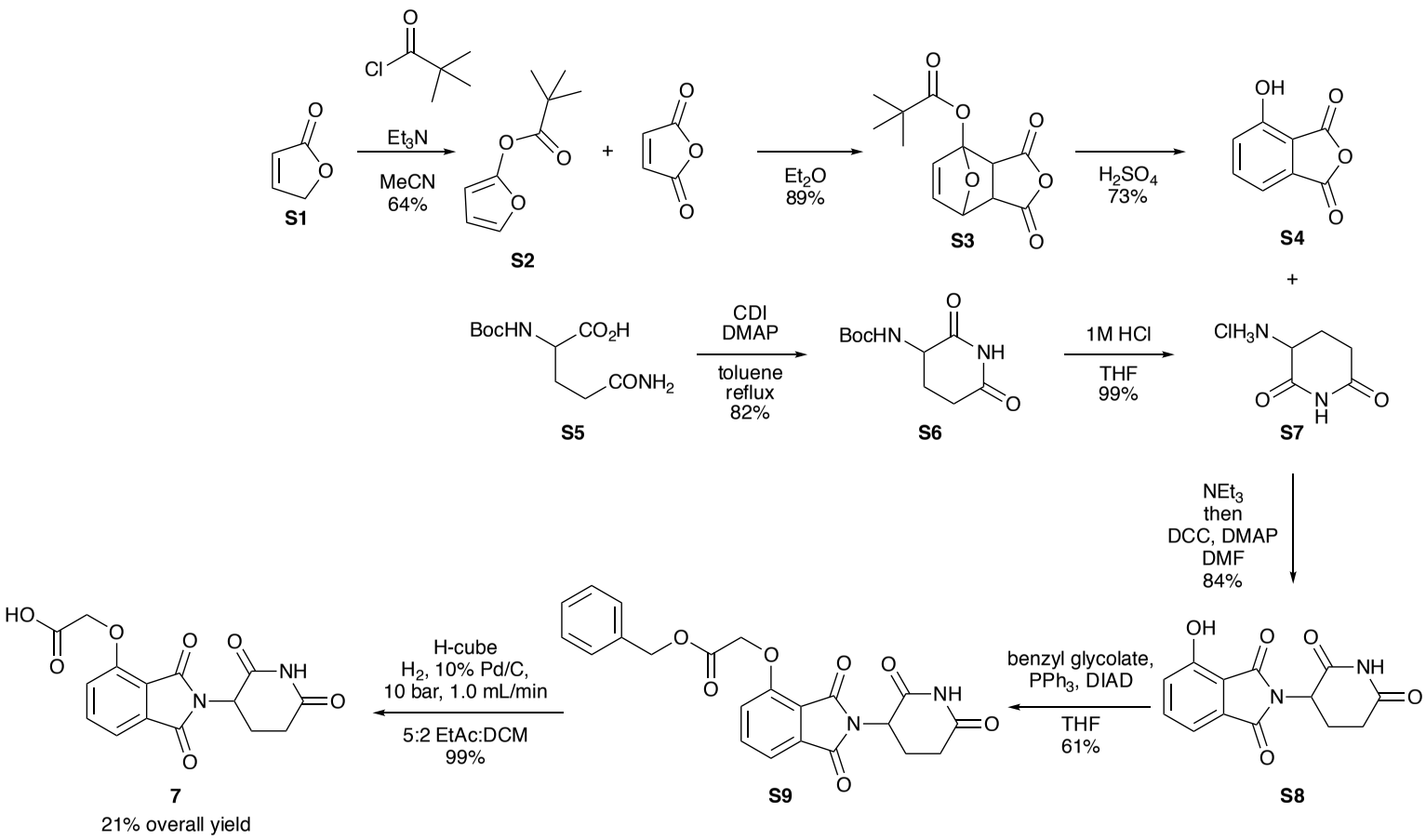
Et3N
MeCN
64%
Et2O
89%
H2SO4
73%
CDI
DMAP
toluene
reflux
82%
1M HCl
THF
99%
NEt3
then
DCC, DMAP
DMF
84%
benzyl glycolate,
PPh3, DIAD
THF
61%
H-cube
H2, 10% Pd/C,
10 bar, 1.0 mL/min
5:2 EtAc:DCM
99%
S1
S2
S3
S4
S5
S6
S7
S8
S9
7
21% overall yield

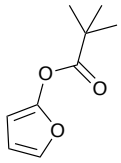

S2

Furan-2-yl pivalate (S2). Furan-2(5*H*)-one (**S1**) (1.7 mL, 23.8 mmol) and pivaloyl chloride (3.5 mL, 28.6 mmol) were dissolved in dry CH_3CN (10 mL) under an Ar atmosphere. Et_3N (4.0 mL, 28.6 mmol) dissolved in dry CH_3CN (5 mL) and added drop wise to the reaction over the course of 5 min *via* a pressure equalizing addition funnel. The reaction was stirred 19 h resulting a brown, opaque solution. The precipitate was filtered off and washed with Et_2O. The organic phase was then washed with 10% w/v Na_2CO_3, dried over Na_2SO_4 and concentrated via nitrogen flow. CAUTION: product is volatile. Crude material was then purified via flash column chromatography (1:20 EtOAc/hexanes), yielding 2.6 g of **S2** (64%), a clear, colorless to pale yellow oil.

Furan **S2**. ^1H NMR (400 MHz, $CDCl_3$) δ 7.05 (m, 1H), 6.36 (m, 1H), 5.86 (m, 1H), 1.34 (s, 9H); ^{13}C NMR (125 MHz, $CDCl_3$) δ 174.7, 151.6, 135.4, 111.3, 92.3, 39.3, 27.0. Spectral signals matched those by Lohbeck and Miller.[29]

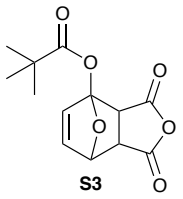

S3

1,3-Dioxo-3,3a,7,7a-tetrahydro-4,7-epoxyisobenzofuran-4(1*H*)-yl pivalate (S3). Furan **S2** (2.58 g, 15.3 mmol) was dissolved in Et_2O (10 mL) under an atmosphere of Ar. Maleic anhydride (1.65 g, 16.9 mmol) was added and the reaction was allowed to stir for 72 h. Yellow solid **S3** (3.63 g, 89%) was collected *via* vacuum filtration, washed with cold Et_2O. Cycloadduct **S3**. ^{1}H-NMR (400 MHz, $CDCl_3$) δ 6.72 (m, 2H), 5.34 (m, 1H), 3.79 (m, 1H), 3.44 (m, 1H), 1.32 (s, 9H); ^{13}C NMR (125 MHz, $CDCl_3$) δ 176.6, 169.4, 166.0, 138.1, 137.2, 111.7, 77.3, 52.7, 49.0, 39.2, 27.0. Spectral signals matched those by Lohbeck and Miller.[29]

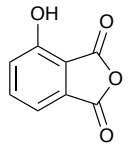

S4

4-Hydroxyisobenzofuran-1,3-dione (S4). Concentrated H_2SO_4 (3 mL) was cooled to -30 °C. Cycloadduct **S3** (1.12 g, 4.20 mmol) was slowly added and stirred for 5 min. The reaction mixture was then poured over crushed ice (3.3 g) and the resulting brown precipitate **S4** (500 mg, 73%) was collected *via* vacuum filtration and dried overnight under vacuum. Anhydride **S4**. ^{1}H NMR (400 MHz, DMSO-d_6) δ 11.74 (s, 1H), 7.78 (dd, J = 8.4, 7.3 Hz, 1H), 7.46 (d, J = 7.3 Hz, 1H), 7.34 (d, J = 8.4 Hz, 1H); ^{13}C NMR (100 MHz, DMSO-d_6) δ 163.5, 160.9, 157.1, 138.2, 132.8, 124.4, 116.1, 114.5. HRMS (+ESI) calc. for $[C_8H_5O_4]^+$ 165.0182 ($[M+H]^+$), found *m/z* 165.0179. Spectral signals matched those by Lohbeck and Miller.[29]

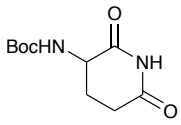

S6

***tert*-Butyl (2,6-dioxopiperidin-3-yl)carbamate (S6). Boc-**glutamine **S5** (2.50 g, 10.15 mmol) was dissolved in THF (12 mL). *N*,*N*-Carbonyldiimidazole (1.86 g, 11.2 mmol) and DMAP (124.0 mg, 1.02 mmol) were added. The solution was brought to reflux for 22 h. The reaction was then cooled to rt and further cooled in an ice bath. The precipitate was filtered off, washed with cold THF yielding 1.89 g of **S6** (82%), a colorless solid.

Carbamate **S6**. ^{1}H NMR (400 MHz, DMSO-d_6) δ 10.75 (s, 1H), 7.13 (d, J = 8.6 Hz, 1H), 4.20 (m, 1H), 2.71 (m, 1H), 2.46 (m, 1H), 1.90 (m, 2H), 1.39 (s, 9H); ^{13}C NMR (100 MHz, DMSO-d_6) δ 173.8, 172.1, 155.4, 78.2, 50.4, 31.0, 28.0, 23.8. HRMS (+ESI) calc. for $[C_{10}H_{16}N_2O_4Na]^+$ 251.1002 ($[M+Na]^+$), found *m/z* 251.1005. Spectral signals matched those by Lohbeck and Miller.[29]

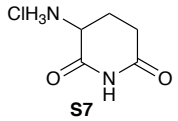

S7

3-Aminopiperidine-2,6-dione hydrochloride (S7). HCl (12 M, 35 mL) was added slowly to MeOH (120 mL) with stirring. *tert*-Butyl (2,6-dioxopiperidin-3-yl)carbamate (**S6**) (1.06 g, 4.66 mmol) was added and the reaction was stirred for 2 h. The solvent was then removed by rotary evaporation yielding 770 mg of **S7** (99%), as a white powder. Glutarimide **S7**. ^{1}H-NMR (400 MHz, DMSO-d_6) δ 11.26 (s, 1H), 8.67 (s, 3H), 4.20 (dd, J = 8.2, 4.5 Hz, 1H), 2.65 (m, 2H), 2.22 (m, 1H), 2.00 (m, 1H). Spectral signals matched those by Lohbeck and Miller.[29]

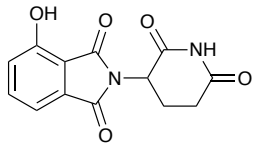

S8

2-(2,6-Dioxopiperidin-3-yl)-4-hydroxyisoindoline-1,3-dione (S8).

Anhydride **S4** (1.04 g, 6.35 mmol) and glutarimide **S7** (0.86 g, 5.20 mmol) and Et_3N (0.76 mL, 5.46 mmol) were dissolved in dry THF (25 mL). The mixture was stirred for 15 min and then brought to reflux for 5 h. After cooling, *N,N*'-dicyclohexylcarbodiimide (1.28 g, 5.85 mmol) and DMAP (64 mg, 0.52 mmol) were added. The reaction mixture was then refluxed overnight. The heat was removed and the reaction was cooled in an ice bath. The precipitate was filtered off via vacuum filtration and washed with THF. The filtrate was concentrate on a rotary evaporator. The crude product was then purified via trituration (CH_2Cl_2/MeOH) yielding 1.19 g of hydroxy-thalidomide **S8** (84%), as a yellow solid. Spectral signals matched those by Lohbeck and Miller.[29]

Hydroxy-thalidomide **S8**. ^{1}H NMR (500 MHz, DMSO-d_6) δ 11.24 (br s, 1H), 11.12 (s, 1H), 7.64 (dd, J = 8.3, 7.2 Hz, 1H), 7.31 (d, J = 7.2 Hz, 1H), 7.24 (d, J = 8.3 Hz, 1H), 5.07 (dd, J = 12.9, 5.4 Hz, 1H), 2.88 (m, 1H), 2.55 (m, 2H), 2.04-1.97 (m, 1H). ^{13}C NMR (125 MHz, DMSO-d_6) δ 172.9, 170.2, 167.2, 166.0, 156.0, 136.3, 133.2, 124.0, 114.2, 113.8, 48.6, 31.0, 22.1.

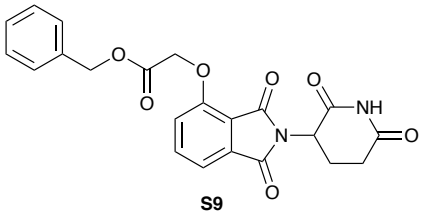

S9

Benzyl 2-((2-(2,6-dioxopiperidin-3-yl)-1,3-dioxoisoindolin-4-yl)oxy)acetate (S9). 2-(2,6-dioxopiperidin-3-yl)-4-hydroxyisoindoline-1,3-dione (**S8**) (49.4 mg, 0.18 mmol) and PPh_3 (72.9 mg, 0.28 mmol) were dissolved in THF (1 mL) under argon with 4Å molecular sieves. Benzyl glycolate (30.0 μL, 0.20 mmol) was added and the mixture was sonicated for 10 min. DIAD (40 μL, 0.20 mmol) was added drop wise to the solution and sonication continued for an additional 30 min. The reaction was then moved to a stir plate and allowed to stir for an additional 20 h. The sieves were filtered off and washed with EtOAc (1 mL) and the reaction mixture was partitioned between EtOAc (30 mL) and water (20 mL). Aqueous layer was extracted with EtOAc (30 mL) and the combined organic phases were dried over Na_2SO_4 and concentrated on a rotary evaporator. The crude material was further purified *via* flash column chromatography (65% EtOAc/hexanes) to yield 46.7 mg of benzyl-thalidomide **S9** (61%), as a white foam.

Benzyl-thalidomide **S9.** ^{1}H NMR (400 MHz, $CDCl_3$) δ 8.25 (s, 1H), 7.61 (dd, J = 8.4, 7.3 Hz, 1H), 7.50 (d, J = 7.3 Hz, 1H), 7.34 (m, 5H), 7.07 (d, J

= 8.4 Hz, 1H), 4.89 (m, 3H), 2.80 (m, 3H), 2.11 (m, 1H); ^{13}C NMR (125 MHz, $CDCl_3$) δ 171.1, 168.1, 167.9, 166.9, 165.5, 155.4, 136.5, 135.0, 134.0, 128.8, 128.8, 128.7, 126.9, 120.1, 117.8, 117.3, 67.5, 66.4, 49.3, 31.5, 22.7; HRMS (+ESI) calc. for $[C_{22}H_{18}N_2O_7NH_4]^+$ 440.1452 ($[M+NH_4]^+$), found *m/z* 440.1452, calc. for $[C_{22}H_{18}N_2O_7Na]^+$ 445.1006 ($[M+Na]^+$), found *m/z* 445.1005. Spectral signals matched those by Lohbeck and Miller.[29]

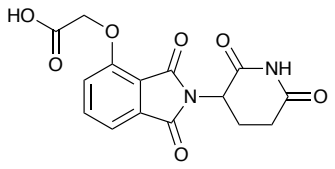

7

2-((2-(2,6-dioxopiperidin-3-yl)-1,3-dioxoisoindolin-4-yl)oxy)acetic acid (7). Benzyl-thalidomide **S9** (258.8 mg, 0.6 mmol) was dissolved in a 5:3 mixture of EtOAc:CH_2Cl_2 (150 mL) and eluted through an H-cube flow hydrogenolysis apparatus (10% Pd/C, 10 bar, 1.0 mL/min). Receiver flask was concentrated on a rotary evaporator yielding 208.6 mg of acid **7** (99%), as a white powder.

Acid **7**. ^{1}H NMR (500 MHz, DMSO-d_6) δ 13.23 (br s, 1H), 11.13 (s, 1H), 7.79 (dd, J = 8.5, 7.3 Hz, 1H), 7.47 (d, J = 7.2 Hz, 1H), 7.39 (d, J = 8.5 Hz, 1H), 5.11 (dd, J = 12.8, 5.4 Hz, 1H), 4.99 (s, 2H), 2.93-2.85 (m, 1H), 2.63-2.47 (m, 2H), 2.06-2.01 (m, 1H). HRMS (-ESI) calc. for $[C_{15}H_{11}N_2O_7]^-$ 331.0569 (M^-), found *m/z* 331.0569. Spectral signals matched those by Lohbeck and Miller.[29]

D. Synthesis of (+)-JQ1 thioester 12. A two-step procedure was used to prepare thioester **12** from (+)-JQ1 as shown in Supplementary Scheme S2.

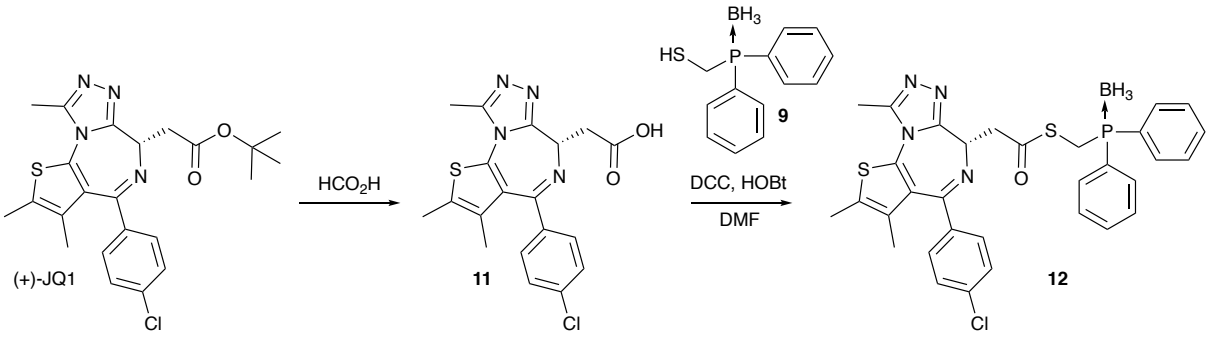

Appendix Scheme 2-2. Synthetic route to (+)-JQ1 thioester **12.** Synthetic route of **11** adapted from Winter *et. al*.[4a]

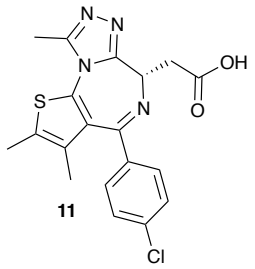

11

(*S*)-2-(4-(4-chlorophenyl)-2,3,9-trimethyl-6*H*-thieno[3,2-*f*][1,2,4]triazolo[4,3-*a*][1,4]diazepin-6-yl)acetic acid (11).

(+)-JQ1 (24.3 mg, 0.053 mmol) was stirred in anhydrous HCO_2H (4 mL) under an Ar atmosphere for 48 h. Solvent was removed by rotary evaporation yielding 22.8 mg of acid **11** (99%) and was used without further purification.

(+)-JQ1 acid **11**. ^{1}H NMR (400 MHz, $CDCl_3$) δ 7.43 (d, J = 8.0 Hz, 2H), 7.34 (d, J = 8.0 Hz, 2H), 4.61 (t, J = 8 Hz, 1H), 3.66 (m, 2H), 2.70 (s, 3H), 2.41 (s, 3H), 1.69 (s, 3H); LRMS (-ESI) calc. for $[C_{19}H_{16}ClN_4O_2S]^-$ 399.07 ($[M-H]^-$), found *m/z* 398.95. Spectral signals matched those by Winter *et. al.*[4a]

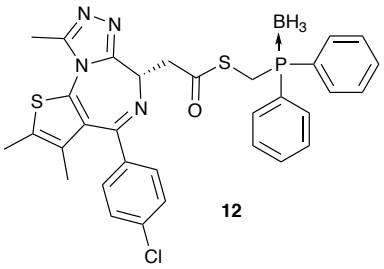

12

***S*-((diphenylphosphaneyl)methyl) (*S*)-2-(4-(4-chlorophenyl)-2,3,9-trimethyl-6*H*-thieno[3,2-*f*][1,2,4]triazolo[4,3-*a*][1,4]diazepin-6-yl)ethanethioate borane complex (12).** Acid **11** (10.0 mg, 0.025 mmol) and HOBt (3.7 mg, 0.027 mmol) were dissolved in DMF (0.3 mL) under an Ar atmosphere. DCC (5.7 mg, 0.027 mmol) was added. After stirring at rt overnight, thiol **9** (6.8 mg, 0.027 mmol) was added as a solution in CH_2Cl_2 (0.2 mL). After stirring overnight, the solvent was removed *via* vacuum and the crude material was purified on a microcolumn containing 1 g of silica gel. Column was eluted first with Et_2O (10 mL) and then EtOAc (10 mL). Rotary evaporation of the EtOAc fraction returned at 5.0 mg of **12** (32%). The reaction product could be used without silica gel purification. Thioester **12**. ^{1}H NMR (500 MHz, $CDCl_3$) δ 7.72 (m, 4H), 7.46 (m, 6H), 7.36 (d, J = 8.7 Hz, 2H), 7.30 (d, J = 8.7 Hz, 2H), 4.57 (dd, J = 9.0, 4.5 Hz, 1H), 3.84 (m, 3H), 3.68 (dd, J = 16.1, 4.5 Hz, 1H), 2.66 (s, 3H), 2.42 (s, 3H), 1.69 (s, 3H); ^{13}C NMR (125 MHz, $CDCl_3$) δ 197.4, 165.0, 154.5, 150.1, 137.0, 136.5, 132.6 (d, J = 9.5 Hz), 132.6 (d, J = 9.5 Hz), 132.3,

132.0 (d, *J* = 2.5 Hz), 131.9 (d, *J* = 2.5 Hz), 131.3 (d, *J* = 9.7 Hz), 131.1 (d, *J* = 10.4 Hz), 130.4, 130.1, 129.5 (d, *J* = 10.5 Hz), 129.3 (d, *J* = 10.2 Hz), 129.1 (d, *J* = 10.0 Hz), 129.0 (d, *J* = 10.0 Hz), 128.8, 127.9 (d, *J* = 55.1 Hz), 127.6 (d, *J* = 55.3 Hz), 124.0, 118.7, 111.2, 53.8, 45.8, 23.7 (d, *J* = 34.5 Hz), 14.6, 13.29, 12.0; LC-MS (+ESI) calc. for $[C_{32}H_{32}BClN_4OPS_2]^+$ 629.15 ($[M+H]^+$), found *m/z* 629.26.

E. Synthesis of thalidomide thioester 10. A two-step procedure was used to prepare thioester **10** from acid **7** and thioester **S10** as shown in Supplementary Scheme S3.

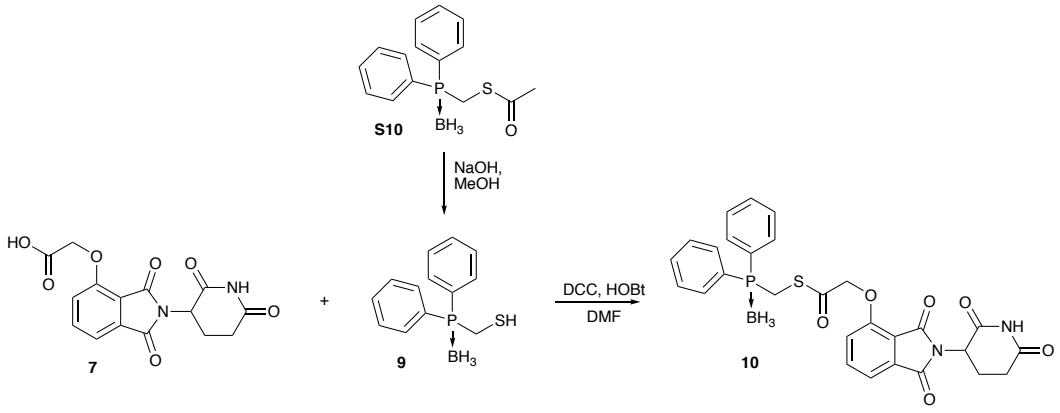

Appendix Scheme 2-3. Synthesis of thalidomide thioester **10** adapted from Mühlberg *et. al.*[21]

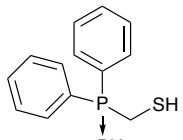

9

Diphenylphosphaneylmethanethiol borane complex (9). Thioester **S10** (91.8 mg, 0.319 mmol) was dissolved in MeOH (2 mL). NaOH (25.1 mg, 0.637 mmol) was added as a solid. After stirring for 3 h at rt, the solvent was removed *via* rotary evaporation. The crude residue partitioned between CH_2Cl_2 (30 mL) and 0.5 M HCl (30 mL). Organic phase was washed with 0.5 M HCl (30 mL), brine (30 mL) and then dried over Na_2SO_4 and concentrated *via* rotary evaporation affording 84.2 mg of **9** (99%), which was used without further purification.

Thiol **9**. ^{1}H NMR (500 MHz, $CDCl_3$) δ 7.60 (m, 10H), 3.19 (dd, J = 8.2, 6.1 Hz, 2H), 1.89 (td, J = 8.2, 8.1, 6.7 Hz, 1H), 1.40-0.72 (br m, 3H); ^{13}C NMR (125 MHz, $CDCl_3$) δ 132.6 (d, J = 9.0 Hz), 131.8 (d, J = 2.4 Hz), 129.1 (d, J = 10.0 Hz), 127.8 (d, J = 55.2 Hz), 19.8 (d, J = 32.6 Hz).

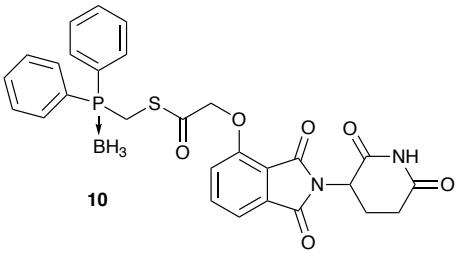

10

***S*-((diphenylphosphaneyl)methyl) 2-((2-(2,6-dioxopiperidin-3-yl)-1,3-dioxoisoindolin-4-yl)oxy)ethanethioate borane complex (10).** Acid **7** (31.5 mg, 0.095 mmol) and HOBt (14.5 mg, 0.100 mmol) were dissolved in DMF (0.4 mL) under an Ar atmosphere. DCC (24.8 mg, 0.120 mmol) was added. After stirring at rt for 30 min, thiol **9** (21.2 mg, 0.086 mmol) was added as a solution in DMF (0.35 mL). The resulting solution was stirred at rt for 18 h. The solution was filtered to remove the precipitate and filtrate concentrated on a rotary evaporator. Note: do not attempt aqueous workup or thioester will hydrolyze. The crude product was then purified by flash column chromatography 7:3 EtOAc/hexanes to yielding 35.3 mg of **10** (73%), as a white wax.

Thioester **10**. ^{1}H NMR (500 MHz, $CDCl_3$) δ 8.13 (s, 1H), 7.60 (m, 12H), 6.98 (d, *J* = 8.4 Hz, 1H), 4.97 (dd, *J* = 12.4, 5.3 Hz, 1H), 4.87 (s, 2H), 3.77 (d, *J* = 6.9 Hz, 2H), 2.82 (m, 3H), 2.16 (m, 1H), 1.24 (m, 3H); ^{13}C NMR (125 MHz, $CDCl_3$) δ 194.6, 171.0, 168.0, 166.7, 165.3, 154.8, 136.7, 134.0, 132.6 (d, *J* = 9.5 Hz), 132.0 (d, *J* = 2.5 Hz), 129.1 (d, *J* = 10.2 Hz),

127.4 (d, J = 55.4 Hz), 120.5, 118.1, 117.9, 73.6, 49.4, 31.5, 22.8 (d, J = 32.4 Hz), 22.7; LRMS **(**+ESI) calc. for $[C_{28}H_{24}N_2O_6PS]^+$ 547.11 ($[M-BH_3+H]^+$), found *m/z* 547.18, $[C_{28}H_{23}N_2NaO_6PS]^+$ 569.09 ($[M-BH_3+Na]^+$), found *m/z* 569.09, $[C_{28}H_{26}BN_2NaO_6PS]^+$ 583.12 ($[M+Na]^+$), found *m/z* 583.07.

F. Synthesis of thalidomide azides 8a and 8c. The following methods were used to prepare thalidomide azides **8a** and **8c**.

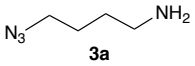

3a

4-azidobutan-1-amine (3a).

Azidoamine **3a** was synthesized using previously published methods and spectral signals matched those provided.[7]

Amine **3a**. ^{1}H NMR (400MHz, $CDCl_3$) δ 3.28 (t, J = 6.7 Hz, 2H), 2.73 (t, J = 6.9 Hz, 2H), 2.67 (br s, 2H), 1.58 (m, 4H); ^{13}C NMR (100 MHz, $CDCl_3$) δ 51.4, 41.4, 30.2, 26.4; HRMS (+ESI) calc. for $[C_4H_{11}N_4]^+$ 115.0978 ($[M+H]^+$), found *m/z* 115.0976.

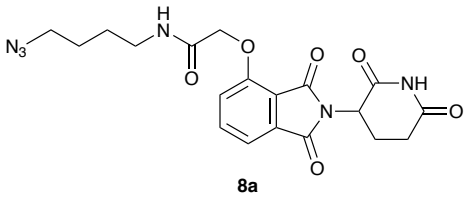

8a

***N*-(4-azidobutyl)-2-((2-(2,6-dioxopiperidin-3-yl)-1,3-dioxoisoindolin-4-yl)oxy)acetamide (8a).** Acid **7** (8.2 mg, 0.025 mmol), azidoamine **3a** (3.4 mg, 0.030 mmol) and Et*i*Pr$_2$ (10 μL, 0.062 mmol) were dissolved in DMF (0.2 mL) under an Ar atmosphere. HATU (12.2 mg, 0.045 mmol) was added and the reaction stirred for 24 h. Reaction was diluted with EtOAc (10 mL). The organic phase was then washed with sat. NH_4Cl (10 mL), 10% w/v Na_2CO_3 (10 mL) and brine (10 mL). The organic layer was then dried over Na_2SO_4 and concentrated on a rotary evaporator to yield 5.4 mg of azide **8a** (50%).

Azide **8a**. ^{1}H NMR (500MHz, $CDCl_3$) δ 8.21 (br s, 1H), 7.75 (m, 1H), 7.55 (m, 2H), 7.20 (d, *J* = 8.3 Hz, 1H), 4.98 (dd, *J* = 12.4, 5.3 Hz, 1H), 4.65 (s, 2H), 3.42 (q, *J* = 6.2 Hz, 2H), 3.32 (t, *J* = 6.2 Hz, 2H), 2.80 (m, 3H), 2.18 (m, 1H), 1.70 (m, 4H); ^{13}C NMR (125 MHz, $CDCl_3$) δ 170.9, 168.1, 167.0, 166.7, 166.3, 154.6, 137.3, 133.6, 119.8, 118.3, 117.7, 68.3, 51.2, 49.4, 38.8, 31.5, 26.7, 26.4, 22.7; LC-MS **(**+ESI) calc. for $[C_{19}H_{21}N_6O_6]^+$ 429.15 ($[M+H]^+$), found *m/z* 429.19. Spectral signals matched those previously reported.[4a]

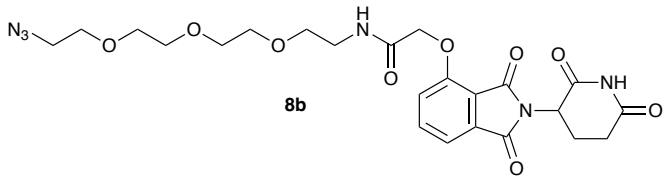

8b

N-(2-(2-(2-(2-azidoethoxy)ethoxy)ethoxy)ethyl)-2-((2-(2,6-dioxopiperidin-3-yl)-1,3-dioxoisoindolin-4-yl)oxy)acetamide (8b). Acid **7** (17.3 mg, 0.052 mmol), azidoamine **3b** (14.8 mg, 0.068 mmol) and Et*i*Pr$_2$ (23 μL, 0.130 mmol) were dissolved in DMF (0.2 mL) under an Ar atmosphere. HATU (25.7 mg, 0.068 mmol) was added and the reaction stirred for 24 h. Reaction was diluted with EtOAc (10 mL). The organic phase was then washed with sat. NH_4Cl (10 mL), 10% w/v Na_2CO_3 (10 mL) and brine (10 mL). The organic layer was then dried over Na_2SO_4 and concentrated on a rotary evaporator to yield 13.1 mg of azide **8b** (47%). Azide **8b**. ^{1}H NMR (500MHz, $CDCl_3$) δ 8.70 (br s, 1H), 7.74 (dd, *J* = 8.4, 7.4 Hz, 1H), 7.63 (t, *J* = 5.1 Hz, 1H), 7.55 (d, *J* = 7.4 Hz, 1H), 7.18 (d, *J* = 8.4 Hz, 1H), 4.95 (dd, *J* = 12.2, 5.5 Hz, 1H), 4.65 (s, 2H), 3.63 (m, 14H) 3.40 (m, 2H), 3.32 (t, *J* = 6.2 Hz, 2H), 2.81 (m, 3H), 2.15 (m, 1H); ^{13}C NMR (125 MHz, $CDCl_3$) δ 171.2, 168.2, 167.0, 166.8, 165.9, 154.5, 137.1, 133.7, 119.4, 118.1, 117.5, 72.6, 70.9, 70.6, 70.5, 70.3, 70.0, 69.5, 68.0, 61.9, 50.7, 49.3, 39.2, 31.5, 22.8; HRMS (+ESI) calc. for $[C_{23}H_{29}N_6O_9]^+$ 533.1991 ($[M+H]^+$), found *m/z* 533.1994.

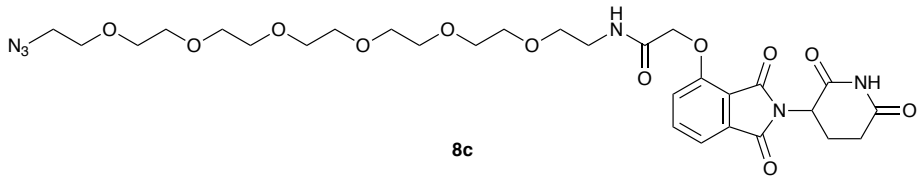

8c

***N*-(20-azido-3,6,9,12,15,18-hexaoxaicosyl)-2-((2-(2,6-dioxopiperidin-3-yl)-1,3-dioxoisoindolin-4-yl)oxy)acetamide (8c).** A solution of **3c** (8.8 mg, 0.025 mmol) in DMF (0.2 mL) was added to thioester **10** (7.0 mg, 0.012 mmol) under an Ar atmosphere. After stirring for 24 h at rt, the reaction was diluted with EtOAc (10 mL). The organic phase was washed with sat. NH_4Cl (10 mL), water (10 mL) and brine (10 mL), dried over Na_2SO_4 and concentrated on a rotary evaporator. Crude material was purified on silica microcolumn containing 1 g of silica gel (EtOAc to 1:4 MeOH/EtOAc) to yield 6.3 mg of azide **8c** (73%).

Azide **8c**. ^{1}H NMR (500MHz, $CDCl_3$) δ 9.02 (br s, 1H), 7.74 (dd, *J* = 8.4, 7.4 Hz), 7.68 (br t, *J* = 5.3 Hz, 1H), 7.55 (d, *J* = 7.3 Hz, 1H), 7.19 (d, *J* = 8.4 Hz, 1H), 4.95 (dd, *J* = 12.3, 5.3 Hz, 1H), 4.65 (s, 2H), 3.64 (m, 26H), 3.39 (t, *J* = 5.0 Hz, 2H), 2.81 (m, 3H), 2.15 (m, 1H); ^{13}C NMR (125 MHz, $CDCl_3$) δ 171.3, 168.38, 166.9, 166.9, 165.9, 154.5, 137.1, 133.8, 119.3, 118.1, 117.4, 70.8, 70.7, 70.7, 70.6, 70.6, 70.5, 70.4, 70.4, 70.1, 69.6, 67.9, 50.8, 49.4, 39.2, 31.6, 22.8; HRMS (+ESI) calc. for $[C_{29}H_{41}N_6O_{12}]^+$ 665.2777 ($[M+H]^+$), found *m/z* 665.2782.

F. Procedures for the one-pot synthetic approach. The following section provides the general synthetic procedure of the one-pot reaction. For all reactions, the solvents were purged with Ar, all reagents evaporated from benzene to minimize water content and all solutions were made under an atmosphere of Ar in order to minimize introduction of oxygen to one-pot reaction. Procedures are given using the compound numbering in Scheme 1.

Preliminary Method. Three methods were examined the first or preliminary method used CDI to engage the coupling of **4** to **3a**-**3b** (Scheme 1). It begins by preparation of stock solutions and then uses these solutions to conduct reactions in parallel using 20 mL vials fitted with rubber septa. It is demonstrated for the preparation of **1a**-**1c**.

Stock solutions (applied to prepare 1a-1c): Anhydrous DMF used for all solutions.

Ligand A and CDI (4, Scheme 1): 55 mM **7** with 85 mM CDI in DMF

Ligand B (6, Scheme 1): 43 mM **6** in DMF

Linkers and DMAP (3a-3c, Scheme 1): 100 mM **3a** with 10 mM DMAP in DMF, 100 mM **3b** with 10 mM DMAP in DMF or 100 mM **3c** with 10 mM DMAP in DMF

DABCO: 460 mM DABCO in DMF

Protocol: Stock solutions were made 24 h within use and stored in rubber septa capped vials. Ligand A **4** and CDI (0.2 mL, 1.1 and 1.5 eq, respectively) added to a reaction vial and stirred at rt for 1 h. Linkers **3** and DMAP (0.1 mL, 1.0 and 0.1 eq, respectively) were added via syringe and the resulting solution was stirred for 3 h. Ligand B **6** (0.3 mL, 1.5 eq) was added *via* syringe, followed by addition of DABCO (0.1 mL, 4.5 eq). The reaction was then heated to 40 °C and stirred for 18 h. After cooling, the reaction was diluted with EtOAc (30 mL). The organic phase was then washed with sat. NH_4Cl (20 mL), 10% w/v Na_2CO_3(20 mL) and brine (20 mL). The organic layer was then dried over Na_2SO_4 and concentrated on a rotary evaporator. Products were then purified via preparative TLC (chamber contained EtOAc), Note: TLC plates had to be loaded as a concentrated solution in DMF due to solubility issues. The plates were then dried under N_2 flow prior to developing them.

Method A. The second or method A used HATU to engage the coupling of **4** to **3b** (Scheme 2-1). It begins by preparation of stock solutions and then uses these solutions to conduct reactions in parallel using 20 mL vials capped with rubber septa. It is demonstrated for the preparation of **2b**.

Stock solutions (applied to prepare 2b): Anhydrous DMF used for all solutions.

Linker: 110 mM **3b** in DMF

Ligand B (6, Scheme 2-1): 73 mM **12** in DMF

DABCO: 900 mM DABCO in DMF

Protocol: Stock solutions were made 24 h within use and stored in rubber septa sealed vials. Ligand A **4** (4.8 mg, 0.014 mmol, 1.3 eq) and HATU (5.5 mg, 0.014 mmol, 1.3 eq) were dissolved in linker **3** stock solution (0.1 mL 1.0 eq) under an Ar atmosphere. DABCO (0.05 mL, 4 eq) was added via syringe and the reaction mixture was stirred at rt for 1.5 h. Ligand B **6** (0.15 mL, 1.0 eq) was added *via* syringe. The reaction was then heated to 40 °C and stirred for 18 h. After cooling, the reaction was diluted with EtOAc (30 mL). The organic phase was then washed with sat. NH_4Cl (20 mL), 10% w/v Na_2CO_3 (20 mL) and brine (20 mL). The organic layer was then dried over Na_2SO_4 and concentrated on a rotary evaporator. The

product was then purified via flash column chromatography (EtOAc to 1:4 MeOH/EtOAc).

Method B (used for compounds 2a and 2c). The third or method B uses purified ligand A azide **5** to engage the coupling of **6** (Scheme 2-1). It begins by preparation of stock solutions and then uses these solutions to conduct reactions in parallel 20 mL vials capped with rubber septa. It is demonstrated for the preparation of compounds **2a**-**2c**. Anhydrous DMF used for all solutions.

Ligand A (5, Scheme 2-1): 87 mM **8a** in DMF or 87 mM **8c** in DMF

Ligand B (6, Scheme 2-1): 87 mM **12** in DMF

DABCO: 760 mM DABCO in DMF

Ligand A **5** (0.15 mL, 1.0 eq) and Ligand B **6** (0.15 mL, 1.0 eq) were added to a vial under an Ar atmosphere. DABCO (0.05 mL, 3 eq) was added *via* syringe. The reaction was then heated to 40 °C and stirred for 18 h. After cooling, the reaction was diluted with EtOAc (30 mL). The organic phase was then washed with sat. NH_4Cl (20 mL), 10% w/v Na_2CO_3 (20 mL) and brine (20 mL). The organic layer was then dried over Na_2SO_4 and concentrated on a rotary evaporator. The product was then purified via flash column chromatography (EtOAc to 1:4 MeOH/EtOAc).

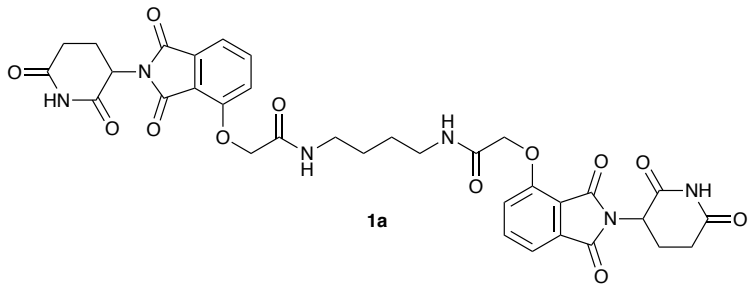

1a

***N,N'*-(butane-1,4-diyl)bis(2-((2-(2,6-dioxopiperidin-3-yl)-1,3-dioxoisoindolin-4-yl)oxy)acetamide) (1a).** Preliminary study was a LCMS based study, and there is no isolated yield to report due to the product being inseparable from the reaction mixture on silica (see Fig. S3). Compound synthesized using general one-pot preliminary method A. HRMS (+ESI) calc. for $[C_{34}H_{33}N_6O_{12}]^+$ 717.2151 ($[M+H]^+$), found *m/z* 717.2157.

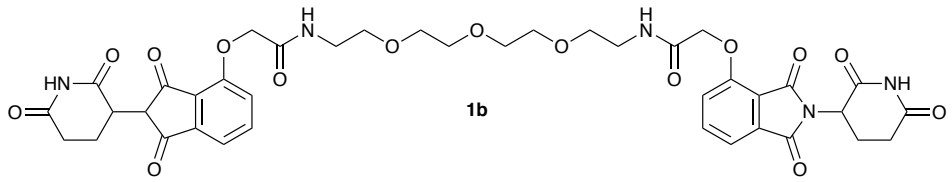

***N,N'*-(((oxybis(ethane-2,1-diyl))bis(oxy))bis(ethane-2,1-diyl))bis(2-((2-(2,6-dioxopiperidin-3-yl)-1,3-dioxoisoindolin-4-yl)oxy)acetamide) (2b).**

Preliminary study was a LCMS based study, and there is no isolated yield to report due to the product being inseparable from the reaction mixture on silica (see Fig. S4). Compound synthesized using general one-pot preliminary method A. HRMS (+ESI) calc. for $[C_{38}H_{40}N_6O_{15}Na]^+$ 843.2444 ($[M+Na]^+$), found *m/z* 843.2434.

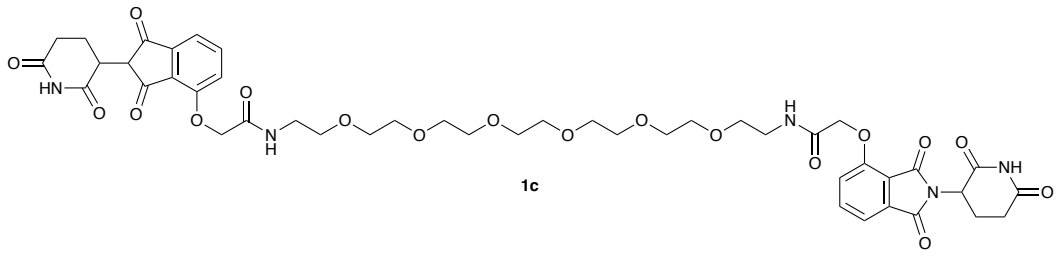

1c

***N,N'*-(3,6,9,12,15,18-hexaoxaicosane-1,20-diyl)bis(2-((2-(2,6-dioxopiperidin-3-yl)-1,3-dioxoisoindolin-4-yl)oxy)acetamide) (1c).**

Compound synthesized using general one-pot preliminary method A. Yield: 1.1 mg (10%). ^{1}H NMR (500 MHz, $CDCl_3$) δ 8.99 (s, 1H), 7.74 (t, *J* = 7.9 Hz, 1H), 7.66 (t, *J* = 5.4 Hz, 1H), 7.55 (d, *J* = 7.3 Hz, 1H), 7.19 (d, *J* = 8.4 Hz, 1H), 4.96 (dd, *J* = 12.4, 5.4 Hz, 1H), 4.65 (s, 2H), 3.70-3.59 (m, 12H), 3.42-3.34 (m, 2H), 2.93-2.70 (m, 3H), 2.18-2.10 (m, 1H); ^{13}C NMR (125 MHz, $CDCl_3$) δ 171.2, 168.3, 166.9, 166.8, 165.9, 154.5, 137.1, 133.8, 119.8, 118.1, 117.4, 71.1, 70.8, 70.8, 70.8, 70.7, 70.6, 70.6, 70.5, 70.5, 70.4, 70.1, 69.6, 67.9, 50.8, 49.9, 39.2, 32.1, 22.9; HRMS (+ESI) calc. for $[C_{44}H_{52}N_6O_{18}NH_4]^+$ 970.3676 ($[M+NH_4]^+$), found *m/z* 970.3647, calc. for $[C_{44}H_{52}N_6O_{18}Na]^+$ 975.3236 ($[M+Na]^+$), found *m/z* 975.3230.

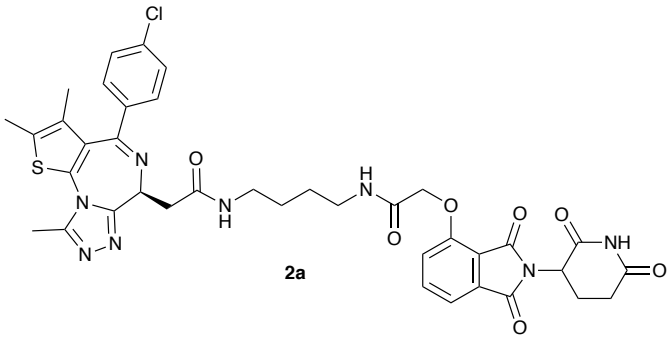

2a

2-((*S*)-4-(4-chlorophenyl)-2,3,9-trimethyl-6*H*-thieno[3,2-*f*][1,2,4]triazolo[4,3-*a*][1,4]diazepin-6-yl)-*N*-(4-(2-((2-(2,6-dioxopiperidin-3-yl)-1,3-dioxoisoindolin-4-yl)oxy)acetamido)butyl)acetamide (2a).

Compound synthesized using general one-pot method B. Yield: 5.4 mg (54%). Spectral signals matched those previously reported.[4a] ^{1}H NMR (500MHz, CD_3OD) δ 7.81 (dd, *J* = 8.5, 7.3 Hz, 1H), 7.53 (d, *J* = 7.4 Hz, 1H), 7.49 (m, 5H), 5.10 (m, 1H), 4.77 (s, 2H), 4.62 (dd, *J* = 8.9, 5.3 Hz, 1H), 3.41 (m, 3H), 3.27 (m, 2H), 2.73 (m, 7H), 2.44 (s, 3H), 2.09 (m, 1H), 1.61 (m, 7H). ^{13}C NMR (125 MHz, D_3COD) δ 174.5, 172.7, 171.4, 170.0, 168.4, 167.8, 166.3, 157.0, 156.3, 152.2, 138.3, 138.1, 138.0, 135.0, 133.6, 133.2, 132.0, 132.0, 131.4, 130.0, 129.4, 121.9, 119.4, 118.0, 69.5, 55.2, 50.5, 40.1, 39.8, 38.8, 32.1, 27.8, 27.6, 23.6, 14.5, 12.9, 11.5; ^{1}H NMR (500 MHz, DMSO-d_6) δ 11.14 (br s, 1H), 8.23 (t, *J* = 5.8 Hz, 1H), 8.01 (t, *J* = 5.8 Hz, 1H), 7.81 (dd, *J* = 8.5, 7.3 Hz, 1H), 7.67 (m, 6H), 5.12

(dd, J = 12.8, 5.5 Hz, 1H), 4.78 (s, 2H), 4.49 (dd, J = 8.1, 6.1 Hz, 1H), 3.15- (m, 6H), 2.88 (m, 1H), 2.53 (m, 5H), 2.40 (s, 3H), 2.03 (m, 1H), 1.61 (s, 3H), 1.56 (m, 4H). ^{13}C NMR (125 MHz, DMSO-d_6) δ 172.9, 169.4, 168.1, 167.0, 166.8, 166.8, 165.6, 163.1, 155.2, 155.1, 149.9, 137.0, 136.8, 135.3, 133.1, 132.3, 130.8, 130.2, 129.9, 129.6, 129.1, 128.5, 120.4, 116.8, 116.1, 66.9, 67.6, 53.9, 48.8, 44.1, 31.3, 26.6, 26.6, 22.2, 14.1, 12.8, 11.4; HRMS (+ESI) calc. for $[C_{38}H_{38}ClN_8O_7S]^+$ 785.2267 ($[M+H]^+$), found *m/z* 785.2264; LC-MS (+ESI) calc. for $[C_{38}H_{38}ClN_8O_7S]^+$ 785.23 ($[M+H]^+$), found *m/z* 785.37.

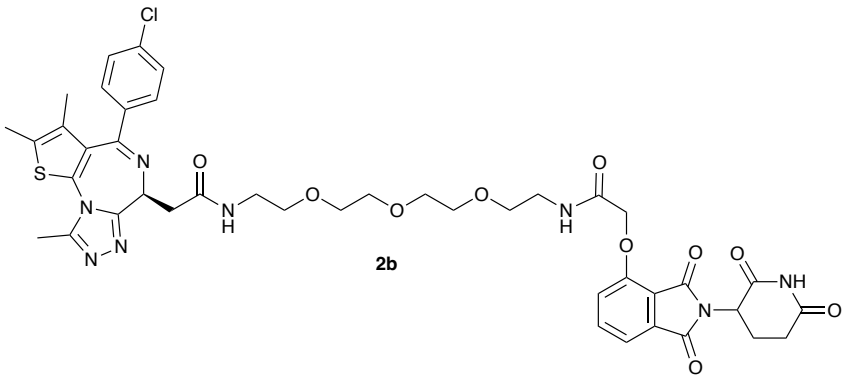

2b

2-((*S*)-4-(4-chlorophenyl)-2,3,9-trimethyl-6*H*-thieno[3,2-*f*][1,2,4]triazolo[4,3-*a*][1,4]diazepin-6-yl)-*N*-(1-((2-(2,6-dioxopiperidin-3-yl)-1,3-dioxoisoindolin-4-yl)oxy)-2-oxo-6,9,12-trioxa-3-azatetradecan-14-yl)acetamide (2b). Yield: 4.8 mg (48%). Note: The reported yield is not fully purified, but represents the mass of the material shown in Fig. S10. For further characterization, this compound was synthesized using general one-pot method B. Yield: 4.2 mg (39%). ^{1}H NMR (500 MHz, DMSO-d_6) δ 11.14 (s, 1H), 8.31 (t, J = 5.7 Hz, 1H), 8.07 (t, J = 5.5 Hz, 1H), 7.80 (t, J = 7.8 Hz, 1H), 7.48 (m, 4H), 7.41 (m, 2H), 5.11 (dd, J = 12.8, 5.4 Hz, 1H), 4.79 (s, 2H), 4.49 (dd, J = 8.2, 6.2 Hz, 1H), 3.54 (m, 16H, H_2O peak present), 2.90 (m, 2H), 2.77 (m, 3H), 2.59 (m, 3H), 2.40 (m, 3H), 2.03 (m, 1H), 1.61 (m, 3H); ^{13}C NMR (125 MHz, DMSO-d_6) δ 172.8, 170.0, 169.7, 167.0, 166.8, 165.5, 163.1, 155.1, 155.0, 149.9, 137.0, 136.8, 135.3, 133.1, 132.3, 130.7, 130.2, 129.9, 129.6, 128.5, 120.3, 116.7, 116.1, 72.4, 69.7, 69.2, 68.9, 67.5, 60.2, 53.9, 51.2, 50.7, 48.8, 45.5, 38.6, 38.4, 37.5,

31.0, 22.0, 14.1, 12.7, 11.4; HRMS (+ESI) calc. for $[C_{42}H_{46}ClN_8O_{10}S]^+$ 889.2741 ($[M+H]^+$), found *m/z* 889.2730, calc. for $[C_{42}H_{45}ClN_8O_{10}SNa]^+$ 911.2560 ($[M+Na]^+$), found *m/z* 911.2558; LC-MS (+ESI) calc. for $[C_{42}H_{46}ClN_8O_{10}S]^+$ 889.27 ($[M+H]^+$), found *m/z* 889.32.

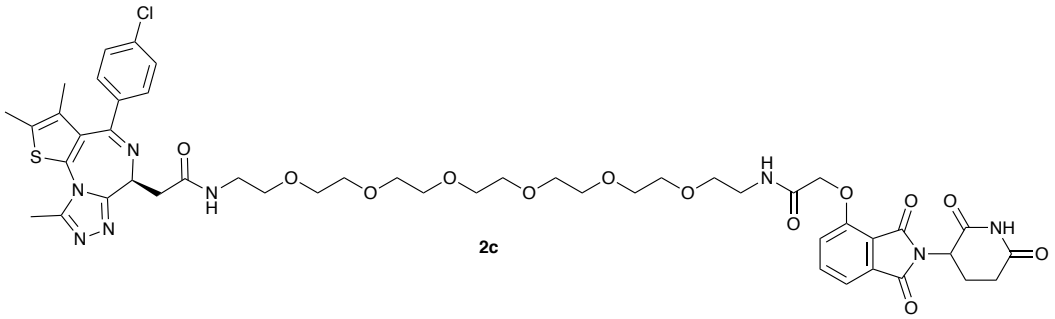

2c

2-((*S*)-4-(4-chlorophenyl)-2,3,9-trimethyl-6*H*-thieno[3,2-*f*][1,2,4]triazolo[4,3-*a*][1,4]diazepin-6-yl)-*N*-(1-((2-(2,6-dioxopiperidin-3-yl)-1,3-dioxoisoindolin-4-yl)oxy)-2-oxo-6,9,12,15,18,21-hexaoxa-3-azatricosan-23-yl)acetamide (2c). Compound synthesized using general one-pot method B. Yield: 9.1 mg (85%). ^{1}H NMR (500 MHz, DMSO-d_6) δ 11.14 (br s, 1H), 8.31 (t, J = 5.7 Hz, 1H), 8.03 (t, J = 5.4 Hz, 1H), 7.80 (dd, J = 8.5, 7.3 Hz, 1H), 7.44 (m, 4H), 6.93 (m, 2H), 5.11 (dd, J = 12.9, 5.5 Hz, 1H), 5.02 (s, 1H), 4.79 (s, 1H), 4.49 (dd, J = 8.2, 6.0 Hz, 1H), 4.46-4.38 (m, 1H), 3.24 (m, 28H, H_2O peak present), 2.90 (m, 2H), 2.54 (m, 3H), 2.38 (m, 3H), 2.03 (m, 2H), 1.77 (dt, J = 14.3, 6.8 Hz, 1H), 1.59 (m, 3H); ^{13}C NMR (125 MHz, DMSO-d_6) δ 173.7, 173.2, 171.5, 167.7, 166.9, 166.2, 164.0, 155.7, 155.4, 150.8, 137.7, 137.2, 136.0, 133.5, 132.6, 131.7, 130.8, 130.5, 130.3, 129.4, 120.9, 117.2, 117.0, 77.4, 72.7, 70.3, 70.3, 70.1, 69.6, 69.2, 68.1, 63.3, 60.6, 55.9, 54.3, 49.4, 44.8, 36.1, 34.2, 33.9, 31.4, 22.7, 13.2, 11.8, 9.4; HRMS (+ESI) calc. for $[C_{48}H_{58}ClN_8O_{13}S]^+$

1021.3527 ([M+H]$^+$), found *m/z* 1021.3530; LC-MS (+ESI) calc. for $[C_{48}H_{58}ClN_8O_{13}S]^+$ 1021.35 ([M+H]$^+$), found *m/z* 1021.42.

I. Representative spectral data. Copies of LC-MS and NMR data has been provided for reactions and purified compounds. LC-MS runs were conducted using the following solvent: A = 0.1% formic acid in water and B = 0.1% formic acid in acetonitrile. Total run time was 8 min. Runs were conducted using an Acquity UPLC Beh C18 column (130Å, 1.7 μm, 2.1 mm × 50 mm) with a flow rate of 0.6 mL/min. Samples were dissolved in acetonitrile.

LC-MS Methods

Method A

Equilibration conditions: 95%A:5%B

time (min)	%A	%B
Initial	95	5
0.50	95	5
4.00	15	85
6.00	5	95
8.00	95	5

Method B

Equilibration conditions: 95%A:5%B

time (min)	%A	%B
Initial	95	5
0.50	95	5
8.00	5	95

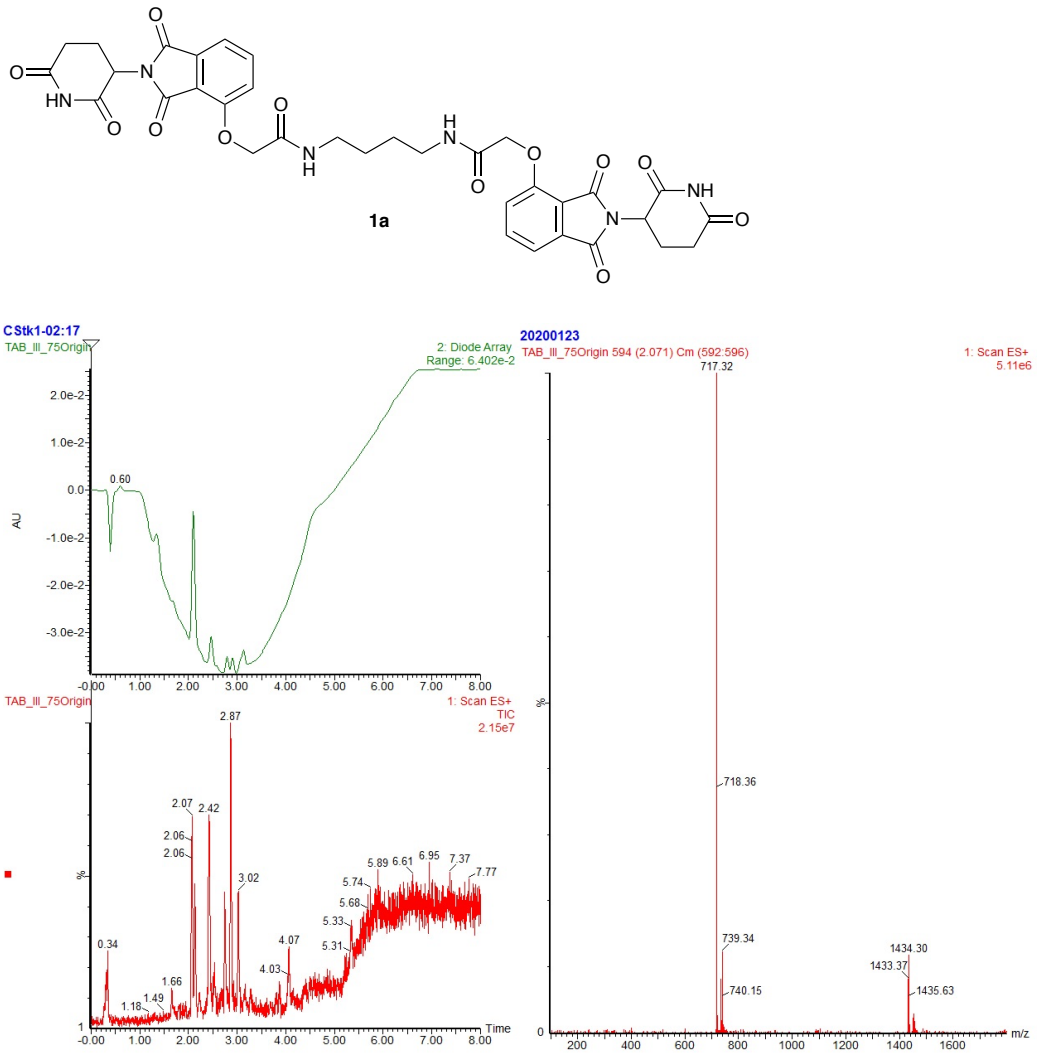

Appendix Figure 2-3: LC-MS trace of **1a** using LC-MS method A. UV-vis detection was at λ = 254 nm. Peak at 2.07 min corresponds to the product. (Note: Peak at 2.15 min corresponds to inseparable intermediate **8a**.)

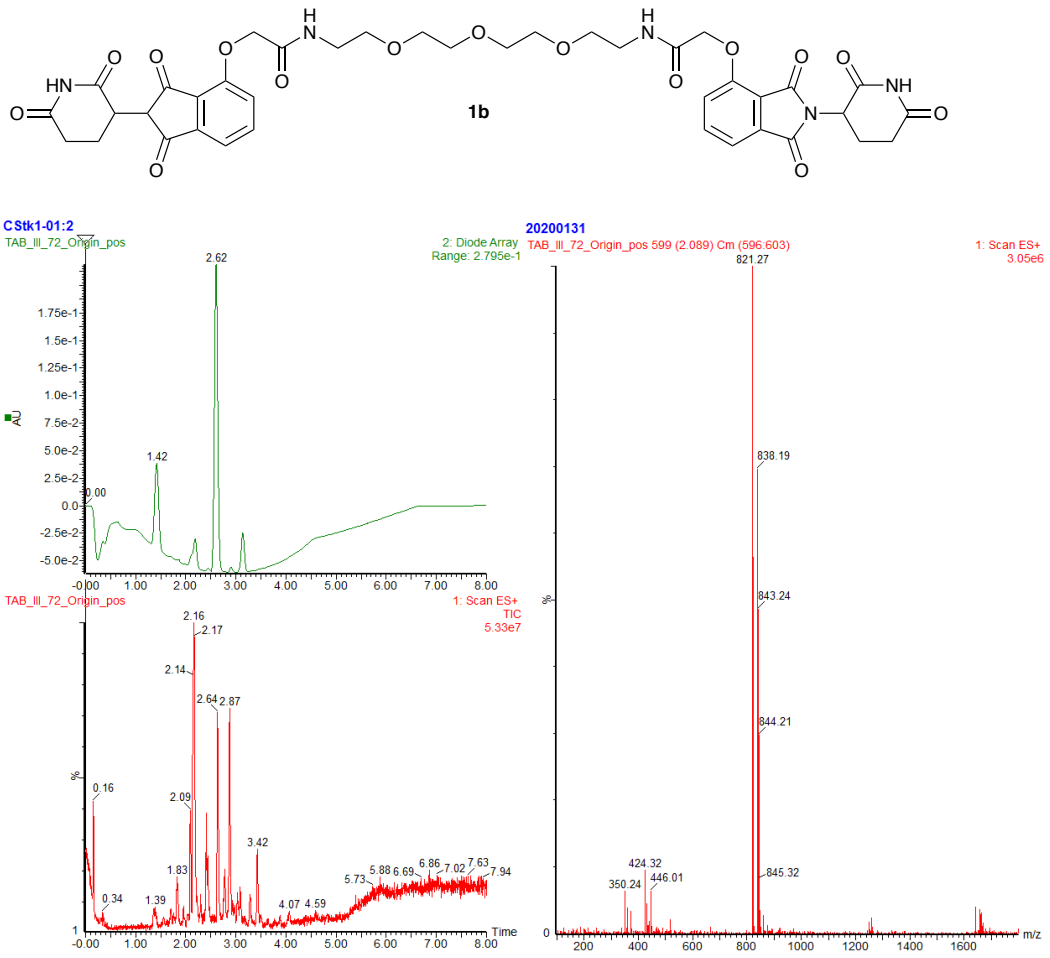

Appendix Figure 2-4: LC-MS trace of **1b** using LC-MS method A. UV-vis detection was at λ = 254 nm. Peak at 2.09 min corresponds to the product. (Note: Peak at 2.16 min corresponds to inseparable intermediate **8b**.)

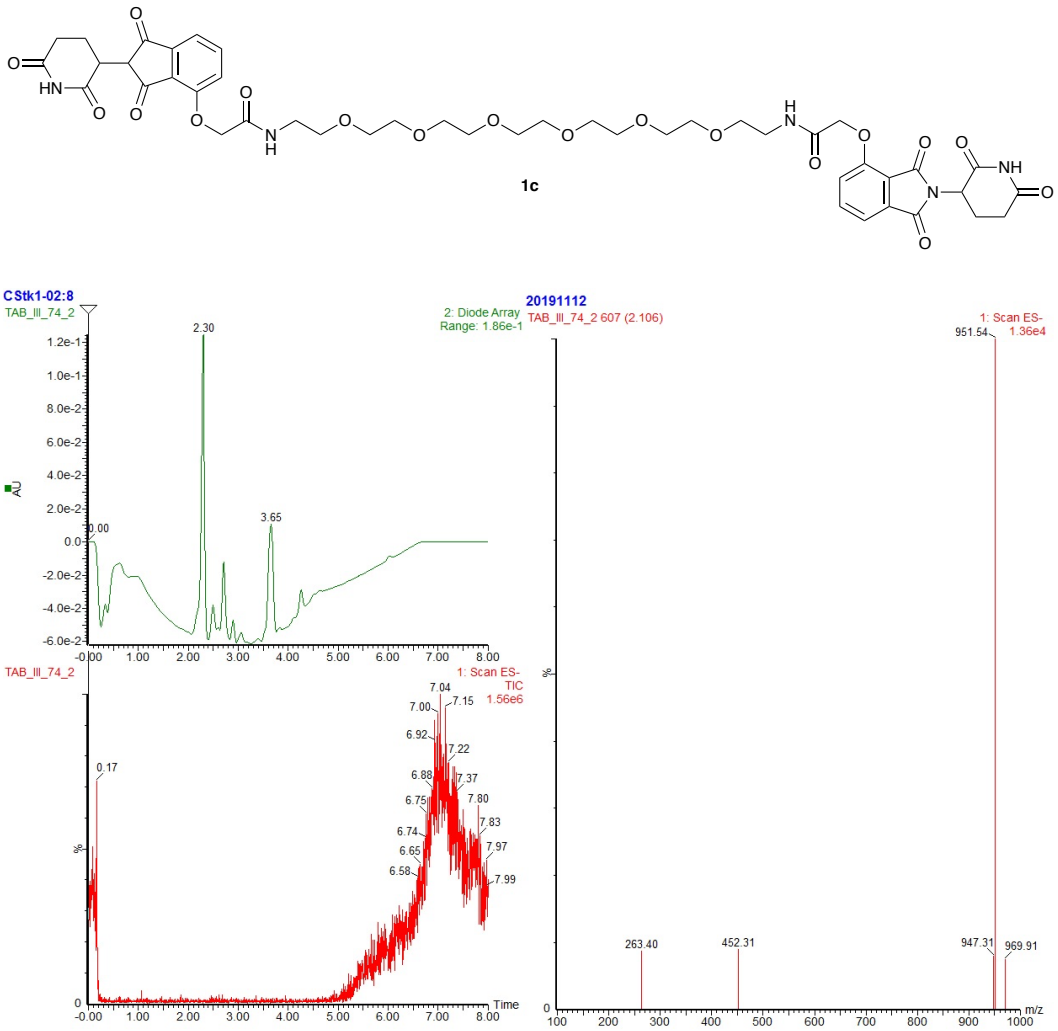

Appendix Figure 2-5: LC-MS trace of **1c** using LC-MS method A. UV-vis detection was at λ = 254 nm. Peak at 2.11 min (front shoulder of large UV signal at 2.30 min) corresponds to the product. The large peak at 2.30 min corresponds to accumulation of intermediate **8c**. Note: compound **1c** was difficult to detect on ES+ detection mode so ES- was used instead.

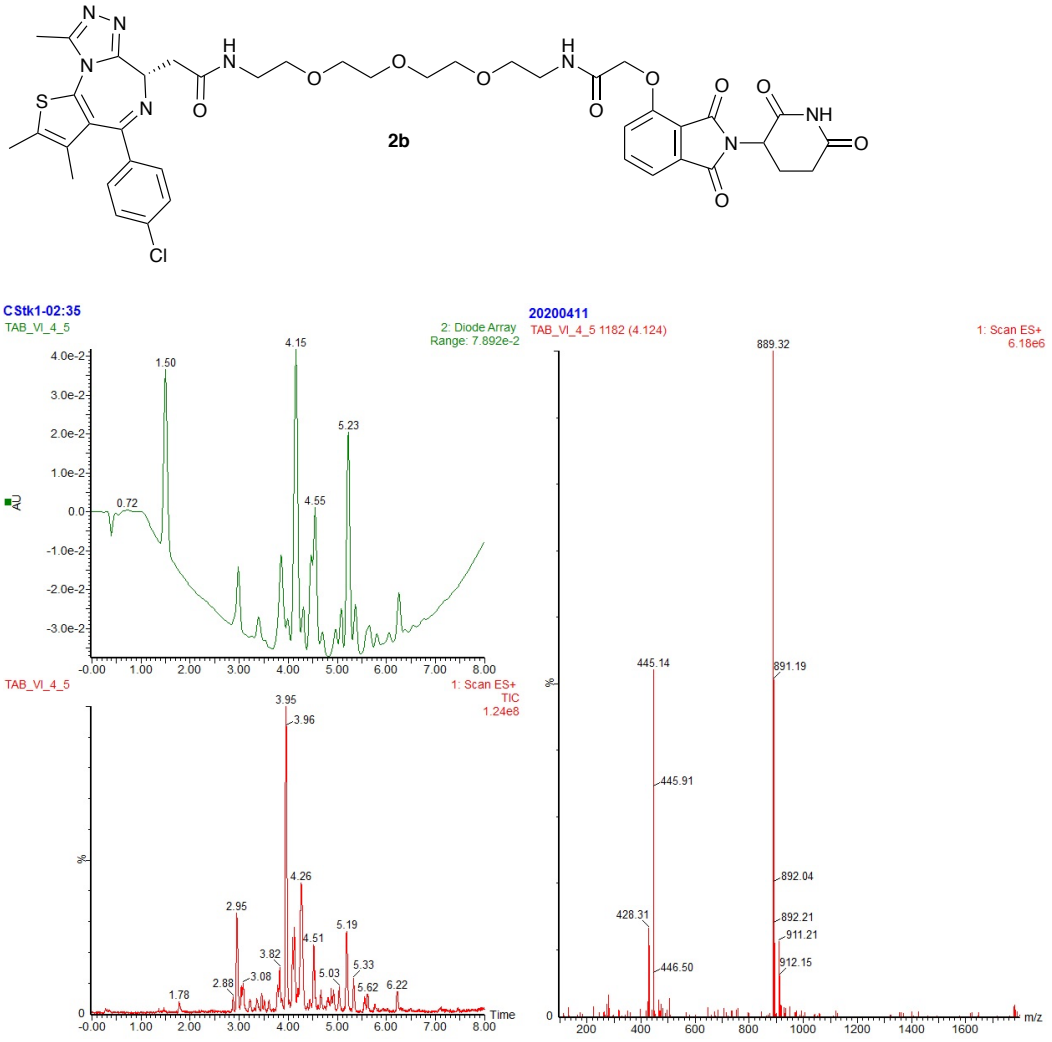

Appendix Figure 2-6: LC-MS trace of **2b** using LC-MS method B. UV-vis detection was at λ = 254 nm. Peak at 4.12 min corresponds to the product.

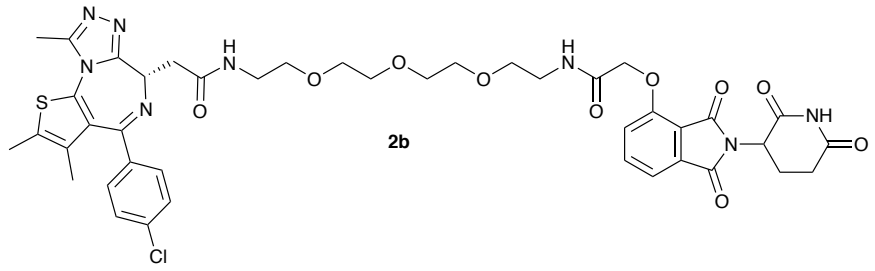

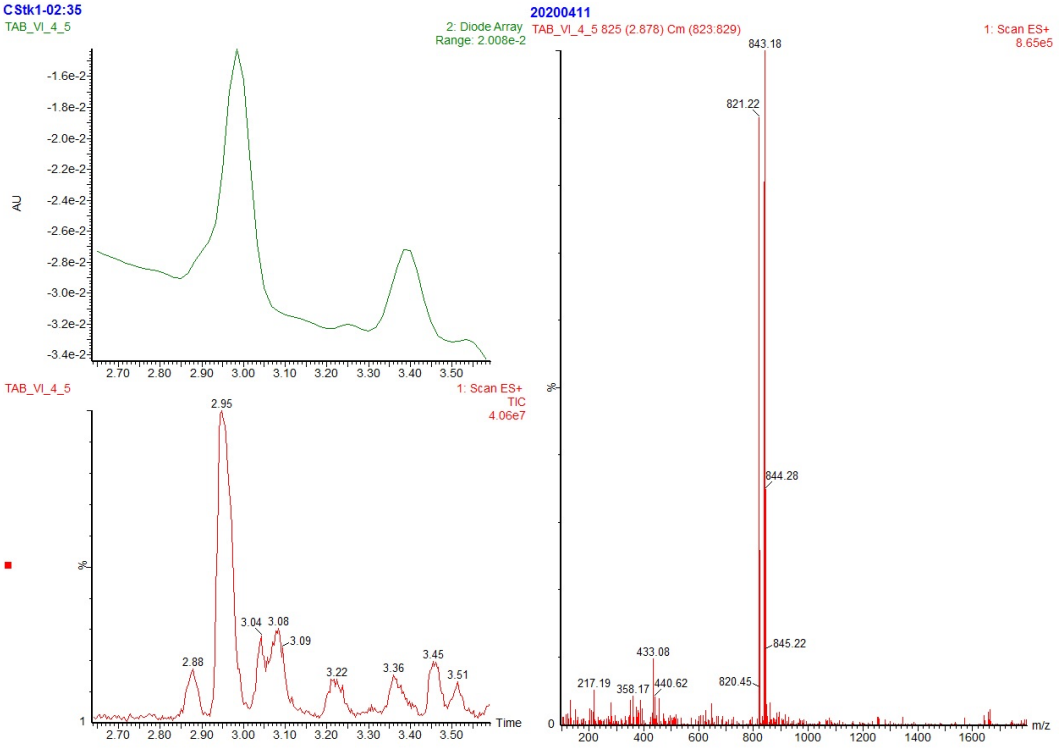

Appendix Figure 2-7: Impurity profile examined via LC-MS during one-pot synthesis of **2b** using LC-MS method B (zoomed in on trace Appendix Figure 2-6) . UV-vis detection was at λ = 254 nm. Peak at 2.88 min corresponds to the aberrant homo-coupled product **1b**. Note: this type of impurity is a liability to biological evaluation, however with our LC method the difference in retention time was 1 min, so it is likely this impurity could be removed via prep-HPLC techniques.

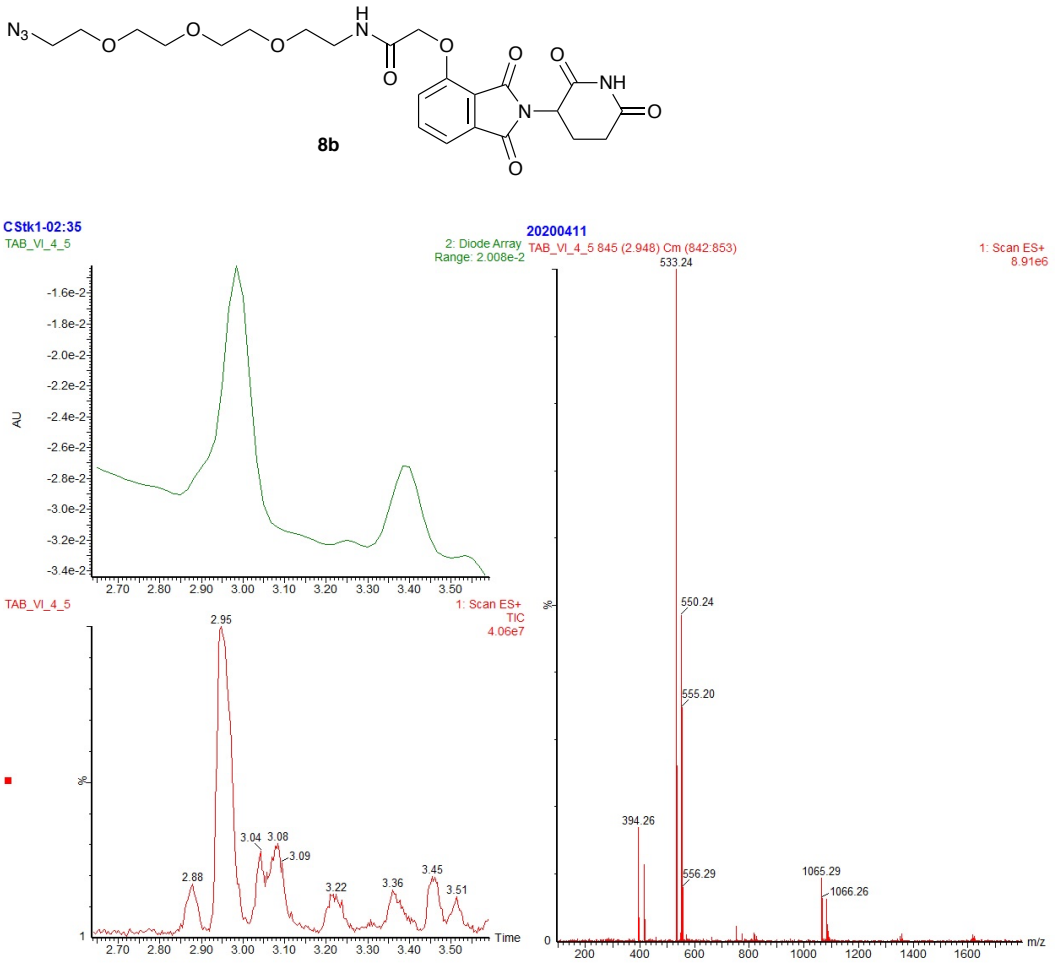

Appendix Figure 2-8: Impurity profile examined via LC-MS during one-pot synthesis of **2b** using LC-MS method B (zoomed in on trace Appendix Figure 2-6) . UV-vis detection was at λ = 254 nm. Peak at 2.95 min corresponds to intermediate **8b**. Note: this type of impurity is a liability to biological evaluation, however with our LC method the difference in retention time was 1 min, so it is likely this impurity could be removed via prep-HPLC techniques.

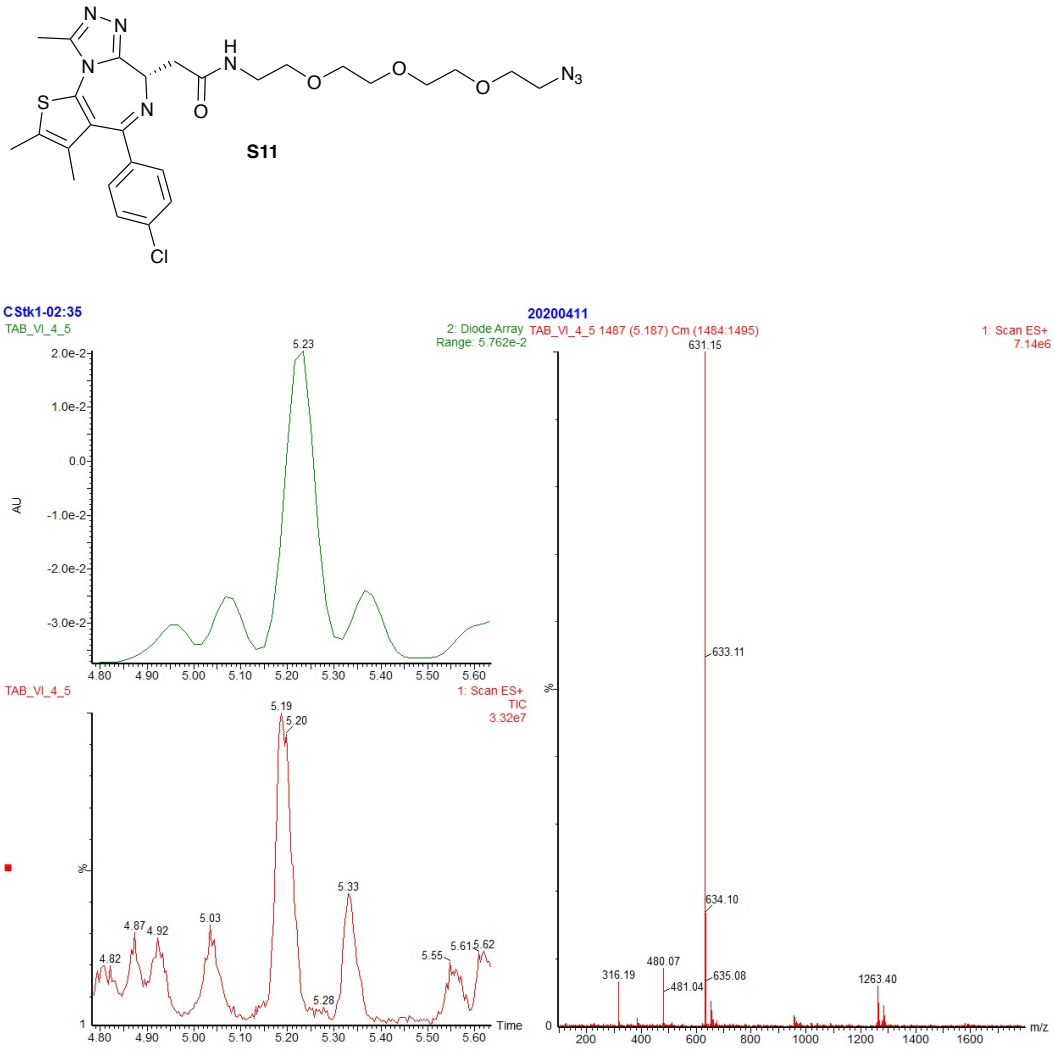

Appendix Figure 2-9: Impurity profile examined via LC-MS during one-pot synthesis of **2b** using LC-MS method B (zoomed in on trace Appendix Figure 2-6) . UV-vis detection was at λ = 254 nm. Peak at 5.19 min corresponds to aberrant formation of **S11.** Note: this type of impurity is a liability to biological evaluation, however with our LC method the difference in retention time was 1 min, so it is likely this impurity could be removed via prep-HPLC techniques.

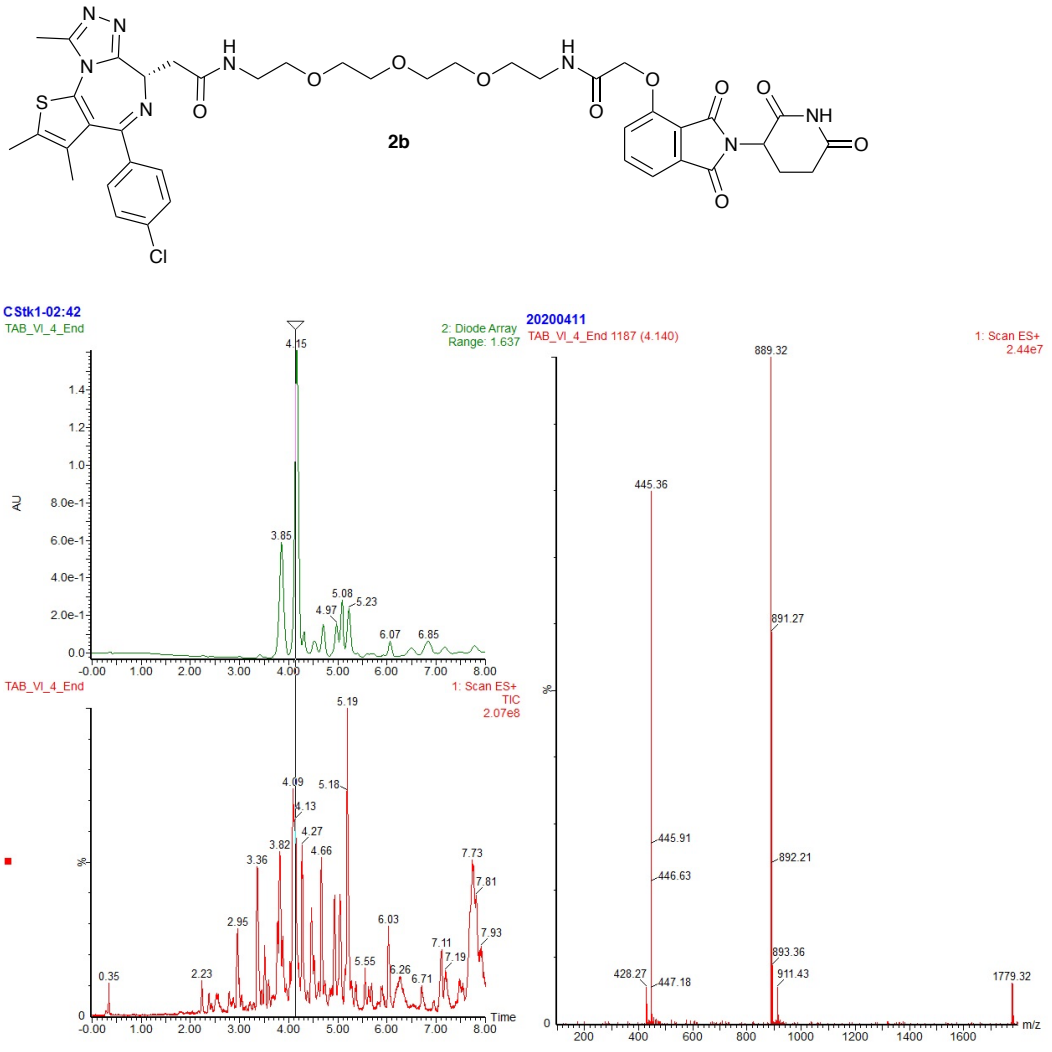

Appendix Figure 2-10: Impurity profile examined via LC-MS during one-pot synthesis of **2b** using LC-MS method B, after flash column chromatography (EtOAc to 1:9 MeOH/EtOAc). UV-vis detection was at λ = 254 nm. Note: Impurities **1b** and **8b** (described in Appendix Figures 2-7 – 2-8), were able to be largely reduced/removed, however impurity **S11** (Appendix Figure 2-9) appears to be present.

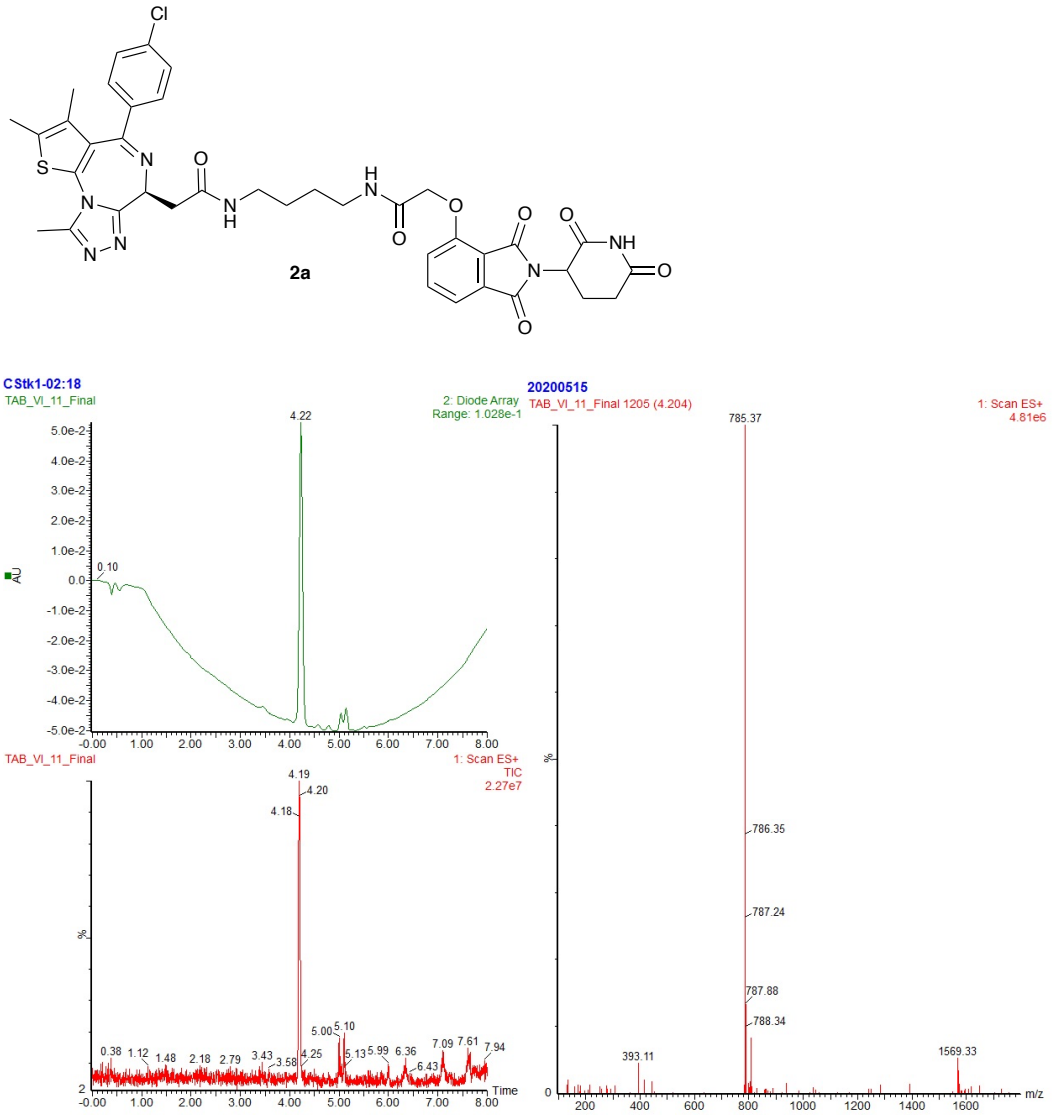

Appendix Figure 2-11: LC-MS trace of **2a** using LC-MS method B. UV-vis detection was at λ = 254 nm. Peak at 4.20 min corresponds to the product. Note: This sample was purified via flash column chromatography (EtOAc to 1:9 MeOH/EtOAc) and does not contain the analogous competitive binders/degraders observed when using one-pot synthetic method B (See Appendix Figures 2-7 – 2-9).

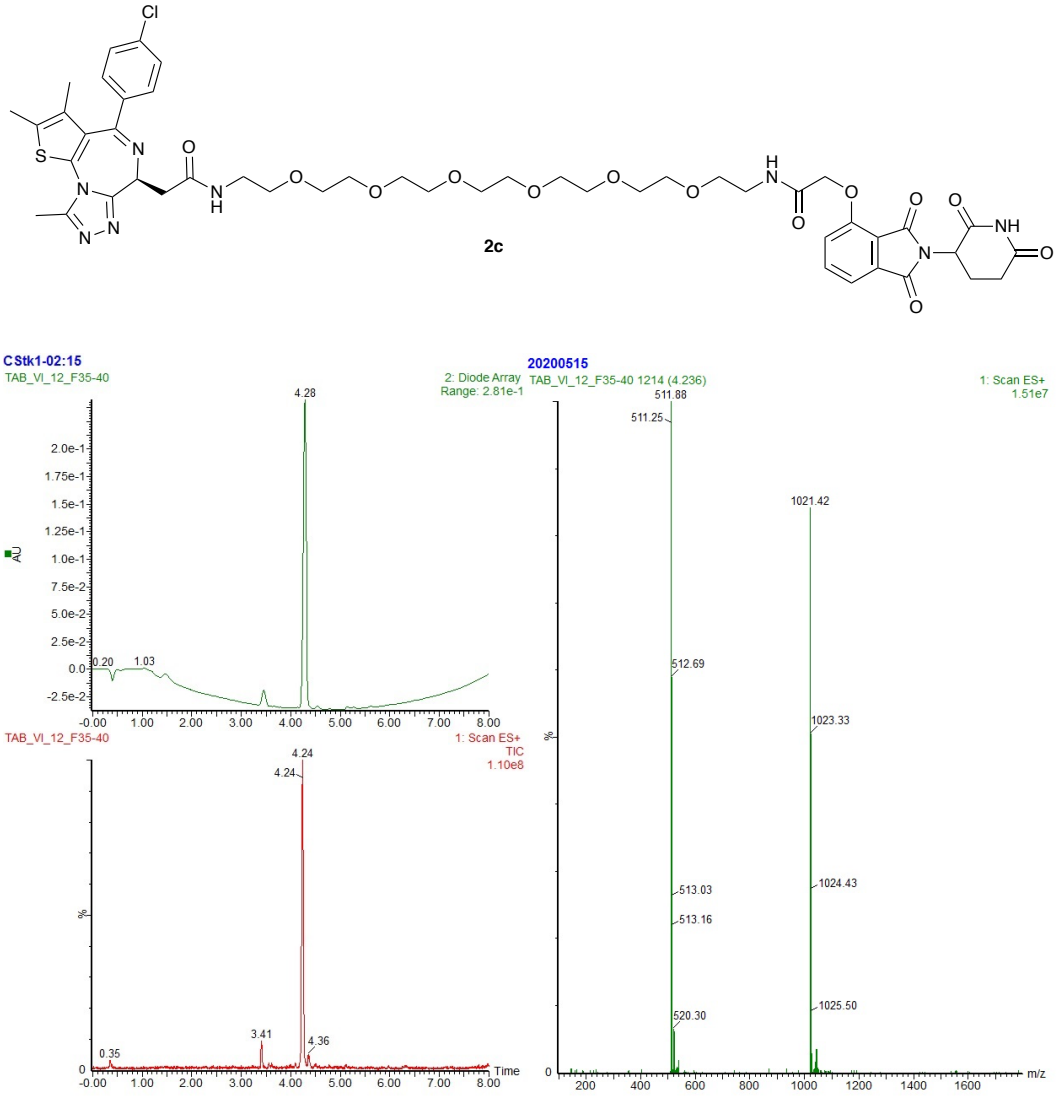

Appendix Figure 2-12: LC-MS trace of **2c** using LC-MS method B. UV-vis detection was at λ = 254 nm. Peak at 4.24 min corresponds to the product. Note: This sample was purified *via* flash column chromatography (EtOAc to 1:9 MeOH/EtOAc) and does not contain the analogous competitive binders/degraders observed when using one-pot synthetic method B (see Appendix Figures 2-7 – 2-9).

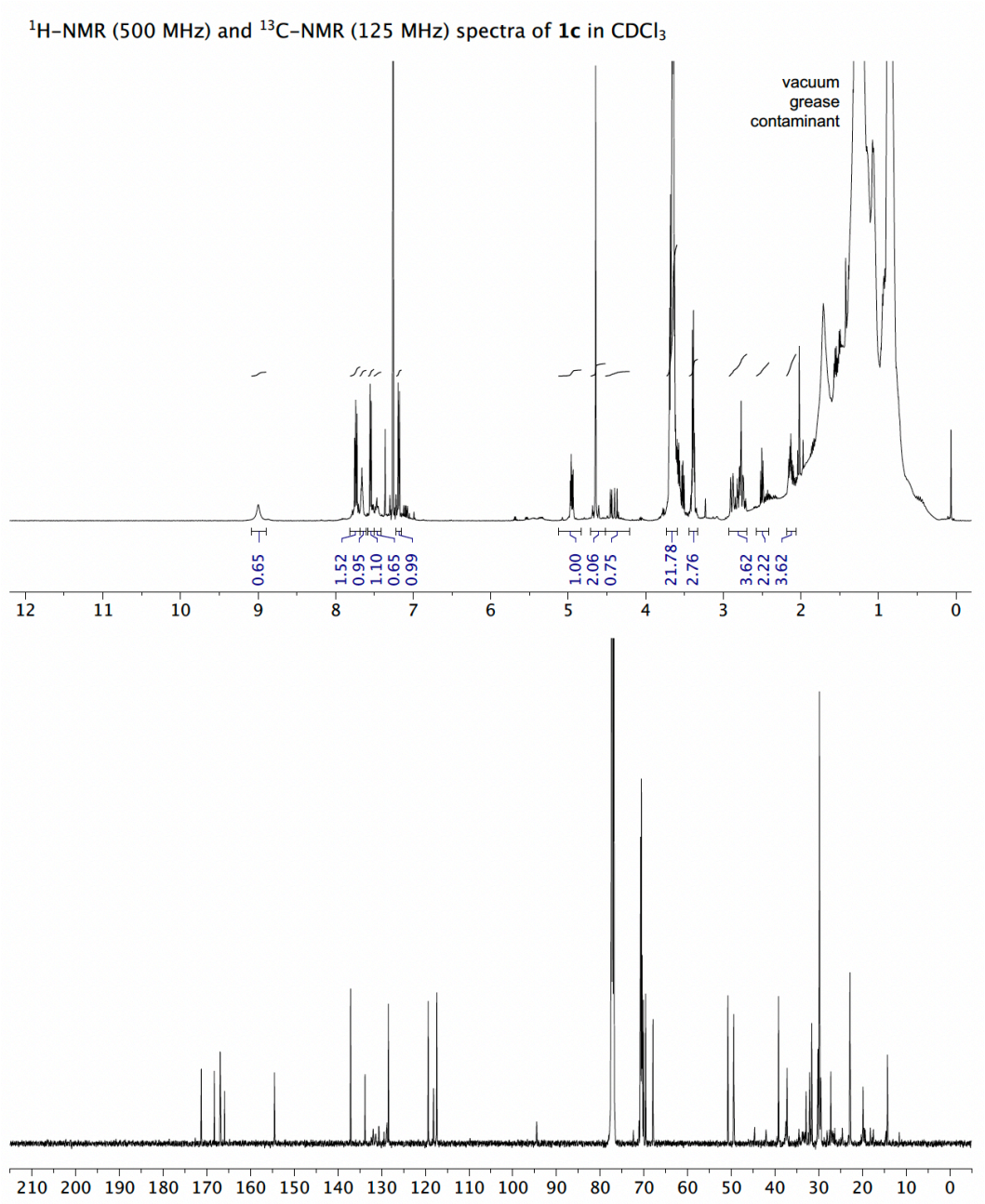

Appendix Figure 2-13: ^{1}H-NMR and ^{13}C-NMR spectra of 1c in $CDCl_3$.

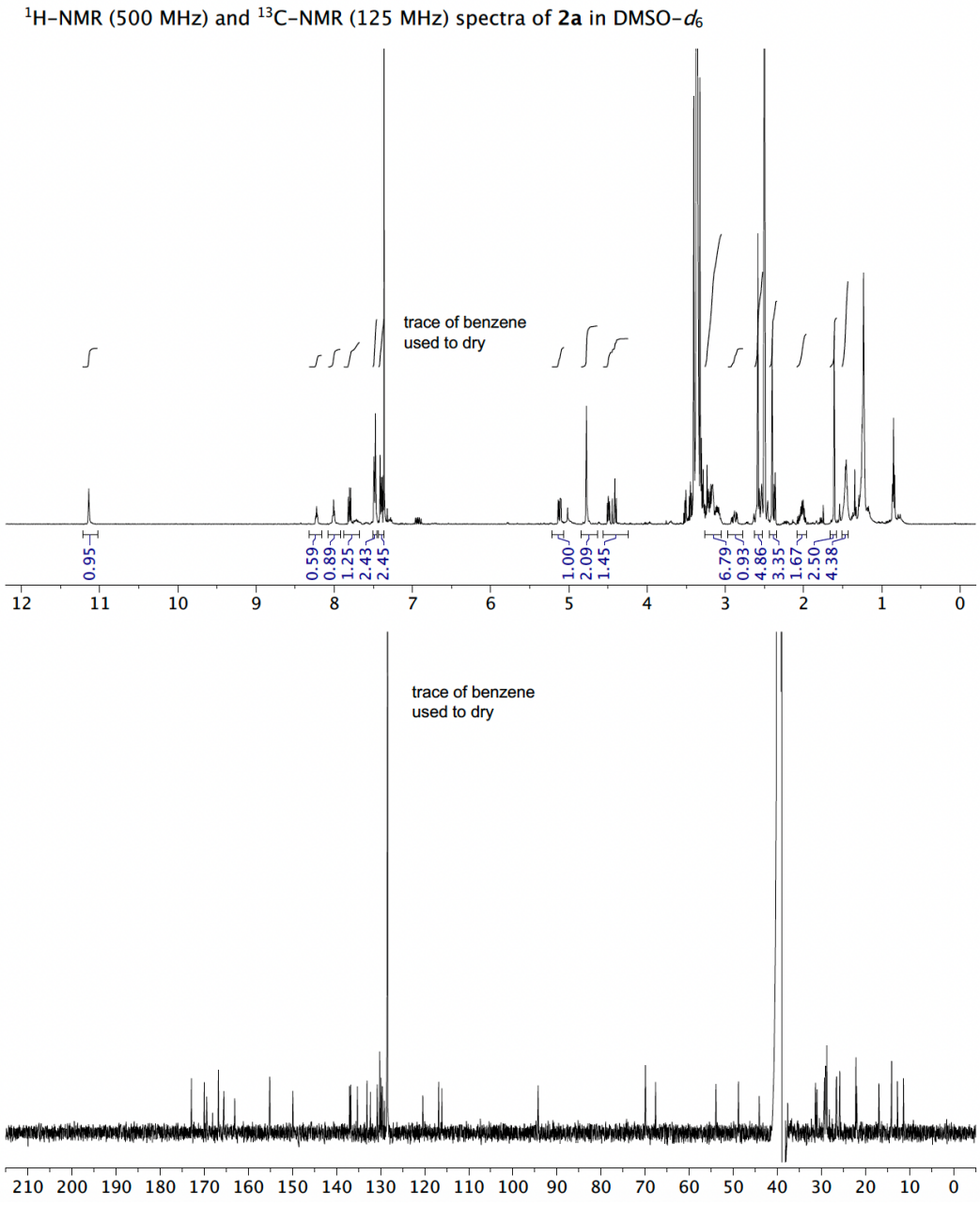

Appendix Figure 2-14: ^{1}H-NMR and ^{13}C-NMR spectra of 2a in DMSO-d_6.

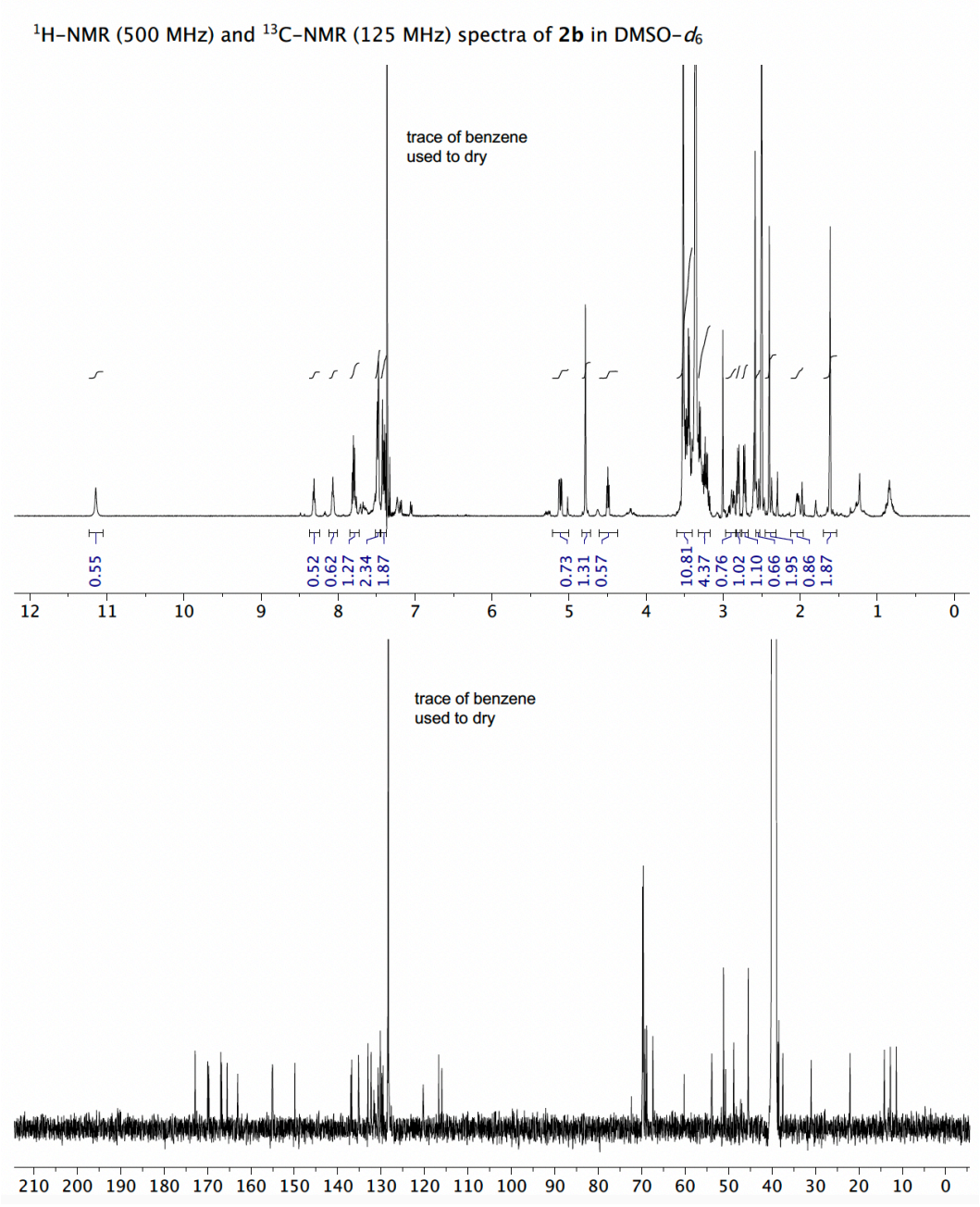

Appendix Figure 2-15: ^{1}H-NMR and ^{13}C-NMR spectra of 2b in DMSO-d_6.

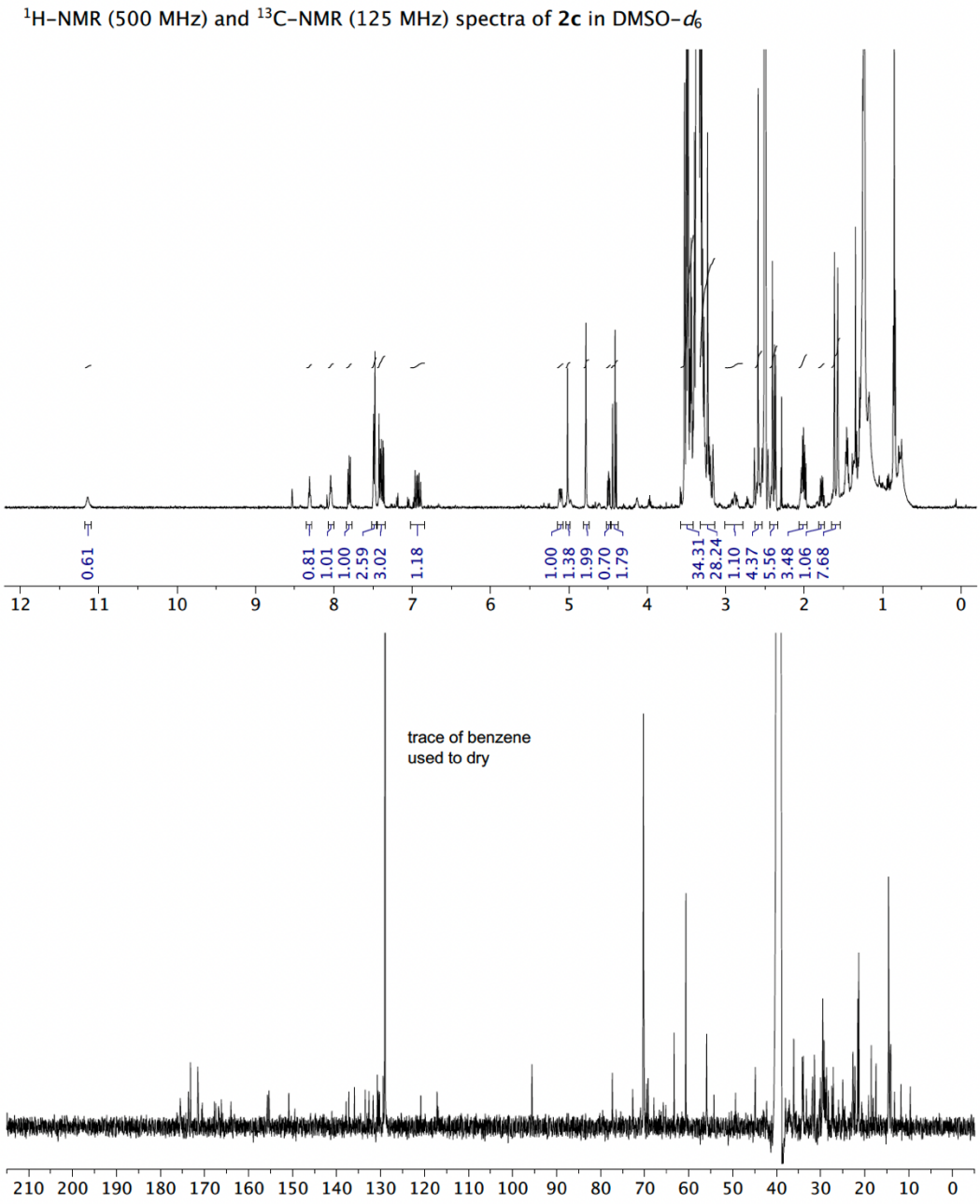

Appendix Figure 2-16: ^{1}H-NMR and ^{13}C-NMR spectra of 2c in DMSO-d_6.

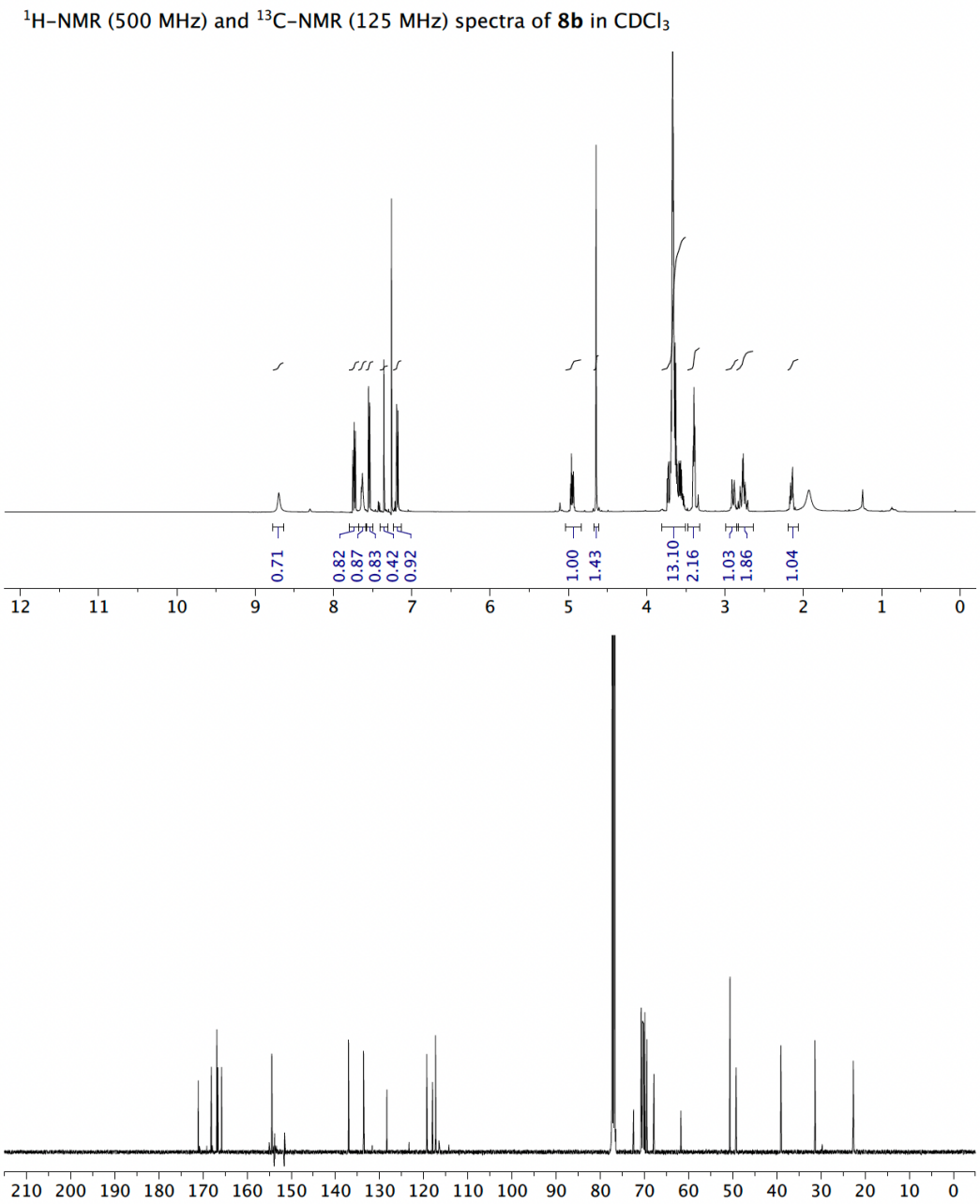

Appendix Figure 2-17: ^{1}H-NMR and ^{13}C-NMR spectra of 8b in $CDCl_3$.

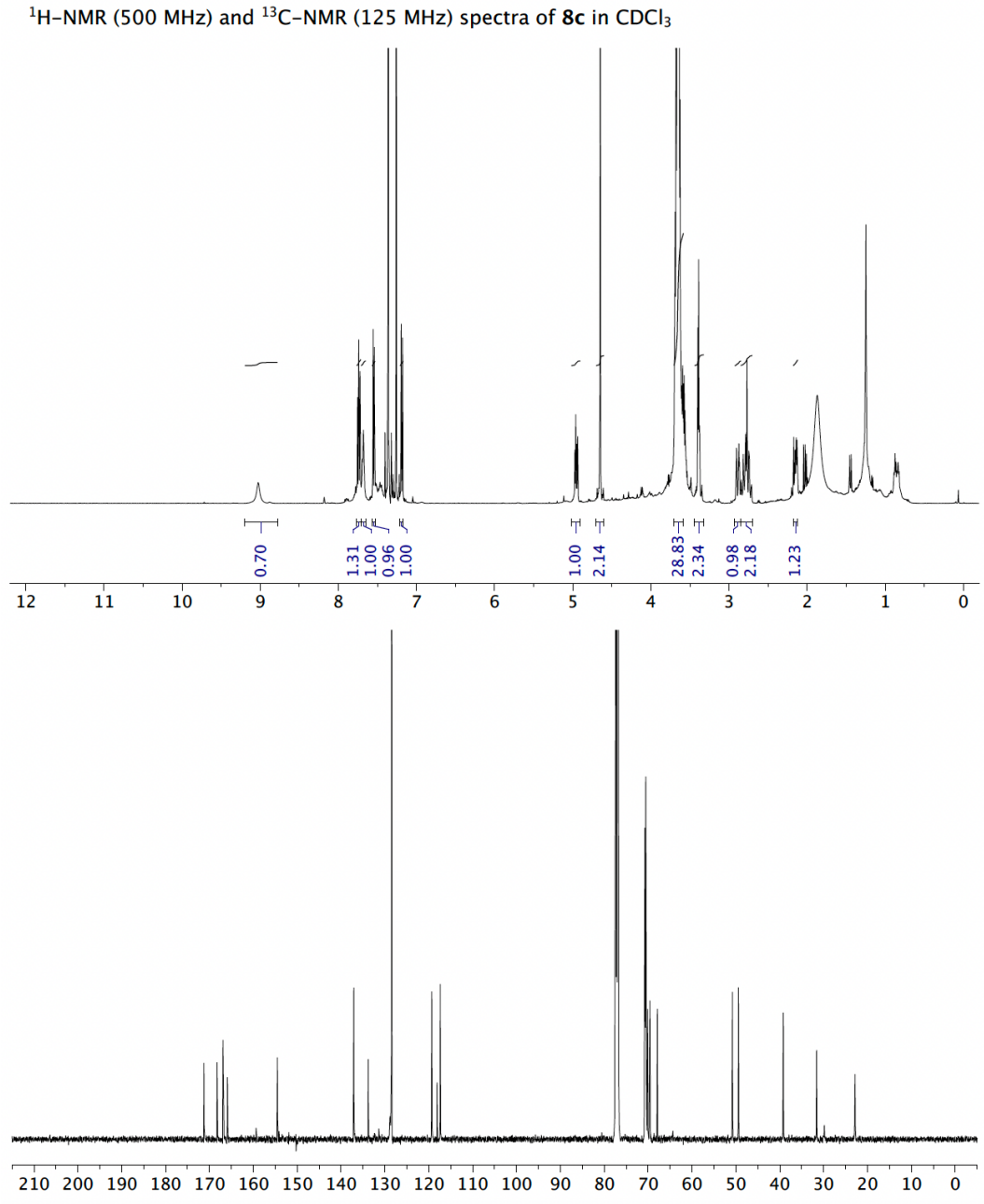

Appendix Figure 2-18: ^{1}H-NMR and ^{13}C-NMR spectra of 8c in $CDCl_3$.

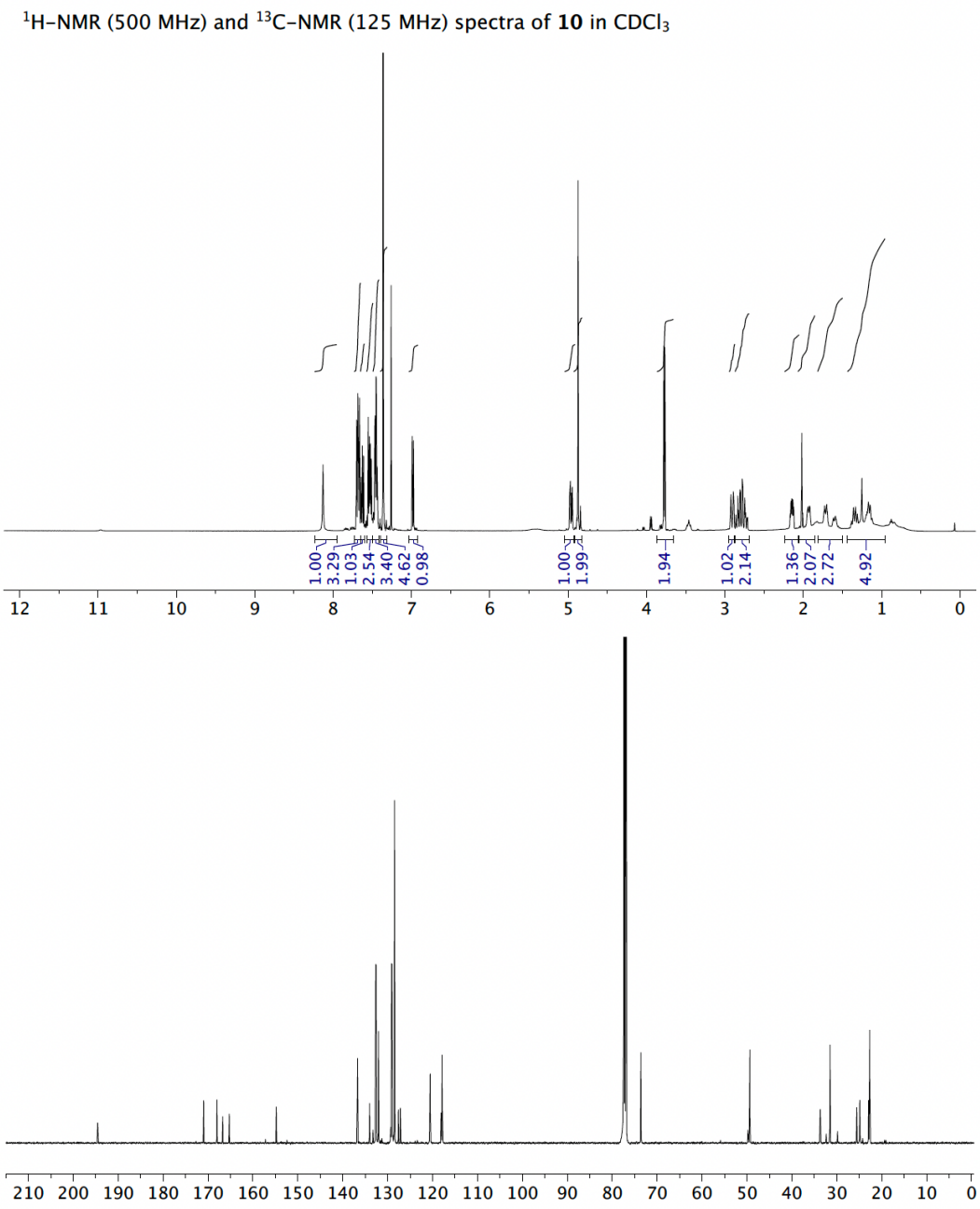

Appendix Figure 2-19: ^{1}H-NMR and ^{13}C-NMR spectra of 10 in $CDCl_3$.

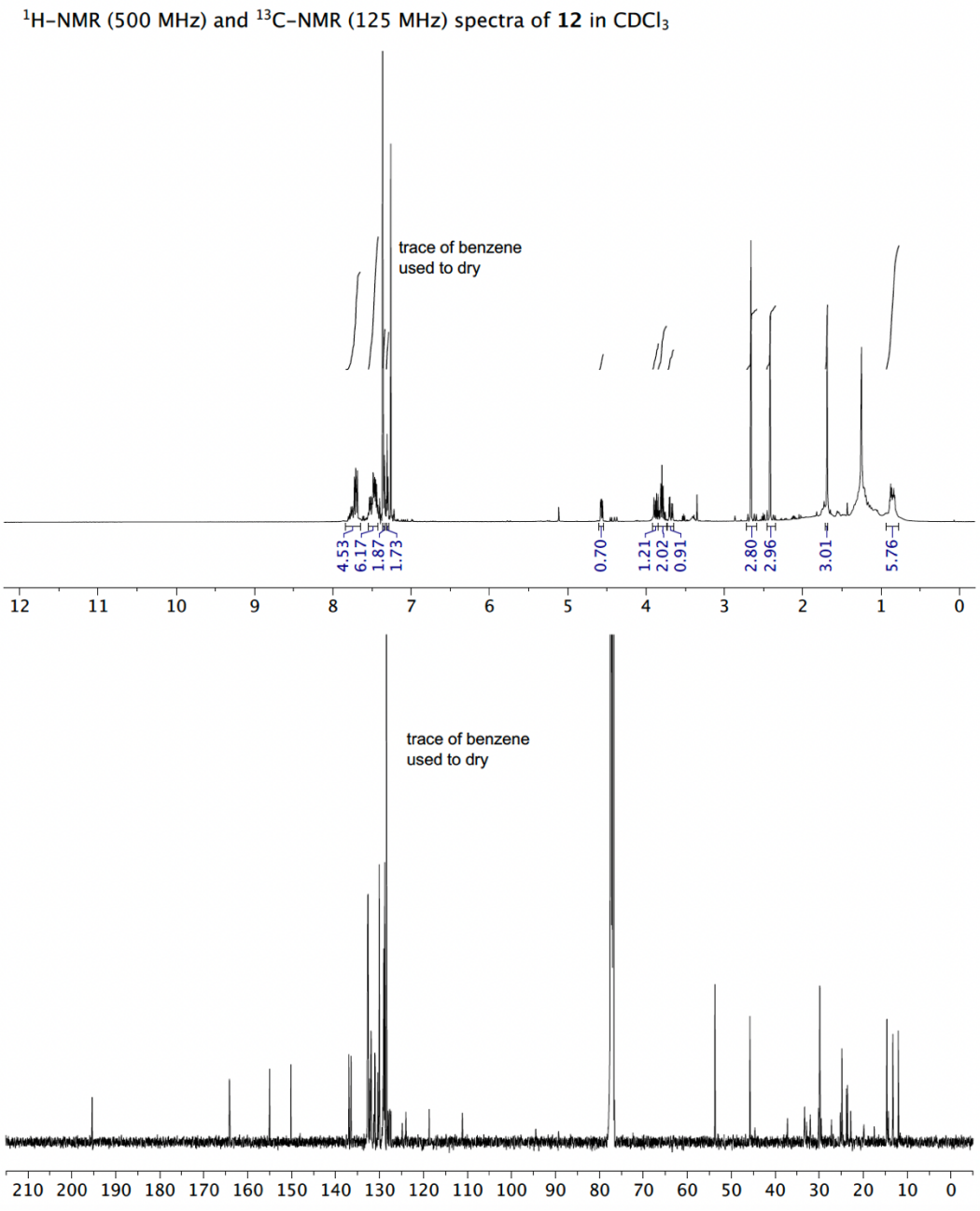

Appendix Figure 2-20: ^{1}H-NMR and ^{13}C-NMR spectra of 12 in $CDCl_3$.

REFERENCES

1. G. Schneider *Nat. Rev. Drug Discovery*, **2018**, *17*, 97-113.

2. (*a*) X. Wang, B. Huang, X. Liu and P. Zhan , *Drug Discovery Today*, **2016**, *21*, 118-132. (*b*) H. C. Kolb , M. G. Finn and B. K. Sharpless , *Angew. Chem., Int. Ed.*, **2001**, *40*, 2004-2021.

3. M. Pettersson and C. M. Crews , *Drug Discovery Today: Technol.*, **2019**, *31*, 15-27.

4. (*a*) M. G. Jaeger and G. E. Winter, *Cell Chem. Biol.*, 2020, **27** , 14 —16. (*b*) I. Churcher *J. Med. Chem.*, 2018, **61** , 444 —452. (*c*) L. Tan and N. S. Gray , *Chin. J. Chem.*, 2018, **36** , 971 —977. (*d*) M. Toure and C. M. Crews , *Angew. Chem., Int. Ed.*, 2016, **55** , 1966 —1973. (*e*) L. Buetow and D. T. Huang , *Nat. Rev. Mol. Cell Biol.*, 2016, **17** , 626 —642. (*f*) R. J. Deshaies *Nat. Chem. Biol.*, 2015, **11** , 634 —635.

5. (*a*) D. P. Bondeson , B. E. Smith , G. M. Burslem , A. D. Buhimschi , J. Hines , S. Jaime-Figueroa , J. Wang , B. D. Hamman , A. Ishchenko and C. M. Crews , *Cell. Chem. Biol.*, 2018, **25** , 78 —87. (*b*) S. Moon and B. H. Lee , *Mol. Cell*, 2018, **41** , 933 —942. (*c*) C. V. Dang , E. P. Reddy , K. M. Shokat and L. Soucek , *Nat. Rev. Cancer*, 2017, **17** , 502 —508. (*d*) C. M. Crews *Chem. Biol.*, 2010, **17** , 551 —555.

6. ClinicalTrials.gov Identifier: NCT03888612

7. K. M. Sakamoto , K. B. Kim , A. Kumagai , F. Mercurio , C. M. Crews and R. J. Deshaies , *Proc. Natl. Acad. Sci. U. S. A.*, 2001, **98** , 8554 —8559.

8. A. Zorba , C. Nguyen , Y. Xu , J. Starr , K. Borzilleri , J. Smith , H. Zhu , K. A. Farley , W. Ding , J. Schiemer , X. Feng , J. S. Chang , D. P. Uccello , J. A. Young , C. N. Garcia-Irrizary , L. Czabaniuk , B. Schuff , R. Oliver , J. Montgomery , M. M. Hayward , J. Coe , J. Chen , M. Niosi , S. Luthra , J. C. Shah , A. El-Kattan , X. Qiu , G. M. West , M. C. Noe , V. Shanmugasundaram , A. M. Gilbert , M. F. Brown and M. F. Calabrese , *Proc. Natl. Acad. Sci. U. S. A.*, 2018, **115** , E7285 —E7292.

9. (*a*) S. Krajcovicova , R. Jorda , D. Hendrychova , V. Krystof and M. Soural , *ChemComm*, 2019, **55** , 929 —932. (*b*) X. Qiu , N. Sun , Y. Kong , Y. Li , X. Yang and B. Jiang , *Org. Lett.*, 2019, **21** , 3838 —3841. (*c*) R. P. Wurz , K. Dellamaggiore , H. Dou , N. Javier , M. Lo , J. D. McCarter , D. Mohl , C. Sastri , J. R. Lipford and V. J. Cee , *J. Med. Chem.*, 2018, **61** , 453 —461. (*d*) J. W. Papatzimas , E. Gorobets , D. K. Brownsey , R. Maity , N. J. Bahlis and D. J. Derksen , *Synlett*, 2017, 2881 —2885.

10. A. Chen , R. N. Re and M. D. Burkart , *Nat. Prod. Rep.*, 2018, **35** , 1029 —1045.

11. K. M. Clarke , A. C. Mercer , J. J. La Clair and M. D. Burkart , *J. Am. Chem. Soc.*, 2005, **127** , 11234 —11235.

12. A. L. Mandel , J. J. La Clair and M. D. Burkart , *Org. Lett.*, 2004, **6** , 4801 —4803.

13. A. S. Worthington and M. D. Burkart , *Org. Biomol. Chem.*, 2006, **4** , 44 —46.

14. (*a*) M. B. Soellner , B. L. Nilsson and R. T. Raines , *J. Am. Chem. Soc.*, 2006, **128** , 8820 —8828. (*b*) B. L. Nilsson , L. L. Kiessling and R. T. Raines , *Org. Lett.*, 2001, **3** , 9 —12.

15. (*a*) Z. A. Wang , C. Tian and J. Zheng , *RSC Adv.*, 2015, **5** , 107192 —107199. (*b*) R. Kleineweischede and C. P. R. Hackenberger , *Angew. Chem., Int. Ed.*, 2008, **47** , 5984 —5988. (*c*) M. Köhn and R. Breinbauer , *Angew. Chem., Int. Ed.*, 2004, **43** , 3106 —3116. (*d*) O. David , W. J. N. Meester , H. Bieräuel , H. E. Schoemaker , H. Hiemstra and J. H. van Maarseveen , *Angew. Chem., Int. Ed.*, 2003, **42** , 4373 —4375. (*e*) E. Saxon , J. I. Armstrong and C. R. Bertozzi , *Org. Lett.*, 2000, **2** , 2141 —2143.

16. H. Schumacher , R. L. Smith and R. T. Williams , *Brit. J. Pharmacol.*, 1965, **25** , 324 —337.

17. (*a*) S. Moon and B. H. Lee , *Mol. Cells*, 2018, **41** , 933 —942. (*b*) C. V. Dang , E. P. Reddy , K. M. Shokat and L. Soucek , *Nat. Rev. Cancer*, 2017, **17** , 502 —508.

18. C. Steinebach , S. Lindner , N. D. Udeshi , D. C. Mani , H. Kehm , S. Köpff , S. A. Carr , M. Gütschow and J. Krönke , *ACS Chem. Biol.*, 2018, **13** , 2771 —2782.

19. J. Lohbeck and A. K. Miller , *Bioorg. Med. Chem. Lett.*, 2016, **26** , 5260 —5262.

20. A. Staubitz , A. P. M. Robertson , M. E. Sloan and I. Manners , *Chem. Rev.*, 2010, **110** , 4023 —4078.

21. M. Mühlberg , D. M. M. Jaradat , R. Kleineweischede , I. Papp , D. Dechtrirat , S. Muth , M. Broncel and C. P. R. Hackenberger , *Biorg. Med. Chem.*, 2010, **18** , 3679 —3686.

22. G. E. Winter , D. L. Buckley , J. Paulk , J. M. Roberts , A. Souza , S. Dhe-paganon and J. E. Bradner , *Science*, 2015, **348** , 1376 —1381.

23. R. P. Nowak , S. L. DeAngelo , D. Buckley , Z. He , K. A. Donovan , J. An , N. Safaee , M. P. Jedrybhowski , C. M. Ponthier , M. Ishoey , T. Zhang , J. D. Mancias , N. S. Gray , J. E. Bradner and E. S. Fischer , *Nat. Chem. Biol.*, 2018, **14** , 706 —714.

24. (*a*) C. S. Kounde , M. M. Shchepinova , C. N. Saunders , M. Muelbaier , M. D. Rackham , J. D. Harling and E. W. Tate , *ChemComm*, 2020, **56** , 5532 —5535. (*b*) A. Testa , S. J. Hughes , X. Lucas , J. E. Wright and A. Ciulli , *Angew. Chem., Int. Ed.*, 2020, 1727 —1734. (*c*) S. Vollmer , D. Cunoosamy , H. Lv , H. Feng , X. Li , Z. Nan , W. Yang and M. W. D. Perry , *J. Med. Chem.*, 2020, **63** , 157 —162.

25. (*a*) M. S. Gadd , A. Testa , X. Lucas , K. Chan , W. Chen , D. J. Lamont , M. Zengerle and A. Ciulli , *Nat. Chem. Biol.*, 2017, **13** , 514 —521. (*b*) K. Cyrus , M. Wehenkel , E. Choi , H. Han , H. Lee , H. Swanson and K. Kim , *Mol. BioSyst.*, 2011, **7** , 359 —364.

26. (*a*) M. Girardini , C. Maniaci , S. J. Hughes , A. Testa and A. Ciulli , *Bioorg. Med. Chem.*, 2019, **27** , 2466 —2479. (*b*) C. Steinebach , H. Kehm , S. Lindner , L. P. Vu , S. Köpff , A. L. Mármol , C. Weiler , K. G. Wagner , M. Reichenzeller , J. Krönke and M. Gütschow , *ChemComm*, 2019, **55** , 1821 —1824.

27. A. Tam , M. B. Soellner and R. T. Raines , *J. Am. Chem. Soc.*, 2007, **129** , 11421 —11430.

28. G. R. Fulmer, A. J. M. Miller, N. H. Sherden, H. E. Gottlieb, A. Nudelman, B. M. Stoltz, J. E. Bercaw and K. I. Goldberg, *Organometallics*, 2010, **29**, 2176-2179.

29. J. Lohbeck and A. K. Miller, *Bioorg. Med. Chem. Lett.*, 2016, **26**, 5260-5262.

CHAPTER 3: Biological evaluation of a series of human carbonic anhydrase II (hCAII) degraders

INTRODUCTION

Human carbonic anhydrase II (hCAII) is a member of a superfamily of metalloenzymes with six known subfamilies, of which, only one subfamily (alpha) is found in vertebrates and will be the focus of this chapter. Alpha carbonic anhydrases have fifteen isoforms and all of which catalyze the reversible conversion of carbon dioxide to bicarbonate.[1] The catalysis is carried out by an active site tetrahedral zinc(II) ion coordinated to three histidine residues and a nucleophilic hydroxide that carries out the attack on carbon dioxide, forming bicarbonate.[2] The active site is bifurcated into a hydrophobic channel and a hydrophilic channel to accommodate the entry/exit of both carbon dioxide (nonpolar) and bicarbonate (polar).[3]

Due to its role in regulating pH and carbon dioxide in cells, hCAII has been implicated in various cancers, glaucoma, edema, epilepsy, morbid obesity, osteopetrosis, renal acidosis, and cerebral calcification.[3,4] It also has secondary effects on pH dependent pathways and could be a viable target for pharmacological intervention in cases, such as, regulation of aquaporins during urine concentration as indicated by diabetes insipidus.[5] Except in special circumstances where localized drug delivery can be accomplished, carbonic anhydrases are seen as difficult drug

targets due issues with isoform selectivity and toxicity associated with systemic inhibition.[6]

Figure 3-1: Strucutre of hCAII in complex with an arylsulphonamide.

There is a long, rich history of targeting metalloenzymes for various indications. A common approach is to use a metal-chelating ligand that inhibits the catalytic metal-center; however, this can lead to extensive off-target binding.[7] Much work has been done to develop metal-binding pharmacophores (MBPs) that exhibit selectivity among various metalloenzyme classes, however the targets of interest usually have many isoforms and pan-inhibition is typically not desired.[8] Prior approaches to achieve isozyme selectivity for a metalloprotein target involve tethering large macrocyclic peptides and polyketides to an MBP in order to induce a selective interaction with a non-conserved peripheral moiety.[9] This strategy can be successful; however, development of these types of molecules can be challenging and selectivity can be limited.

Building upon this approach, the selectivity inducing peripheral interactions described above have a relatively small surface area. It has been shown that a proteolysis targeting chimera (PROTAC) approach can be used with MBPs to degrade metalloprotein targets[10] and the ternary complex formed between the target protein, PROTAC, and E3 ligase ostensibly has potential to induce a peripheral interaction with a larger surface area. With this in mind, we sought to use hCAII as a model system to develop a metalloprotein degradation platform. Due to the extensive

crystallographic data available for hCAII,[11] we planned to get co-crystal structures of our various degrader molecules which could then be used as training sets for *in silico* degrader design for future metalloprotein targets (See Chapter 2 for details on *in silico* degrader design).

COMPOUND DESIGN AND CHARACTERIZATION

The design of our suite of degrader molecules centered around the use of an aryl-sulphonamide MBP, which had been shown to be selective for carbonic anhydrases,[8] linked to an E3 ligase ($CRL4^{CRBN}$) recruiting moiety[12] or linked to a hydrophobic tag (adamantyl).[13] Unlike the degraders discussed previously, the hydrophobic tag (HyT) degraders mechanism of action is to stimulate the cells endogenous protein quality control machinery, mimicking a partially unfolded protein and triggering degradation through the unfolded protein response (UPR).[14]

To ensure that our aryl-sulphonamide MBPs retained their binding to hCAII after being linked to the E3 ligase ligand, we first obtained data on our binary binding. This was accomplished via an established competitive inhibition assay.[15] It has been shown that carbonic anhydrases can facilitate the hydrolysis of *para*-nitrophenylacetate into the corresponding phenolate. Heterologously expressed hCAII was preincubated with varying concentrations of a compound of interest and enzyme inhibition was measured after addition of *para*-nitrophenylacetate and subsequent comparison of absorbance to a positive control without aryl-sulphonamide present. The data showed (Figure 3-2) that conjugating the aryl-sulphonamide to either the E3 ligase ligand or the hydrophobic tag

did not abolish hCAII binding *in vitro* and we attribute minor differences in binary binding to the various peripheral contacts made by both the linker and external moiety.

Figure 3-2: hCAII degrader library and binary affinities. Binary affinities were measure in triplicate via the enzyme-catalyzed hydrolysis of para-nitrophenylacetate and accumulation of phenolate product as described in reference 15. All compounds were synthesized, and binary affinities measured by Conor O'Herin in the laboratory of Professor Seth Cohen.

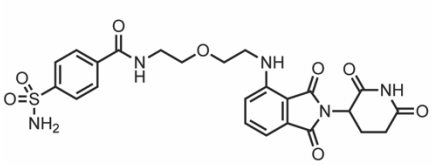

Compound	IC_{50} (nM)
COH-52	66 ± 6

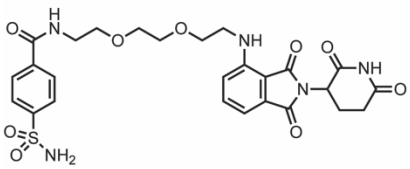

COH-49	62 ± 12

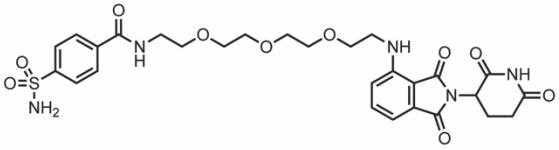

COH-67	60 ± 6

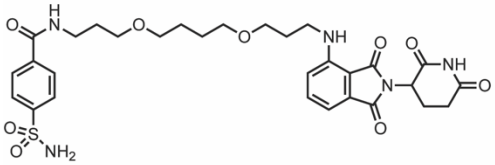

COH-68	31 ± 4

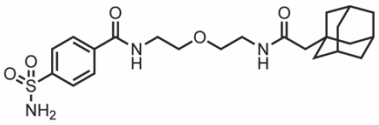

COH-100	88 ± 8

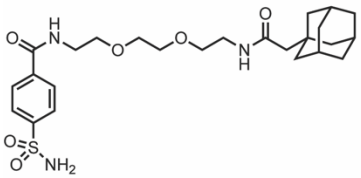

COH-72	43 ± 8

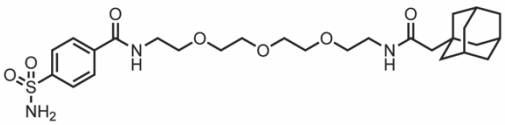

COH-101	54 ± 5

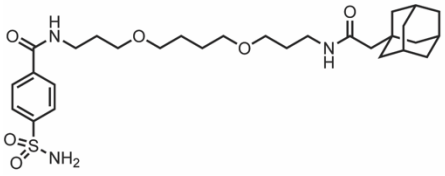

COH-99	19 ± 3

We then moved on to *in cellulo* studies with HEK293T cells which have been shown to robustly express hCAII as well as our chosen E3 ligase ($CRL4^{CRBN}$).[16] For our first pass we opted to screen all compounds in our series at 5 μM for 24 hours (See appendix for details). For the PROTACs, we observed (Figure 3-3) an approximately 5% reduction of hCAII with the compound COH-52 and COH-67. More interestingly, COH-68 showed an approximately 30% reduction of hCAII abundance. The HyT compounds COH-100 and COH-101 yielded an approximately 10% and 5% reductions in hCAII, respectively. All other compounds showed very little activity.

From this data we were able to draw two conclusions for this set of compounds. The first was that the linker lengths of COH-49 and COH-72 were too short to make an effective degrader. The second conclusion was that the best PROTAC (COH-68) showed more robust degradation than the best HyT (COH-100). We then chose to move forward with our hit compound COH-68 for further characterization and future lead optimization.

Figure 3-3: Exploratory degradation screen. Preliminary degradation screening was done with all eight compounds in a single experiment. For experimental details please see the Appendix. All compounds were synthesized by Conor O'Herin in the laboratory of Professor Seth Cohen.

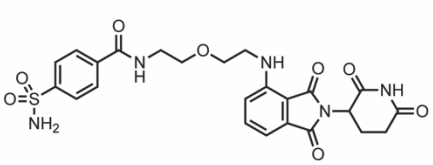

Compound	% hCAII
COH-52	100.1

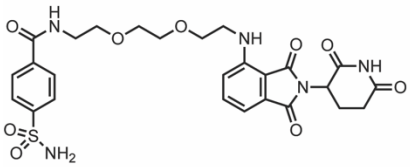

COH-49	94.5

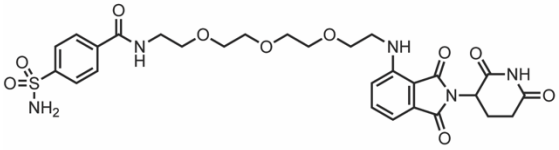

COH-67	94.6

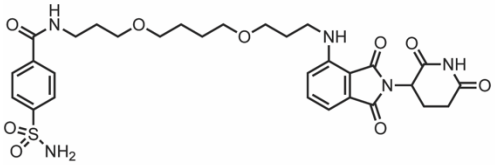

COH-68	70.8

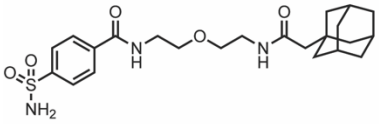

COH-100	90.4

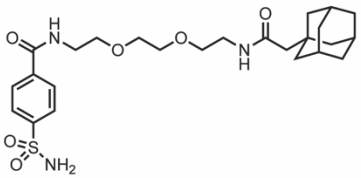

COH-72	99.6

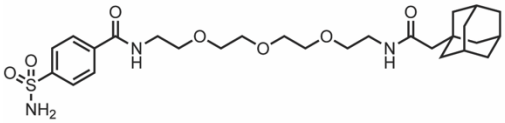

COH-101	94.3

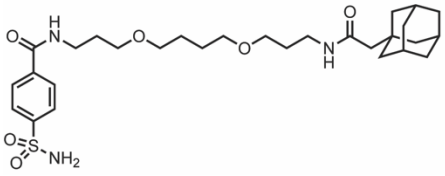

COH-99	98.8

To further understand the chemical properties responsible for successful hCAII degradation among our series of PROTACs we did a rudimentary structure-property relationship (SPR) analysis (Figure 3-4).[17] It is of no surprise that PROTACs often fall outside of drug-like chemical space as defined by rule-of-five dogma,[18] however the most flagrant violations typically stem from their large molecular weight (MW). Many of the typical pharmacokinetic trends as it pertains to total polar surface area (TPSA) membrane permeability (cLogP, LogP), and solubility still hold true[19] and degrader SPR optimization entails constructing molecules that are as drug-like as possible. Typical drug-like properties include having a MW < 500 (g/mol), TPSA < 140 Å^2, and 0 < LogP < 5.[18,20] It is likely that the success of COH-68 can be attributed to its permeability relative to the other PROTACs. Beyond having such large MWs, the PROTACs here are quite hydrophilic (negative Log P and cLogP values) and COH-68 is the least hydrophilic of the series with a LogP = -0.52 and a cLogP = 0.00. For comparison, archetypal BRD4 degrader, dBET1[12] (see Chapter 1), has a LogP = 1.49 and a cLogP = 1.69 suggesting it has better membrane permeability. Additionally, once in the cell large molecules (MW > 400) with numerous hydrogen bond acceptors (N+O ≥ 8) having an increasing likelihood to be substrates for P-glycoprotein (P-gp) efflux.[21] This is a

potential liability for most all PROTACs, however oxygenated linkers could increase this liability.

The HyT compounds showed more favorable PK properties, however as demonstrated in the pan compound screen, the degradation was not as robust in the face of cellular hCAII resynthesis.

Figure 3-4: Predicted physiochemical properties of hCAII degraders. Physiochemical properties were determined utilizing ChemDraw software from Perkin Elmer. All compounds were synthesized by Conor O'Herin in the laboratory of Professor Seth Cohen.

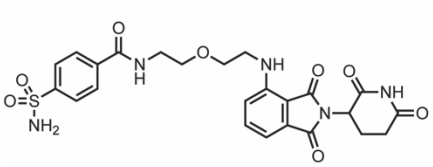

ID	MW	TPSA	cLogP	LogP
COH-52	543.55	194.1	-0.84	-1.13

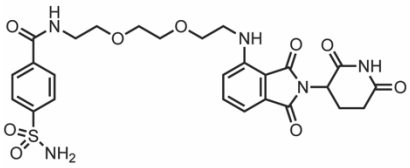

COH-49	587.60	203.3	-0.98	-1.29

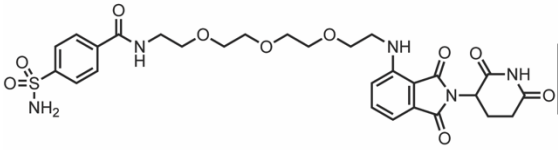

COH-67	631.66	212.5	-1.11	-1.44

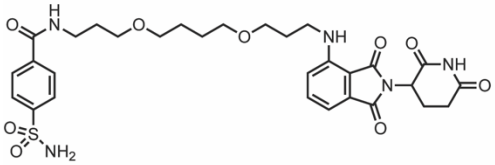

COH-68	643.71	203.3	0.00	-0.52

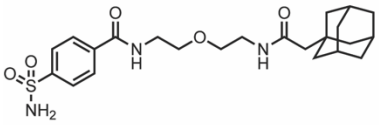

COH-100	463.59	127.6	2.81	1.42

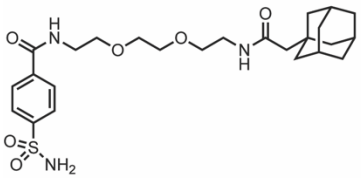

COH-72	507.65	136.8	2.67	1.26

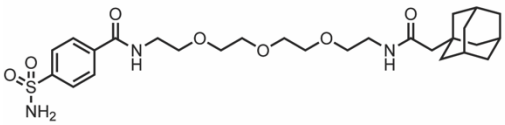

COH-101	551.70	146.1	2.54	1.11

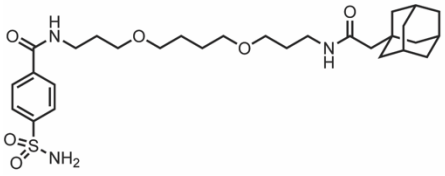

COH-99	563.75	136.8	3.55	2.03

Observing targeted protein degradation is a difficult task complicated by the kinetics of event-driven pharmacology.[22] On top of the usual PK considerations (permeability, solubility, efflux, chemical stability, metabolic stability, ect.) in developing a drug-like compound, there are target protein degradation kinetics, target protein resynthesis kinetics, and variable E3 ligase expression levels that confound the data.[23] In short, there must be all three components of the ternary complex (target protein, PROTAC, E3 ligase) present and the degradation must occur faster than the cell can resynthesize the target in order to observe target degradation via western blot. The reliance on degradation kinetics yields variable optimal dosing times for different protein targets. In order to determine our optimal dosing time, we performed a time course experiment where HEK293T cells were treated with 7.5 μM of COH-68, incubated, and lysed and various time points. What we observed (Figure 3-5) was that the compound had little effect on hCAII levels after 2 hours, at 4 hours the cells began to overexpress hCAII leading to a 27% increase in hCAII levels, maximal degradation was observed after 24 hours, and this degradation/resynthesis equilibrium was sustained at 48 hours. From this data, we concluded that 24-hour treatment was adequate to move forward with for further characterization of COH-68.

Figure 3-5: COH-68 time course degradation study. HEK293T cells were treated with compound or vehicle and cells were lysed at various timepoints. For experimental details please see the Appendix. Western blot optimization was performed by the author, Conor O'Herin and Alysia Kohlbrand. The blot depicted was performed by Conor O'Herin in the laboratory of Seth Cohen.

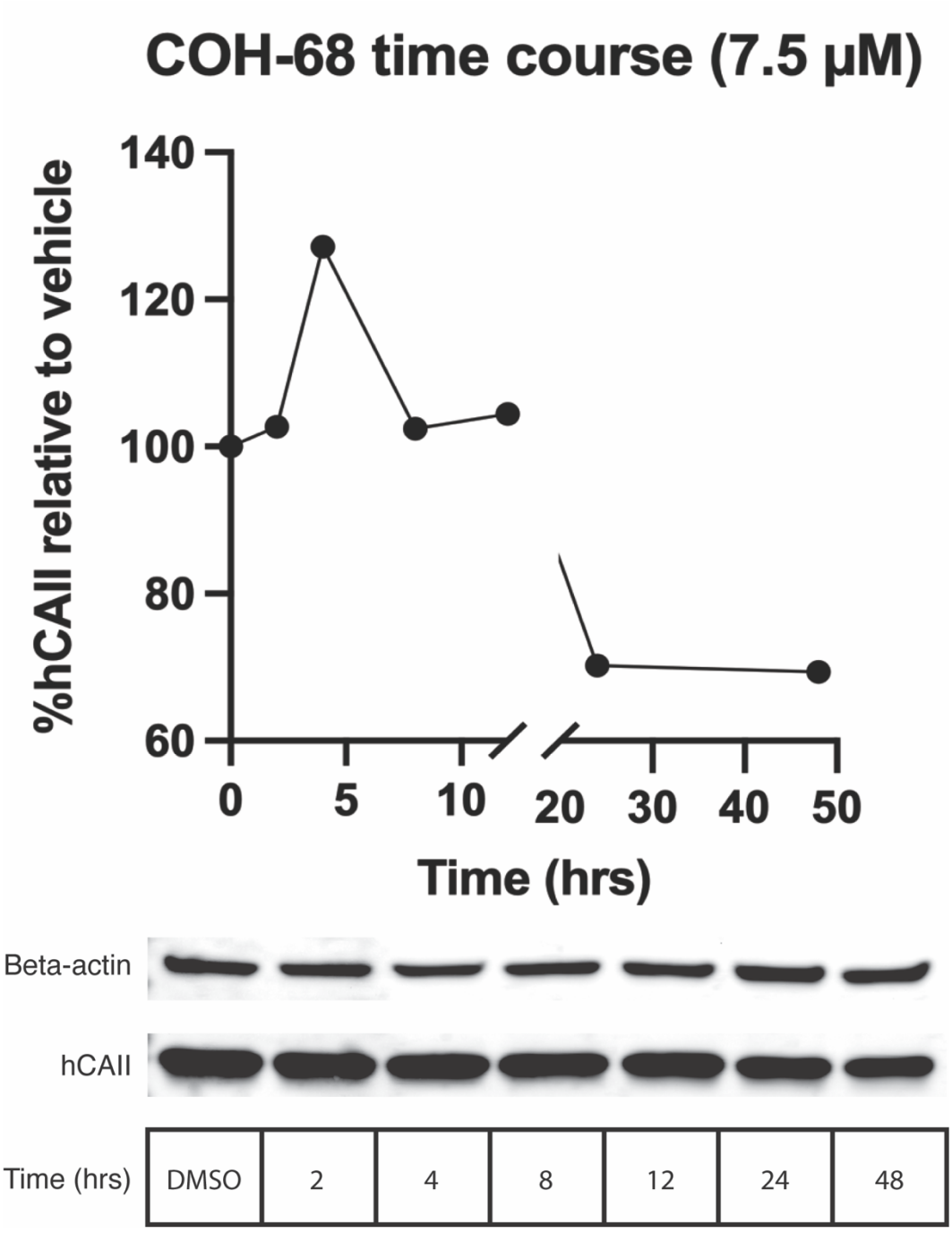
COH-68 time course (7.5 µM)
%hCAII relative to vehicle
140
120
100
80
60
0
5
10
20
30
40
50
Time (hrs)
Beta-actin
hCAII
Time (hrs)
DMSO
2
4
8
12
24
48

With an optimal timepoint in hand, we proceeded with an initial hCAII degradation dose-response experiment ranging from 0.75 nM to 7500 nM (Figure 3-6). Interestingly, low doses of COH-68 stimulated an overexpression of hCAII to 138% relative to DMSO vehicle controls and overproduction was maintained until doses higher than 75 nM where degradation below endogenous hCAII levels was observed. Furthermore, we observed a dose-responsive degradation of hCAII with a D_{max} = 74% and a DC_{50} = 930 nM relative to the DMSO treated cells. It is of note that DC_{50} here is calculated relative to DMSO (100% hCAII), however as previously discussed, treatment with COH-68 stimulates 38% excess production of hCAII, indicating robust degradation in the face of cellular hCAII resynthesis.

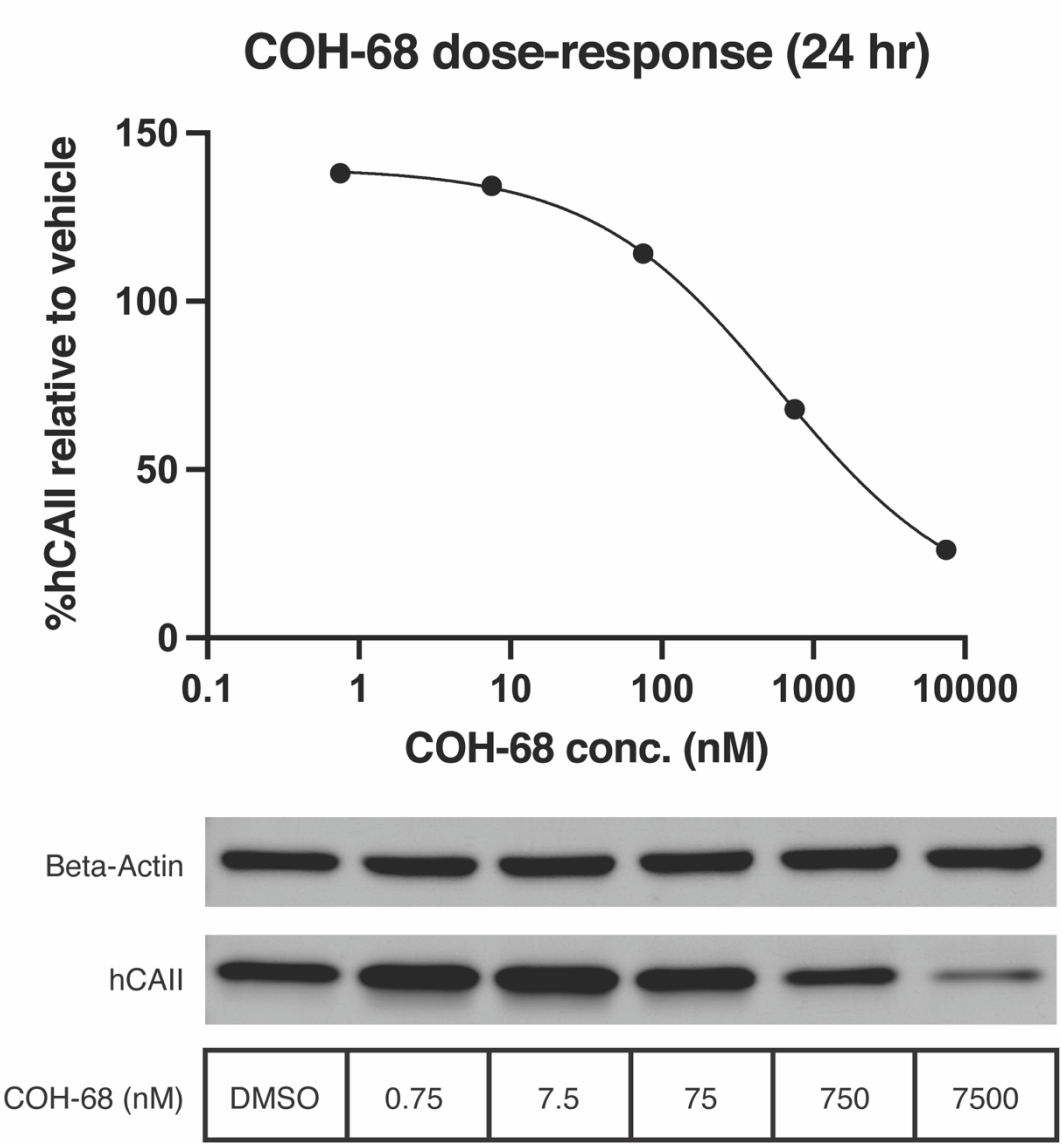

Figure 3-6: COH-68 preliminary dose-response study. HEK293T cells were treated with vehicle or compound at various concentrations and lysed after 24 hours. For full experimental details please see the Appendix. Western blot optimization was performed by the author, Conor O'Herin and Alysia Kohlbrand. The blot depicted was performed by Conor O'Herin in the laboratory of Seth Cohen.

Before moving into final characterization of hCAII degradation by COH-68, we wanted to observe how cell confluence affected the observed degradation (Figure 3-7). It was hypothesized that exponentially growing cells (i.e. lower confluence levels) would yield a higher expression of hCAII and therefore a lower observed degradation. To explore this hypothesis HEK293T cells were treated with either DMSO (0.5%) or 7.5 μM COH-68 in DMSO (0.5%) at increasing cellular confluences. We observed that higher levels of hCAII degradation was observed at higher cellular confluences.

Figure 3-7: Effects of confluence on hCAII degradation via COH-68. HEK293T cells were grown to different levels of confluence, photographed before and after a 24-hour treatment with compound or vehicle and lysed. For full experimental details please see the Appendix. Western blot optimization was performed by the author, Conor O'Herin and Alysia Kohlbrand. The blot depicted was performed by Conor O'Herin in the laboratory of Seth Cohen.

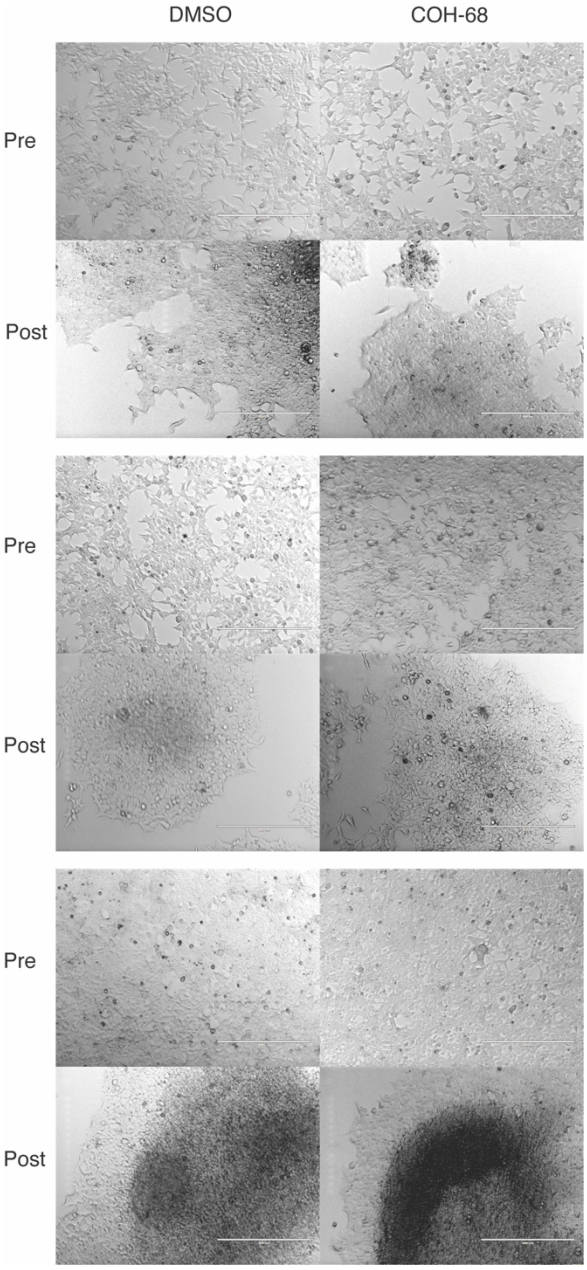

Timepoint	% hCAII
1	72.4

Timepoint	% hCAII
2	78.5

Timepoint	% hCAII
3	63.2

Targeting hCAII for PROTAC degradation presented unique challenges that have not been addressed previously. Firstly, hCAII is highly expressed relative to other PROTAC target proteins. It has been reported that hCAII abundance is approximately 0.1 mM in red blood cells,[24] where the expression has been independently reported at 2,448.1 normalized transcripts per million (nTPM).[16a,25] The HEK293 cell line has a reported hCAII expression of 1097.8 nTPM,[16] providing a back of the napkin calculated hCAII abundance of approximately 0.045 mM. It is remarkable that COH-68 was able to achieve meaningful levels of hCAII degradation in the face of both the endogenous protein levels and observed overexpression induced at low compound concentrations (Figure 3-6).

Moving forward, we are currently working on the design and synthesis of second generation hCAII degraders with the same number of linear linker atoms as COH-68, however designed to have potentially better PK properties. The approach for second-generation design is to decrease the TPSA and increase the cLogP and LogP to increase membrane permeability and decrease P-gp efflux liabilities.[18-21] Compound 1 (Figure 3-8) replaces the oxygenated linker with a linear aliphatic linker. This alteration fulfills our designated second-generation

design criteria, however the tradeoff for increased membrane permeability (lipophilicity) is a decrease in solubility in aqueous media. Compound 2 was designed to offset the decrease in aqueous solubility while still maintaining an increase in permeability relative to first-generation degraders through the introduction of an ionizable piperazine linker moiety,[26] which also serves to reduce the number of rotatable bonds, increasing rigidity. Drawing upon previous degrader studies[27] reporting favorable PK properties through the further rigidification of the linker via introduction of an alkynl moiety, compound 3 was designed. As previously stated, the hCAII active site is bifurcated into both hydrophobic and hydrophilic channels so we do not anticipate that this change in linker chemistry will be prohibitive to hCAII degradation.

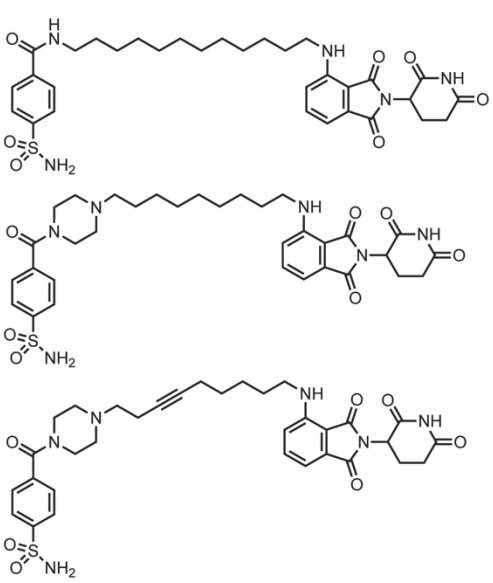

ID	MW	TPSA	cLogP	LogP
1	639.77	184.8	3.65	2.92
2	666.79	179.3	2.41	1.66
3	662.76	179.3	1.41	1.09

Figure 3-8: Second-generation hCAII degrader design. Exemplary structures of potential second-generation hCAII degraders bearing more favorable predicted physiochemical properties.

CONCLUSION AND FUTURE DIRECTIONS

Here we have identified COH-68 as an active degrader of hCAII in HEK293T cells. The initial dose-response experiments have shown an interesting dual activity, where at low doses we observed an upregulation of hCAII production relative to DMSO controls which was sustained until doses above 75 nM. Above 75 nM we observed effective degradation of hCAII with no observed hook-effect up to 7.5 μM. The upregulation of hCAII at low doses could be of interest as a potential therapeutic for indications where hCAII expression is depressed, such as renal acidosis or diabetes insipidus. To date, hCAII as a degradation target serves as the most highly expressed protein of interest to be successfully degraded and the ability to stimulate hCAII overproduction at very low COH-68 concentrations indicates a unique oxymoronic activity.

Future studies will involve replicates of the COH-68 dose-response assay for publication, however we will include four more doses (0.325 nM, 0.163 nM, 15 μM, and 30 μM). The two lowest doses will serve as a benchmark to observe how much compound is necessary to stimulate the overexpression of hCAII. The two highest doses will ensure that we are observing our true maximum degradation and will also allow observation of the stereotypical hook-effect common to bifunctional degraders. Due to

the high expression levels of hCAII, I do not believe a true hook-effect will be observed due to an inability to saturate all possible hCAII binding sites.

Chapter 3, in part, is currently being prepared for submission for publicaiton of the material. O'Herin, Conor; Bemis, Troy A.; Kohlbrand, Alysia J.; La Clair, James J.; Burkart, Michael D.; Cohen, Seth M. The dissertation author is a primary coauthor of the manuscript in preparation with O'Herin, Conor and the primary author of this chapter.

APPENDIX

Compounds

All compounds in this study were prepared by Conor O'Herin in the laboratory of Professor Seth Cohen.

Cell Culture

The HEK293T cell line was cultured in DMEM (Life Technologies) supplemented with 10% fetal bovine serum, 2 mM L-glutamine, 100 U mL^{-1} penicillin and 100 μg mL^{-1} streptomycin at 37 ^{o}C in an atmosphere of 5% CO_2.

Cellular Drug Treatments

Compounds were dissolved in DMSO (MilliporeSigma). Cells were treated with 0.5% DMSO or compound dissolved in DMSO.

Pan-Compound Activity Screen

HEK293T cells were plated in 6-well plates at 0.3 x 10^6 cells/well in 2 mL warm media and allowed to grow to 80% confluence. The media was removed and replaced with 2 mL fresh warm media. DMSO (10 μL) or compound (10 μL, 5 μM final concentration) was added and the cells were incubated for 24 hours. The media was removed, the cells were washed with cold PBS (1 mL), and 1x modified RIPA lysis buffer (Cell Signaling) containing 1% human protease and phosphatase inhibitor (Cell signaling) at 4 ^{o}C for 20 minutes. The cells were then scraped from their wells,

transferred to epi tubes, centrifuged for at 14,000 rpm for 10 minutes at 4 ^{o}C, the supernatant collected and transferred into new epi tubes, and stored at -80 ^{o}C overnight. Protein concentration was measured via the Pierce BCA Assay (Thermo Fisher).

Time Course Assay

HEK293T cells were plated in 6-well plates at 0.3 x 10^6 cells/well in 2 mL warm media and allowed to grow to 80% confluence. The media was removed and replaced with 2 mL fresh warm media. DMSO (10 μL) or compound (10 μL, 7.5 μM final concentration) was added and the cells were incubated for 2, 4, 8 ,12, 24, or 48 hours. The media was removed, the cells were washed with cold PBS (1 mL), and 1x modified RIPA lysis buffer (Cell Signaling) containing 1% human protease and phosphatase inhibitor (Cell signaling) at 4 ^{o}C for 20 minutes. The cells were then scraped from their wells, transferred to epi tubes, centrifuged for at 14,000 rpm for 10 minutes at 4 ^{o}C, the supernatant collected and transferred into new epi tubes, and stored at -80 ^{o}C overnight. Protein concentration was measured via the Pierce BCA Assay (Thermo Fisher).

Dose-Response Assay

HEK293T cells were plated in 6-well plates at 0.3 x 10^6 cells/well in 2 mL warm media and allowed to grow to 80% confluence. The media was

removed and replaced with 2 mL fresh warm media. DMSO (10 μL) or compound (10 μL) at 0.75 nM, 7.5 nM, 75 nM, 750 nM, or 7.5 μM final concentration was added and the cells were incubated for 24 hours. The media was removed, the cells were washed with cold PBS (1 mL), and 1x modified RIPA lysis buffer (Cell Signaling) containing 1% human protease and phosphatase inhibitor (Cell signaling) at 4 ^{o}C for 20 minutes. The cells were then scraped from their wells, transferred to epi tubes, centrifuged for at 14,000 rpm for 10 minutes at 4 ^{o}C, the supernatant collected and transferred into new epi tubes, and stored at -80 ^{o}C overnight. Protein concentration was measured via the Pierce BCA Assay (Thermo Fisher).

Confluence Assay

HEK293T cells were plated in 6-well plates at 0.3 x 10^6 cells/well in 2 mL warm media and allowed to grow to three different levels of confluence. Images were obtained of the cells prior to dosing. The media was removed and replaced with 2 mL fresh warm media. DMSO (10 μL) or compound (10 μL, 7.5 μM final concentration) was added and the cells were incubated for 24 hours. Images were obtained of the cells after treatment. The media was removed, the cells were washed with cold PBS (1 mL), and 1x modified RIPA lysis buffer (Cell Signaling) containing 1% human protease and phosphatase inhibitor (Cell signaling) at 4 ^{o}C for 20

minutes. The cells were then scraped from their wells, transferred to epi tubes, centrifuged for at 14,000 rpm for 10 minutes at 4 ^{o}C, the supernatant collected and transferred into new epi tubes, and stored at -80 ^{o}C overnight. Protein concentration was measured via the Pierce BCA Assay (Thermo Fisher).

REFERENCES

1. Boone, C. D.; Habibzadegan, A.; Gill, S.; Mckenna, R. Carbonic Anhydrases and Their Biotechnological Applications. *Biomolecules* **2013**, *3*, 553.

2. Fisher, S. Z.; Aggarwal, M.; Kovalevsky, A. Y.; Silverman, D. N.; McKenna, R. Neutron Diffraction of Acetazolamide-Bound Human Carbonic Anhydrase II Reveals Atomic Details of Drug Binding. *J. Am. Chem. Soc.* **2012**, *134*, 14726–14729.

3. Lindskog, S. Structure and Mechanism of Carbonic Anhydrase. *Pharmacol. Ther.* **1997**, *74*, 1–20.

4. Morrison, H. Enzyme Active Sites and Their Reaction Mechanisms; Academic Press, **2020**.

5. Krishnan, D.; Pan, W.; Beggs, M. R.; Trepiccione, F.; Chambrey, R.; Eladari, D.; Cordat, E.; Dimke, H.; Alexander, R. T. Deficiency of Carbonic Anhydrase II Results in a Urinary Concentrating Defect. *Front. Physiol.* **2018**, *8*, 1108.

6. Ghorai, S.; Pulya, S.; Ghosh, K.; Panda, P.; Ghosh, B.; Gayen, S. Structure-Activity Relationship of Human Carbonic Anhydrase-II Inhibitors: Detailed Insight for Future Development as Anti-Glaucoma Agents. *Bioorg. Chem.* **2020**, *95*, 103557.

7. Chen, A. Y.; Adamek, R. N.; Dick, B. L.; Credille, C. V; Morrison, C. N.; Cohen, S. M. Targeting Metalloenzymes for Therapeutic Intervention. *Chem. Rev.* **2018**, *119*, 1323-1455.

8. Day, J. A.; Cohen, S. M. Investigating the Selectivity of Metalloenzyme Inhibitors. *J. Med. Chem.* **2013**, *56*, 7997–8007.

9. Riccardi, L.; Genna, V.; De Vivo, M. Metal–Ligand Interactions in Drug Design. *Nat. Rev. Chem.* **2018**, *2*, 100–112.

10. (*a*) *Yang*, K.; Wu, H.; Zhang, Z.; Leisten, E. D.; Nie, X.; Liu, B.; Wen, Z.; Zhang, J.; Cunningham, M. D.; Tang, W. Development of Selective

Histone Deacetylase 6 (HDAC6) Degraders Recruiting von Hippel-Lindau (VHL) E3 Ubiquitin Ligase. *ACS Med. Chem. Lett.* **2020**, *11*, 575–581. (*b*) Wu, H.; Yang, K.; Zhang, Z.; Leisten, E. D.; Li, Z.; Xie, H.; Liu, J.; Smith, K. A.; Novakova, Z.; Barinka, C.; Tang, W. Development of Multifunctional Histone Deacetylase 6 Degraders with Potent Antimyeloma Activity. *J. Med. Chem.* **2019**, *62*, 7042–7057.

11. Aggarwal, M.; Boone, C. D.; Kondeti, B.; McKenna, R. Structural Annotation of Human Carbonic Anhydrases. *Journal of Enzyme Inhibition and Medicinal Chemistry*. **2013**, *28*, 267–277.

12. Winter, G. E.; Buckley, D. L.; Paulk, J.; Roberts, J. M.; Souza, A.; Dhe-Paganon, S.; Bradner, J. E. Phthalimide Conjugation as a Strategy for in Vivo Target Protein Degradation. *Science*. **2015**, *348*, 1376-1381.

13. Neklesa, T. K.; Crews, C. M. Greasy Tags for Protein Removal. *Nature*. **2012**, *487*, 308–309.

14. Cromm, P. M.; Crews, C. M. Targeted Protein Degradation: From Chemical Biology to Drug Discovery. *Cell Chemical Biology*. **2017**, *24*, 1181–1190.

15. Tu, C.; Thomas, H. G.; Wynns, G. C.; Silverman, D. N. Hydrolysis of 4-Nitrophenyl Acetate Catalyzed by Carbonic Anhydrase III from Bovine Skeletal Muscle. *J. Biol. Chem.* **1986**, *261*, 10100–10103.

16. (*a*) Berglund, L.; Björling, E.; Oksvold, P.; Fagerberg, L.; Asplund, A.; Szigyarto, C. A. K.; Persson, A.; Ottosson, J.; Wernérus, H.; Nilsson, P.; Lundberg, E.; Sivertsson, Å.; Navani, S.; Wester, K.; Kampf, C.; Hobert, S.; Pontén, F.; Uhlén, M. A Genecentric Human Protein Atlas for Expression Profiles Based on Antibodies. *Mol. Cell. Proteomics* **2008**, *7*, 2019–2027. (*b*) *Human Protein Atlas* https://www.proteinatlas.org/ENSG00000104267-CA2/cell+line (accessed 2021-12-02).

17. Di, L.; Kerns, E. H. Drug-Like Properties: Concepts, Structure Design and Methods from ADME to Toxicity Optimization; Elsevier, **2016**.

18. Lipinski, C. A.; Lombardo, F.; Dominy, B. W.; Feeney, P. J. Experimental and Computational Approaches to Estimate Solubility and Permeability in Drug Discovery and Development Settings. *Adv. Drug Deliv. Rev.* **2001**, *46*, 3–26.

19. Maple, H. J.; Clayden, N.; Baron, A.; Stacey, C.; Felix, R. Developing Degraders: Principles and Perspectives on Design and Chemical Space. *Medchemcomm.* **2019**, *10*, 1755–1764.

20. Veber, D. F.; Johnson, S. R.; Cheng, H. Y.; Smith, B. R.; Ward, K. W.; Kopple, K. D. Molecular Properties That Influence the Oral Bioavailability of Drug Candidates. *J. Med. Chem.* **2002**, *45*, 2615–2623.

21. Didziapetris, R.; Japertas, P.; Avdeef, A.; Petrauskas, A. Classification Analysis of P-Glycoprotein Substrate Specificity. *Journal of Drug Targeting.* **2008**, *11*, 391–406.

22. Pettersson, M.; Crews, C. M. PROteolysis TArgeting Chimeras (PROTACs) — Past, Present and Future. *Drug Discov. Today Technol.* **2019**, *31*, 15–27.

23. Roy, M. J.; Winkler, S.; Hughes, S. J.; Whitworth, C.; Galant, M.; Farnaby, W.; Rumpel, K.; Ciulli, A. SPR-Measured Dissociation Kinetics of PROTAC Ternary Complexes Influence Target Degradation Rate. *ACS Chem. Biol.* **2019**, *14*, 361–368.

24. (*a*) Moini, M.; Demars, S. M.; Huang, H. Analysis of Carbonic Anhydrase in Human Red Blood Cells Using Capillary Electrophoresis/Electrospray Ionization-Mass Spectrometry. *Anal. Chem.* **2002**, *74*, 3772–3776. (*b*) Donaldson, T. L.; Quinn, J. A. Kinetic Constants Determined from Membrane Transport Measurements: Carbonic Anhydrase Activity at High Concentrations. *Proc. Natl. Acad. Sci.* **1974**, *71*, 4995–4999.

25. *Human Protein Atlas.* https://www.proteinatlas.org/ENSG00000104267-CA2/single+cell+type (accessed 2021-12-02).

26. Cecchini, C.; Pannilunghi, S.; Tardy, S.; Scapozza, L. From Conception to Development: Investigating PROTACs Features for Improved Cell Permeability and Successful Protein Degradation. *Front. Chem.* **2021**, *9*, 215.

27. Han, X.; Wang, C.; Qin, C.; Xiang, W.; Fernandez-Salas, E.; Yang, C. Y.; Wang, M.; Zhao, L.; Xu, T.; Chinnaswamy, K.; Delproposto, J.; Stuckey, J.; Wang, S. Discovery of ARD-69 as a Highly Potent Proteolysis Targeting Chimera (PROTAC) Degrader of Androgen Receptor (AR) for the Treatment of Prostate Cancer. *J. Med. Chem.* **2019**, *62*, 941–964.

CONCLUSION

Here we present a platform for the development of chimeric small molecules, targeted protein degraders specifically. The platform consists of a parallel synthetic methodology enabling rapid access to chimeric small molecule linker variants (See Chapter 1). Application of the synthetic platform in a lab environment without access to preparative-HPLC purification will entail the preparation of azide-terminal linked E3 ligase ligand stocks (Chapter 1, compound 8) with a diverse array of linker chemistries aliquoted for rapid availability in parallel synthesis. Application of the methodology for a new target entails elaboration of the target protein ligand with a peripheral carboxylic acid handle (solvent exposed). The carboxylic acid will then be elaborated into the borane-protected phosphine thioester (example shown in Chapter 1, compound 12). The thioester stock solution will then be added in a parallel fashion to aliquots of the linked E3 ligase ligands described above, yielding the entire linker variant suite in a single effort. With access to preparative-HPLC, the entire process can be choreographed from the carboxylic acids of the two ligands in a parallel, one-pot fashion, albeit, yielding a complicated reaction mixture. Overall, this methodology expands access to linker

variants necessary for structure-activity relationship (SAR) studies that, to date, remain a rather empirical endeavor.

In an effort to reduce the empiricism in chimeric small molecule development, we performed a meta-analysis of previously performed linker-variant SAR studies (see Chapter 2). The model developed from this endeavor provides insight into how to choose linker lengths and chemistries in a methodical way in order to screen for degradation activity. The prescription of this study is to be cautious when screening for ternary complex compatibility at shorter linker lengths where steric clashes can quickly abolish biological activity. The model is to be used for first-pass degrader hit identification and is not intended to inform lead optimization where the linker should be optimized for favorable pharmacokinetic properties and shortened as much as possible to limit the degrees of freedom in the ternary complex.

The platform described here was specifically designed for use in targeted protein degradation, however, as previously described (See Introduction) we are currently witnessing a chimeric small molecule renaissance. The ability to rewire cellular metabolism through the use of chimeric small molecules has opened Pandora's box of opportunities for the development of molecular tools to aide in fundamental understanding

of biology. It also provides exciting new modalities for pharmaceutical intervention and has expanded our definition of what a “drug-like” molecule looks like. We anxiously await the results as the first chimeric protein degraders work their way through the clinic.

Moving forward I expect the empirical nature of linker SAR and ternary complex formation to be largely alleviated due to advances in computational modeling and further structural characterization of ternary complexes (See Chapter 2 for details). Furthermore, I expect there to be a number of new E3 ligase ligands discovered for use in targeted protein degradation with better pharmacokinetic properties than the options currently available. Although chimeric degraders exist outside the typical “drug-like” chemical space, future development will consist of maintaining the event-driven pharmacological activity while simultaneously attempting to make the chimeric small molecules as “drug-like” as possible. For this reason, new ligands for E3 ligase recruitment will be paramount to the success of chimeric small molecules in the clinic.